Global Carbon Budget 2016

Corinne Le Quéré[1], Robbie M. Andrew[2], Josep G. Canadell[3], Stephen Sitch[4], Jan Ivar Korsbakken[2], Glen P. Peters[2], Andrew C. Manning[5], Thomas A. Boden[6], Pieter P. Tans[7], Richard A. Houghton[8], Ralph F. Keeling[9], Simone Alin[10], Oliver D. Andrews[1], Peter Anthoni[11], Leticia Barbero[12,13], Laurent Bopp[14], Frédéric Chevallier[14], Louise P. Chini[15], Philippe Ciais[14], Kim Currie[16], Christine Delire[17], Scott C. Doney[18], Pierre Friedlingstein[19], Thanos Gkritzalis[20], Ian Harris[21], Judith Hauck[22], Vanessa Haverd[23], Mario Hoppema[22], Kees Klein Goldewijk[24], Atul K. Jain[25], Etsushi Kato[26], Arne Körtzinger[27], Peter Landschützer[28], Nathalie Lefèvre[29], Andrew Lenton[30], Sebastian Lienert[31,32], Danica Lombardozzi[33], Joe R. Melton[34], Nicolas Metzl[29], Frank Millero[35], Pedro M. S. Monteiro[36], David R. Munro[37], Julia E. M. S. Nabel[28], Shin-ichiro Nakaoka[38], Kevin O'Brien[39], Are Olsen[40], Abdirahman M. Omar[40], Tsuneo Ono[41], Denis Pierrot[12,13], Benjamin Poulter[42,43], Christian Rödenbeck[44], Joe Salisbury[45], Ute Schuster[4], Jörg Schwinger[46], Roland Séférian[17], Ingunn Skjelvan[46], Benjamin D. Stocker[47], Adrienne J. Sutton[39,10], Taro Takahashi[48], Hanqin Tian[49], Bronte Tilbrook[50], Ingrid T. van der Laan-Luijkx[51], Guido R. van der Werf[52], Nicolas Viovy[14], Anthony P. Walker[53], Andrew J. Wiltshire[54], and Sönke Zaehle[44]

[1]Tyndall Centre for Climate Change Research, University of East Anglia, Norwich Research Park, Norwich, NR4 7TJ, UK
[2]Center for International Climate and Environmental Research – Oslo (CICERO), Oslo, Norway
[3]Global Carbon Project, CSIRO Oceans and Atmosphere, GPO Box 3023, Canberra, ACT 2601, Australia
[4]College of Life and Environmental Sciences, University of Exeter, Exeter, EX4 4RJ, UK
[5]Centre for Ocean and Atmospheric Sciences, School of Environmental Sciences, University of East Anglia, Norwich Research Park, Norwich, NR4 7TJ, UK
[6]Carbon Dioxide Information Analysis Center (CDIAC), Oak Ridge National Laboratory, Oak Ridge, TN, USA
[7]National Oceanic & Atmospheric Administration, Earth System Research Laboratory (NOAA/ESRL), Boulder, CO 80305, USA
[8]Woods Hole Research Center (WHRC), Falmouth, MA 02540, USA
[9]University of California, San Diego, Scripps Institution of Oceanography, La Jolla, CA 92093-0244, USA
[10]National Oceanic & Atmospheric Administration/Pacific Marine Environmental Laboratory (NOAA/PMEL), 7600 Sand Point Way NE, Seattle, WA 98115, USA
[11]Karlsruhe Institute of Technology, Institute of Meteorology and Climate Research/Atmospheric Environmental Research, 82467 Garmisch-Partenkirchen, Germany
[12]Cooperative Institute for Marine and Atmospheric Studies, Rosenstiel School for Marine and Atmospheric Science, University of Miami, Miami, FL 33149, USA
[13]National Oceanic & Atmospheric Administration/Atlantic Oceanographic & Meteorological Laboratory (NOAA/AOML), Miami, FL 33149, USA
[14]Laboratoire des Sciences du Climat et de l'Environnement, Institut Pierre-Simon Laplace, CEA-CNRS-UVSQ, CE Orme des Merisiers, 91191 Gif sur Yvette CEDEX, France
[15]Department of Geographical Sciences, University of Maryland, College Park, MD 20742, USA
[16]National Institute of Water and Atmospheric Research (NIWA), Dunedin 9054, New Zealand
[17]Centre National de Recherche Météorologique, Unite mixte de recherche 3589 Météo-France/CNRS, 42 Avenue Gaspard Coriolis, 31100 Toulouse, France
[18]Woods Hole Oceanographic Institution (WHOI), Woods Hole, MA 02543, USA
[19]College of Engineering, Mathematics and Physical Sciences, University of Exeter, Exeter, EX4 4QF, UK
[20]Flanders Marine Institute, InnovOcean, Wandelaarkaai 7, 8400 Ostend, Belgium
[21]Climatic Research Unit, University of East Anglia, Norwich Research Park, Norwich, NR4 7TJ, UK

[22]Alfred Wegener Institute Helmholtz Centre for Polar and Marine Research, Postfach 120161, 27515 Bremerhaven, Germany

[23]CSIRO Oceans and Atmosphere, GPO Box 1700, Canberra, ACT 2601, Australia

[24]PBL Netherlands Environmental Assessment Agency, The Hague/Bilthoven and Utrecht University, Utrecht, the Netherlands

[25]Department of Atmospheric Sciences, University of Illinois, Urbana, IL 61821, USA

[26]Institute of Applied Energy (IAE), Minato-ku, Tokyo 105-0003, Japan

[27]GEOMAR Helmholtz Centre for Ocean Research Kiel, Düsternbrooker Weg 20, 24105 Kiel, Germany

[28]Max Planck Institute for Meteorology, Bundesstr. 53, 20146 Hamburg, Germany

[29]Sorbonne Universités (UPMC, Univ Paris 06), CNRS, IRD, MNHN, LOCEAN/IPSL Laboratory, 75252 Paris, France

[30]CSIRO Oceans and Atmosphere, P.O. Box 1538, Hobart, TAS, Australia

[31]Climate and Environmental Physics, Physics Institute, University of Bern, Bern, Switzerland

[32]Oeschger Centre for Climate Change Research, University of Bern, Bern, Switzerland

[33]National Center for Atmospheric Research, Climate and Global Dynamics, Terrestrial Sciences Section, Boulder, CO 80305, USA

[34]Climate Research Division, Environment and Climate Change Canada, Victoria, Canada

[35]Department of Ocean Sciences, RSMAS/MAC, University of Miami, 4600 Rickenbacker Causeway, Miami, FL 33149, USA

[36]Ocean Systems and Climate, CSIR-CHPC, Cape Town, 7700, South Africa

[37]Department of Atmospheric and Oceanic Sciences and Institute of Arctic and Alpine Research, University of Colorado, Campus Box 450, Boulder, CO 80309-0450, USA

[38]Center for Global Environmental Research, National Institute for Environmental Studies (NIES), 16-2 Onogawa, Tsukuba, Ibaraki 305-8506, Japan

[39]Joint Institute for the Study of the Atmosphere and Ocean, University of Washington, Seattle, WA 98195, USA

[40]Geophysical Institute, University of Bergen and Bjerknes Centre for Climate Research, Allégaten 70, 5007 Bergen, Norway

[41]National Research Institute for Far Sea Fisheries, Japan Fisheries Research and Education Agency 2-12-4 Fukuura, Kanazawa-Ku, Yokohama 236-8648, Japan

[42]NASA Goddard Space Flight Center, Biospheric Science Laboratory, Greenbelt, MD 20771, USA

[43]Department of Ecology, Montana State University, Bozeman, MT 59717, USA

[44]Max Planck Institute for Biogeochemistry, P.O. Box 600164, Hans-Knöll-Str. 10, 07745 Jena, Germany

[45]University of New Hampshire, Ocean Process Analysis Laboratory, 161 Morse Hall, 8 College Road, Durham, NH 03824, USA

[46]Uni Research Climate, Bjerknes Centre for Climate Research, Nygårdsgaten 112, 5008 Bergen, Norway

[47]Imperial College London, Life Science Department, Silwood Park, Ascot, Berkshire, SL5 7PY, UK

[48]Lamont-Doherty Earth Observatory of Columbia University, Palisades, NY 10964, USA

[49]School of Forestry and Wildlife Sciences, Auburn University, 602 Ducan Drive, Auburn, AL 36849, USA

[50]CSIRO Oceans and Atmosphere and Antarctic Climate and Ecosystems Cooperative Research Centre, Hobart, TAS, Australia

[51]Department of Meteorology and Air Quality, Wageningen University & Research, P.O. Box 47, 6700AA Wageningen, the Netherlands

[52]Faculty of Earth and Life Sciences, VU University Amsterdam, Amsterdam, the Netherlands

[53]Environmental Sciences Division & Climate Change Science Institute, Oak Ridge National Laboratory, Oak Ridge, TN, USA

[54]Met Office Hadley Centre, FitzRoy Road, Exeter, EX1 3PB, UK

Correspondence to: Corinne Le Quéré (c.lequere@uea.ac.uk)

Abstract. Accurate assessment of anthropogenic carbon dioxide (CO_2) emissions and their redistribution among the atmosphere, ocean, and terrestrial biosphere – the "global carbon budget" – is important to better understand the global carbon cycle, support the development of climate policies, and project future climate

change. Here we describe data sets and methodology to quantify all major components of the global carbon budget, including their uncertainties, based on the combination of a range of data, algorithms, statistics, and model estimates and their interpretation by a broad scientific community. We discuss changes compared to previous estimates and consistency within and among components, alongside methodology and data limitations. CO_2 emissions from fossil fuels and industry (E_{FF}) are based on energy statistics and cement production data, respectively, while emissions from land-use change (E_{LUC}), mainly deforestation, are based on combined evidence from land-cover change data, fire activity associated with deforestation, and models. The global atmospheric CO_2 concentration is measured directly and its rate of growth (G_{ATM}) is computed from the annual changes in concentration. The mean ocean CO_2 sink (S_{OCEAN}) is based on observations from the 1990s, while the annual anomalies and trends are estimated with ocean models. The variability in S_{OCEAN} is evaluated with data products based on surveys of ocean CO_2 measurements. The global residual terrestrial CO_2 sink (S_{LAND}) is estimated by the difference of the other terms of the global carbon budget and compared to results of independent dynamic global vegetation models. We compare the mean land and ocean fluxes and their variability to estimates from three atmospheric inverse methods for three broad latitude bands. All uncertainties are reported as $\pm 1\sigma$, reflecting the current capacity to characterise the annual estimates of each component of the global carbon budget. For the last decade available (2006–2015), E_{FF} was 9.3 ± 0.5 GtC yr^{-1}, E_{LUC} 1.0 ± 0.5 GtC yr^{-1}, G_{ATM} 4.5 ± 0.1 GtC yr^{-1}, S_{OCEAN} 2.6 ± 0.5 GtC yr^{-1}, and S_{LAND} 3.1 ± 0.9 GtC yr^{-1}. For year 2015 alone, the growth in E_{FF} was approximately zero and emissions remained at 9.9 ± 0.5 GtC yr^{-1}, showing a slowdown in growth of these emissions compared to the average growth of 1.8% yr^{-1} that took place during 2006–2015. Also, for 2015, E_{LUC} was 1.3 ± 0.5 GtC yr^{-1}, G_{ATM} was 6.3 ± 0.2 GtC yr^{-1}, S_{OCEAN} was 3.0 ± 0.5 GtC yr^{-1}, and S_{LAND} was 1.9 ± 0.9 GtC yr^{-1}. G_{ATM} was higher in 2015 compared to the past decade (2006–2015), reflecting a smaller S_{LAND} for that year. The global atmospheric CO_2 concentration reached 399.4 ± 0.1 ppm averaged over 2015. For 2016, preliminary data indicate the continuation of low growth in E_{FF} with $+0.2\%$ (range of -1.0 to $+1.8\%$) based on national emissions projections for China and USA, and projections of gross domestic product corrected for recent changes in the carbon intensity of the economy for the rest of the world. In spite of the low growth of E_{FF} in 2016, the growth rate in atmospheric CO_2 concentration is expected to be relatively high because of the persistence of the smaller residual terrestrial sink (S_{LAND}) in response to El Niño conditions of 2015–2016. From this projection of E_{FF} and assumed constant E_{LUC} for 2016, cumulative emissions of CO_2 will reach 565 ± 55 GtC (2075 ± 205 GtCO$_2$) for 1870–2016, about 75% from E_{FF} and 25% from E_{LUC}. This living data update documents changes in the methods and data sets used in this new carbon budget compared with previous publications of this data set (Le Quéré et al., 2015b, a, 2014, 2013). All observations presented here can be downloaded from the Carbon Dioxide Information Analysis Center (doi:10.3334/CDIAC/GCP_2016).

1 Introduction

The concentration of carbon dioxide (CO_2) in the atmosphere has increased from approximately 277 parts per million (ppm) in 1750 (Joos and Spahni, 2008), the beginning of the industrial era, to 399.4 ± 0.1 ppm in 2015 (Dlugokencky and Tans, 2016). The Mauna Loa station, which holds the longest running record of direct measurements of atmospheric CO_2 concentration (Tans and Keeling, 2014), went above 400 ppm for the first time in May 2013 (Scripps, 2013). The global monthly average concentration was above 400 ppm in March through May 2015 and again since November 2015 (Dlugokencky and Tans, 2016; Fig. 1). The atmospheric CO_2 increase above pre-industrial levels was, initially, primarily caused by the release of carbon to the atmosphere from deforestation and other land-use-change activities (Ciais et al., 2013). While emissions from fossil fuels started before the industrial era, they only became the dominant source of anthropogenic emissions to the atmosphere from around 1920, and their relative share has continued to increase until present. Anthropogenic emissions occur on top of an active natural carbon cycle that circulates carbon between the reservoirs of the atmosphere, ocean, and terrestrial biosphere on timescales from sub-daily to millennia, while exchanges with geologic reservoirs occur at longer timescales (Archer et al., 2009).

The global carbon budget presented here refers to the mean, variations, and trends in the perturbation of CO_2 in the atmosphere, referenced to the beginning of the industrial era. It quantifies the input of CO_2 to the atmosphere by emissions from human activities, the growth rate of atmospheric CO_2 concentration, and the resulting changes in the storage of carbon in the land and ocean reservoirs in response to increasing atmospheric CO_2 levels, climate change and variability, and other anthropogenic and natural changes (Fig. 2). An understanding of this perturbation budget over time and the underlying variability and trends of the natural carbon cycle is necessary to understand the response of natural sinks
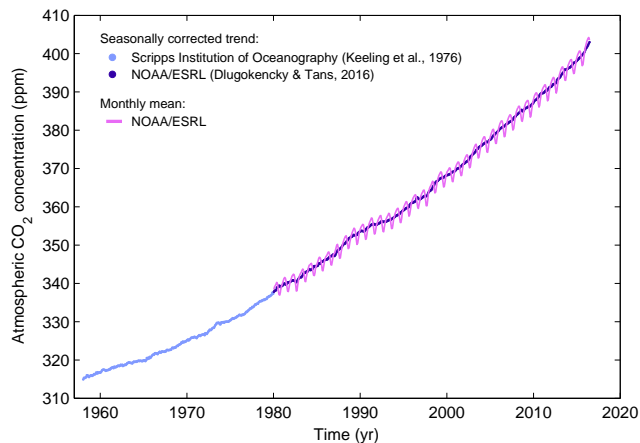
Figure 1. Surface average atmospheric CO_2 concentration, deseasonalised (ppm). The 1980–2016 monthly data are from NOAA/ESRL (Dlugokencky and Tans, 2016) and are based on an average of direct atmospheric CO_2 measurements from multiple stations in the marine boundary layer (Masarie and Tans, 1995). The 1958–1979 monthly data are from the Scripps Institution of Oceanography, based on an average of direct atmospheric CO_2 measurements from the Mauna Loa and South Pole stations (Keeling et al., 1976). To take into account the difference of mean CO_2 between the NOAA/ESRL and the Scripps station networks used here, the Scripps surface average (from two stations) was harmonised to match the NOAA/ESRL surface average (from multiple stations) by adding the mean difference of 0.542 ppm, calculated here from overlapping data during 1980–2012. The mean seasonal cycle is also shown from 1980 (in pink).

to changes in climate, CO_2, and land-use-change drivers, and the permissible emissions for a given climate stabilisation target.

The components of the CO_2 budget that are reported annually in this paper include separate estimates for the CO_2 emissions from (1) fossil fuel combustion and oxidation and cement production (E_{FF}; GtC yr^{-1}) and (2) the emissions resulting from deliberate human activities on land leading to land-use change (E_{LUC}; GtC yr^{-1}), as well as their partitioning among (3) the growth rate of atmospheric CO_2 concentration (G_{ATM}; GtC yr^{-1}), and the uptake of CO_2 by the "CO_2 sinks" in (4) the ocean (S_{OCEAN}; GtC yr^{-1}) and (5) on land (S_{LAND}; GtC yr^{-1}). The CO_2 sinks as defined here include the response of the land and ocean to elevated CO_2 and changes in climate and other environmental conditions. The global emissions and their partitioning among the atmosphere, ocean, and land are in balance:

$$E_{FF} + E_{LUC} = G_{ATM} + S_{OCEAN} + S_{LAND}. \quad (1)$$

G_{ATM} is usually reported in ppm yr^{-1}, which we convert to units of carbon mass per year, GtC yr^{-1}, using 1 ppm = 2.12 GtC (Ballantyne et al., 2012; Prather et al., 2012; Table 1). We also include a quantification of E_{FF} by
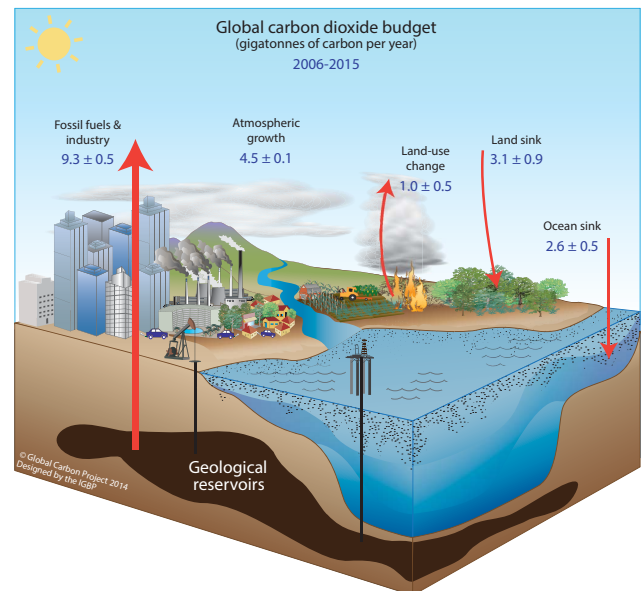

Figure 2. Schematic representation of the overall perturbation of the global carbon cycle caused by anthropogenic activities, averaged globally for the decade 2006–2015. The arrows represent emission from fossil fuels and industry (E_{FF}), emissions from deforestation and other land-use change (E_{LUC}), the growth rate in atmospheric CO_2 concentration (G_{ATM}), and the uptake of carbon by the "sinks" in the ocean (S_{OCEAN}) and land (S_{LAND}) reservoirs. All fluxes are in units of GtC yr^{-1}, with uncertainties reported as $\pm 1\sigma$ (68 % confidence that the real value lies within the given interval) as described in the text. This figure is an update of one prepared by the International Geosphere-Biosphere Programme for the Global Carbon Project (GCP), first presented in Le Quéré (2009).

country, computed with both territorial and consumption-based accounting (see Sect. 2).

Equation (1) partly omits two kinds of processes. The first is the net input of CO_2 to the atmosphere from the chemical oxidation of reactive carbon-containing gases from sources other than the combustion of fossil fuels (e.g. fugitive anthropogenic CH_4 emissions, industrial processes, and biogenic emissions from changes in vegetation, fires, wetlands), primarily methane (CH_4), carbon monoxide (CO), and volatile organic compounds such as isoprene and terpene (Gonzalez-Gaya et al., 2016). CO emissions are currently implicit in E_{FF}, while fugitive anthropogenic CH_4 emissions are not and thus their inclusion would result in a small increase in E_{FF}. The second is the anthropogenic perturbation to carbon cycling in terrestrial freshwaters, estuaries, and coastal areas, which modifies lateral fluxes from land ecosystems to the open ocean; the evasion of CO_2 flux from rivers, lakes, and estuaries to the atmosphere; and the net air–sea anthropogenic CO_2 flux of coastal areas (Regnier et al., 2013). The inclusion of freshwater fluxes of anthropogenic CO_2 would affect the estimates of, and partitioning between, S_{LAND} and S_{OCEAN} in Eq. (1) in complementary ways, but it would not

Table 1. Factors used to convert carbon in various units (by convention, unit 1 = unit 2 · conversion).

Unit 1	Unit 2	Conversion	Source
GtC (gigatonnes of carbon)	ppm (parts per million)[a]	2.12[b]	Ballantyne et al. (2012)
GtC (gigatonnes of carbon)	PgC (petagrams of carbon)	1	SI unit conversion
GtCO$_2$ (gigatonnes of carbon dioxide)	GtC (gigatonnes of carbon)	3.664	44.01/12.011 in mass equivalent
GtC (gigatonnes of carbon)	MtC (megatonnes of carbon)	1000	SI unit conversion

[a] Measurements of atmospheric CO_2 concentration have units of dry-air mole fraction. "ppm" is an abbreviation for micromole per mole of dry air. [b] The use of a factor of 2.12 assumes that all the atmosphere is well mixed within one year. In reality, only the troposphere is well mixed and the growth rate of CO_2 concentration in the less well-mixed stratosphere is not measured by sites from the NOAA network. Using a factor of 2.12 makes the approximation that the growth rate of CO_2 concentration in the stratosphere equals that of the troposphere on a yearly basis.

affect the other terms. These flows are omitted in the absence of annual information on the natural vs. anthropogenic perturbation terms of these loops of the carbon cycle, and they are discussed in Sect. 2.7.

The CO_2 budget has been assessed by the Intergovernmental Panel on Climate Change (IPCC) in all assessment reports (Ciais et al., 2013; Denman et al., 2007; Prentice et al., 2001; Schimel et al., 1995; Watson et al., 1990), as well as by others (e.g. Ballantyne et al., 2012). These assessments included budget estimates for the decades of the 1980s and 1990s (Denman et al., 2007) and, most recently, the period 2002–2011 (Ciais et al., 2013). The IPCC methodology has been adapted and used by the Global Carbon Project (GCP, http://www.globalcarbonproject.org), which has coordinated a cooperative community effort for the annual publication of global carbon budgets up to year 2005 (Raupach et al., 2007; including fossil emissions only), year 2006 (Canadell et al., 2007), year 2007 (published online; GCP, 2007), year 2008 (Le Quéré et al., 2009), year 2009 (Friedlingstein et al., 2010), year 2010 (Peters et al., 2012b), year 2012 (Le Quéré et al., 2013; Peters et al., 2013), year 2013 (Le Quéré et al., 2014), year 2014 (Friedlingstein et al., 2014; Le Quéré et al., 2015b), and most recently year 2015 (Jackson et al., 2016; Le Quéré et al., 2015a). Each of these papers updated previous estimates with the latest available information for the entire time series. From 2008, these publications projected fossil fuel emissions for one additional year.

We adopt a range of ±1 standard deviation (σ) to report the uncertainties in our estimates, representing a likelihood of 68 % that the true value will be within the provided range if the errors have a Gaussian distribution. This choice reflects the difficulty of characterising the uncertainty in the CO_2 fluxes between the atmosphere and the ocean and land reservoirs individually, particularly on an annual basis, as well as the difficulty of updating the CO_2 emissions from land-use change. A likelihood of 68 % provides an indication of our current capability to quantify each term and its uncertainty given the available information. For comparison, the Fifth Assessment Report of the IPCC (AR5) generally reported a likelihood of 90 % for large data sets whose uncertainty is well characterised, or for long time intervals less affected by year-to-year variability. Our 68 % uncertainty value is near

the 66 % which the IPCC characterises as "likely" for values falling into the ±1σ interval. The uncertainties reported here combine statistical analysis of the underlying data and expert judgement of the likelihood of results lying outside this range. The limitations of current information are discussed in the paper and have been examined in detail elsewhere (Ballantyne et al., 2015).

All quantities are presented in units of gigatonnes of carbon (GtC, 10^{15} gC), which is the same as petagrams of carbon (PgC; Table 1). Units of gigatonnes of CO_2 (or billion tonnes of CO_2) used in policy are equal to 3.664 multiplied by the value in units of GtC.

This paper provides a detailed description of the data sets and methodology used to compute the global carbon budget estimates for the period pre-industrial (1750) to 2015 and in more detail for the period 1959 to 2015. We also provide decadal averages starting in 1960 including the last decade (2006–2015), results for the year 2015, and a projection for year 2016. Finally, we provide cumulative emissions from fossil fuels and land-use change since year 1750, the pre-industrial period, and since year 1870, the reference year for the cumulative carbon estimate used by the IPCC (AR5) based on the availability of global temperature data (Stocker et al., 2013). This paper will be updated every year using the format of "living data" to keep a record of budget versions and the changes in new data, revision of data, and changes in methodology that lead to changes in estimates of the carbon budget. Additional materials associated with the release of each new version will be posted at the Global Carbon Project (GCP) website (http://www.globalcarbonproject.org/carbonbudget), with fossil fuel emissions also available through the Global Carbon Atlas (http://www.globalcarbonatlas.org). With this approach, we aim to provide the highest transparency and traceability in the reporting of CO_2, the key driver of climate change.

2 Methods

Multiple organisations and research groups around the world generated the original measurements and data used to complete the global carbon budget. The effort presented here is

Table 2. How to cite the individual components of the global carbon budget presented here.

Component	Primary reference
Global emissions from fossil fuels and industry (E_{FF}), total and by fuel type	Boden and Andres (2016; CDIAC; http://cdiac.ornl.gov/trends/emis/meth_reg.html)
National territorial emissions from fossil fuels and industry (E_{FF})	CDIAC source: Boden and Andres (2016; as above) UNFCCC source: (2016; http://unfccc.int/national_reports/annex_i_ghg_inventories/national_inventories_submissions/items/8108.php; last access: June 2016)
National consumption-based emissions from fossil fuels and industry (E_{FF}) by country (consumption)	Peters et al. (2011b) updated as described in this paper
Land-use-change emissions (E_{LUC})	Houghton et al. (2012) combined with Giglio et al. (2013)
Growth rate in atmospheric CO_2 concentration (G_{ATM})	Dlugokencky and Tans (2016; NOAA/ESRL: http://www.esrl.noaa.gov/gmd/ccgg/trends/global.html; last access: July 2016)
Ocean and land CO_2 sinks (S_{OCEAN} and S_{LAND})	This paper for S_{OCEAN} and S_{LAND} and references in Table 6 for individual models

thus mainly one of synthesis, where results from individual groups are collated, analysed, and evaluated for consistency. We facilitate access to original data with the understanding that primary data sets will be referenced in future work (see Table 2 for how to cite the data sets). Descriptions of the measurements, models, and methodologies follow below and in-depth descriptions of each component are described elsewhere.

This is the 11th version of the global carbon budget and the fifth revised version in the format of a living data update. It builds on the latest published global carbon budget of Le Quéré et al. (2015a). The main changes are (1) the inclusion of data to year 2015 (inclusive) and a projection for fossil fuel emissions for year 2016; (2) the introduction of a projection for the full carbon budget for year 2016 using our fossil fuel projection, combined with preliminary data (Dlugokencky and Tans, 2016) and analysis by others (Betts et al., 2016) of the growth rate in atmospheric CO_2 concentration; and (3) the use of BP data from 1990 (BP, 2016b) to estimate emissions in China to ensure all recent revisions in Chinese statistics are incorporated. The main methodological differences between annual carbon budgets are summarised in Table 3.

2.1 CO_2 emissions from fossil fuels and industry (E_{FF})

2.1.1 Emissions from fossil fuels and industry and their uncertainty

The calculation of global and national CO_2 emissions from fossil fuels, including gas flaring and cement production (E_{FF}), relies primarily on energy consumption data, specifically data on hydrocarbon fuels, collated and archived by

several organisations (Andres et al., 2012). These include the Carbon Dioxide Information Analysis Center (CDIAC), the International Energy Agency (IEA), the United Nations (UN), the United States Department of Energy (DoE) Energy Information Administration (EIA), and more recently also the Planbureau voor de Leefomgeving (PBL) Netherlands Environmental Assessment Agency. Where available, we use national emissions estimated by the countries themselves and reported to the UNFCCC for the period 1990–2014 (40 countries). We assume that national emissions reported to the UNFCCC are the most accurate because national experts have access to additional and country-specific information, and because these emission estimates are periodically audited for each country through an established international methodology overseen by the UNFCCC. We also use global and national emissions estimated by CDIAC (Boden and Andres, 2016). The CDIAC emission estimates are the only data set that extends back in time to 1751 with consistent and well-documented emissions from fossil fuels, cement production, and gas flaring for all countries and their uncertainty (Andres et al., 2014, 2012, 1999); this makes the data set a unique resource for research of the carbon cycle during the fossil fuel era.

The global emissions presented here are based on CDIAC's analysis, which provides an internally consistent global estimate including bunker fuels, minimising the effects of lower-quality energy trade data. Thus, the comparison of global emissions with previous annual carbon budgets is not influenced by the use of national data from UNFCCC reports.

During the period 1959–2013, the emissions from fossil fuels estimated by CDIAC are based primarily on energy data provided by the UN Statistics Division (UN, 2015a, b; Ta-

Table 3. Main methodological changes in the global carbon budget since first publication. Unless specified below, the methodology was identical to that described in the current paper. Furthermore, methodological changes introduced in one year are kept for the following years unless noted. Empty cells mean there were no methodological changes introduced that year.

Publication year[a]	Fossil fuel emissions			LUC emissions	Reservoirs			Uncertainty and other changes
	Global	Country (territorial)	Country (consumption)		Atmosphere	Ocean	Land	
2006 Raupach et al. (2007)	Split into regions							
2007 Canadell et al. (2007)				E_{LUC} based on FAO-FRA 2005; constant E_{LUC} for 2006	1959–1979 data from Mauna Loa; data after 1980 from global average	Based on one ocean model tuned to reproduced observed 1990s sink		±1σ provided for all components
2008 (online)				Constant E_{LUC} for 2007				
2009 Le Quéré et al. (2009)		Split between Annex B and non-Annex B	Results from an independent study discussed	Fire-based emission anomalies used for 2006–2008		Based on four ocean models normalised to observations with constant delta	First use of five DGVMs to compare with budget residual	
2010 Friedlingstein et al. (2010)	Projection for current year based on GDP	Emissions for top emitters		E_{LUC} updated with FAO-FRA 2010				
2011 Peters et al. (2012b)			Split between Annex B and non-Annex B					
2012 Le Quéré et al. (2013) Peters et al. (2013)		129 countries from 1959	129 countries and regions from 1990 to 2010 based on GTAP8.0	E_{LUC} for 1997–2011 includes interannual anomalies from fire-based emissions	All years from global average	Based on five ocean models normalised to observations with ratio	Ten DGVMs available for S_{LAND}; first use of four models to compare with E_{LUC}	
2013 Le Quéré et al. (2014)		250 countries[b]	134 countries and regions 1990–2011 based on GTAP8.1, with detailed estimates for years 1997, 2001, 2004, and 2007	E_{LUC} for 2012 estimated from 2001–2010 average		Based on six models compared with two data products to year 2011	Coordinated DGVM experiments for S_{LAND} and E_{LUC}	Confidence levels; cumulative emissions; budget from 1750
2014 Le Quéré et al. (2015b)	Three years of BP data		Extended to 2012 with updated GDP data	E_{LUC} for 1997–2013 includes interannual anomalies from fire-based emissions		Based on seven models compared with three data products to year 2013	Based on 10 models	Inclusion of breakdown of the sinks in three latitude bands and comparison with three atmospheric inversions
2015 Le Quéré et al. (2015a) Jackson et al. (2016)	Projection for current year based on Jan–Aug data	National emissions from UNFCCC extended to 2014 also provided (along with CDIAC)	Detailed estimates introduced for 2011 based on GTAP9			Based on eight models compared with two data products	Based on 10 models with assessment of minimum realism	The decadal uncertainty for the DGVM ensemble mean now uses ±1σ of the decadal spread across models
2016 (this study)	Two years of BP data; CHN emissions from 1990 from BP data	Added three small countries; CHN emissions from 1990 from BP data		Preliminary E_{LUC} using FRA-2015 shown for comparison; use of five DGVMs		Based on seven models compared with two data products	Based on 14 models	Discussion of projection for full budget for current year

[a] The naming convention of the budgets has changed. Up to and including 2010, the budget year (Carbon Budget 2010) represented the latest year of the data. From 2012, the budget year (Carbon Budget 2012) refers to the initial publication year. [b] The CDIAC database has about 250 countries, but we show data for 219 countries since we aggregate and disaggregate some countries to be consistent with current country definitions (see Sect. 2.1.1 for more details).

Table 4. Data sources used to compute each component of the global carbon budget.

Component	Process	Data source	Data reference
E_{FF} (global and CDIAC national)	Fossil fuel combustion and gas flaring	UN Statistics Division to 2013	UN (2015a, b)
		BP for 2014–2015	BP (BP, 2016b)
	Cement production	US Geological Survey	USGS (2016a, b)
E_{LUC}	Land-cover change (deforestation, afforestation, and forest regrowth)	Forest Resource Assessment (FRA) of the Food and Agriculture Organization (FAO)	FAO (2010)
	Wood harvest Shifting agriculture	FAO Statistics Division FAO FRA and Statistics Division	FAOSTAT (2010) FAO (2010) FAOSTAT (2010)
	Interannual variability from peat fires and climate–land management interactions (1997–2013)	Global Fire Emissions Database (GFED4)	Giglio et al. (2013)
G_{ATM}	Change in atmospheric CO_2 concentration	1959–1980: CO_2 Program at Scripps Institution of Oceanography and other research groups	Keeling et al. (1976)
		1980–2015: US National Oceanic and Atmospheric Administration Earth System Research Laboratory	Dlugokencky and Tans (2016) Ballantyne et al. (2012)
S_{OCEAN}	Uptake of anthropogenic CO_2	1990–1999 average: indirect estimates based on CFCs, atmospheric O_2, and other tracer observations	Manning and Keeling (2006) McNeil et al. (2003) Mikaloff Fletcher et al. (2006) as assessed by the IPCC in Denman et al. (2007)
	Impact of increasing atmospheric CO_2, climate, and variability	Ocean models	Table 6
S_{LAND}	Response of land vegetation to increasing atmospheric CO_2 concentration, climate and variability, and other environmental changes	Budget residual	

ble 4). When necessary, fuel masses/volumes are converted to fuel energy content using coefficients provided by the UN and then to CO_2 emissions using conversion factors that take into account the relationship between carbon content and energy (heat) content of the different fuel types (coal, oil, gas, gas flaring) and the combustion efficiency (to account, for example, for soot left in the combustor or fuel otherwise lost or discharged without oxidation). Most data on energy consumption and fuel quality (carbon content and heat content) are available at the country level (UN, 2015a). In general, CO_2 emissions for equivalent primary energy consumption are about 30 % higher for coal compared to oil, and 70 % higher for coal compared to natural gas (Marland et al., 2007).

Recent revisions in energy data for China (Korsbakken et al., 2016) have not yet fully propagated to the UN energy statistics used by CDIAC but are available through the BP energy statistics (BP, 2016b). We thus use the BP energy statistics (BP, 2016b) and estimate the emissions by fuel type using the BP methodology (BP, 2016a) to be consistent with the format of the CDIAC data. Emissions in China calculated from the BP statistics differ from those provided by CDIAC emissions mostly between 1997 and 2009. The revised emissions are higher by 5 % on average between 1990 and 2015 for a total additional emissions of 2.0 GtC during that period (41.3 GtC using the BP statistics and methodology compared to 39.3 provided by CDIAC). The two estimates converge to similar values from 2011 onwards (< 2 % differ-

ence). We propagate these new estimates for China through to the global total to ensure consistency.

Our emission totals for the UNFCCC-reporting countries were recorded as in the UNFCCC submissions, which have a slightly larger system boundary than CDIAC. Additional emissions come from carbonates other than in cement manufacture, and thus UNFCCC totals will be slightly higher than CDIAC totals in general, although there are multiple sources of differences. We use the CDIAC method to report emissions by fuel type (e.g. all coal oxidation is reported under "coal", regardless of whether oxidation results from combustion as an energy source), which differs slightly from UNFCCC.

For the most recent 1–2 years when the UNFCCC estimates (1 year) and UN statistics (2 years) used by CDIAC are not yet available, we generated preliminary estimates based on the BP annual energy review by applying the growth rates of energy consumption (coal, oil, gas) for 2015 to the national and global emissions from the UN national data in 2014, and for 2014 and 2015 to the CDIAC national and global emissions in 2013. BP's sources for energy statistics overlap with those of the UN data but are compiled more rapidly from about 70 countries covering about 96 % of global emissions. We use the BP values only for the year-to-year rate of change, because the rates of change are less uncertain than the absolute values and to avoid discontinuities in the time series when linking the UN-based data with the BP data. These preliminary estimates are replaced by the more complete UNFCCC or CDIAC data based on UN statistics when they become available. Past experience and work by others (Andres et al., 2014; Myhre et al., 2009) show that projections based on the BP rate of change are within the uncertainty provided (see Sect. 3.2 and Supplement from Peters et al., 2013).

Estimates of emissions from cement production by CDIAC are based on data on growth rates of cement production from the US Geological Survey up to year 2013 (USGS, 2016a). For 2014 and 2015 we use estimates of cement production made by the USGS for the top 18 countries (representing 85 % of global production; USGS, 2016b), while for all other countries we use the 2013 values (zero growth). Some fraction of the CaO and MgO in cement is returned to the carbonate form during cement weathering, but this is neglected here.

Estimates of emissions from gas flaring by CDIAC are calculated in a similar manner to those from solid, liquid, and gaseous fuels and rely on the UN energy statistics to supply the amount of flared or vented fuel. For the most recent 1–2 emission years, flaring is assumed constant from the most recent available year of data (2014 for countries that report to the UNFCCC, and 2013 for the remainder). The basic data on gas flaring report atmospheric losses during petroleum production and processing that have large uncertainty and do not distinguish between gas that is flared as CO_2 or vented as CH_4. Fugitive emissions of CH_4 from the so-called upstream

sector (e.g. coal mining and natural gas distribution) are not included in the accounts of CO_2 emissions except to the extent that they are captured in the UN energy data and counted as gas "flared or lost".

The published CDIAC data set includes 255 countries and regions. This list includes countries that no longer exist, such as the USSR and East Pakistan. For the carbon budget, we reduce the list to 219 countries by reallocating emissions to the currently defined territories. This involved both aggregation and disaggregation, and does not change global emissions. Examples of aggregation include merging East and West Germany to the currently defined Germany. Examples of disaggregation include reallocating the emissions from the former USSR to the resulting independent countries. For disaggregation, we use the emission shares when the current territories first appeared. The disaggregated estimates should be treated with care when examining countries' emissions trends prior to their disaggregation. For the most recent years, 2014 and 2015, the BP statistics are more aggregated, but we retain the detail of CDIAC by applying the growth rates of each aggregated region in the BP data set to its constituent individual countries in CDIAC.

Estimates of CO_2 emissions show that the global total of emissions is not equal to the sum of emissions from all countries. This is largely attributable to emissions that occur in international territory, in particular the combustion of fuels used in international shipping and aviation (bunker fuels), where the emissions are included in the global totals but are not attributed to individual countries. In practice, the emissions from international bunker fuels are calculated based on where the fuels were loaded, but they are not included with national emissions estimates. Other differences occur because globally the sum of imports in all countries is not equal to the sum of exports and because of inconsistent national reporting, differing treatment of oxidation of non-fuel uses of hydrocarbons (e.g. as solvents, lubricants, feedstocks), and changes in stock (Andres et al., 2012).

The uncertainty in the annual emissions from fossil fuels and industry for the globe has been estimated at ±5 % (scaled down from the published ±10 % at ±2σ to the use of ±1σ bounds reported here; Andres et al., 2012). This is consistent with a more detailed recent analysis of uncertainty of ±8.4 % at ±2σ (Andres et al., 2014) and at the high end of the range of ±5–10 % at ±2σ reported by Ballantyne et al. (2015). This includes an assessment of uncertainties in the amounts of fuel consumed, the carbon and heat contents of fuels, and the combustion efficiency. While we consider a fixed uncertainty of ±5 % for all years, in reality the uncertainty, as a percentage of the emissions, is growing with time because of the larger share of global emissions from non-Annex B countries (emerging economies and developing countries) with less precise statistical systems (Marland et al., 2009). For example, the uncertainty in Chinese emissions has been estimated at around ±10 % (for ±1σ; Gregg et al., 2008), and important potential biases have been iden-

tified suggesting China's emissions could be overestimated in published studies (Liu et al., 2015). Generally, emissions from mature economies with good statistical bases have an uncertainty of only a few percent (Marland, 2008). Further research is needed before we can quantify the time evolution of the uncertainty, as well as its temporal error correlation structure. We note that even if they are presented as 1σ estimates, uncertainties in emissions are likely to be mainly country-specific systematic errors related to underlying biases of energy statistics and to the accounting method used by each country. We assign a medium confidence to the results presented here because they are based on indirect estimates of emissions using energy data (Durant et al., 2011). There is only limited and indirect evidence for emissions, although there is a high agreement among the available estimates within the given uncertainty (Andres et al., 2014, 2012), and emission estimates are consistent with a range of other observations (Ciais et al., 2013), even though their regional and national partitioning is more uncertain (Francey et al., 2013).

2.1.2 Emissions embodied in goods and services

National emission inventories take a territorial (production) perspective and "include greenhouse gas emissions and removals taking place within national territory and offshore areas over which the country has jurisdiction" (Rypdal et al., 2006). That is, emissions are allocated to the country where and when the emissions actually occur. The territorial emission inventory of an individual country does not include the emissions from the production of goods and services produced in other countries (e.g. food and clothes) that are used for consumption. Consumption-based emission inventories for an individual country are another attribution point of view that allocates global emissions to products that are consumed within a country; these inventories are conceptually calculated as the territorial emissions minus the "embedded" territorial emissions to produce exported products plus the emissions in other countries to produce imported products (consumption = territorial − exports + imports). The difference between the territorial- and consumption-based emission inventories is the net transfer (exports minus imports) of emissions from the production of internationally traded products. Consumption-based emission attribution results (e.g. Davis and Caldeira, 2010) provide additional information to territorial-based emissions that can be used to understand emission drivers (Hertwich and Peters, 2009), quantify emission transfers by the trade of products between countries (Peters et al., 2011b), and potentially design more effective and efficient climate policy (Peters and Hertwich, 2008).

We estimate consumption-based emissions from 1990 to 2014 by enumerating the global supply chain using a global model of the economic relationships between economic sectors within and between every country (Andrew and Peters, 2013; Peters et al., 2011a). Our analysis is based on the eco-

nomic and trade data from the Global Trade and Analysis Project (GTAP; Narayanan et al., 2015), and we make detailed estimates for the years 1997 (GTAP version 5), 2001 (GTAP6), and 2004, 2007, and 2011 (GTAP9.1) (using the methodology of Peters et al., 2011b). The results cover 57 sectors and up to 141 countries and regions. The detailed results are then extended into an annual time series from 1990 to the latest year of the GDP data (2014 in this budget), using GDP data by expenditure in current exchange rate of US dollars (USD; from the UN National Accounts Main Aggregates Database; UN, 2015c) and time series of trade data from GTAP (based on the methodology in Peters et al., 2011b).

We estimate the sector-level CO_2 emissions using our own calculations based on the GTAP data and methodology, include flaring and cement emissions from CDIAC, and then scale the national totals (excluding bunker fuels) to match the CDIAC estimates from the most recent carbon budget. We do not include international transportation in our estimates of national totals, but include them in the global total. The time series of trade data provided by GTAP covers the period 1995–2013 and our methodology uses the trade shares as this data set. For the period 1990–1994 we assume the trade shares of 1995, while for 2014 we assume the trade shares of 2013.

Comprehensive analysis of the uncertainty in consumption emissions accounts is still lacking in the literature, although several analyses of components of this uncertainty have been made (e.g. Dietzenbacher et al., 2012; Inomata and Owen, 2014; Karstensen et al., 2015; Moran and Wood, 2014). For this reason we do not provide an uncertainty estimate for these emissions, but based on model comparisons and sensitivity analysis, they are unlikely to be larger than for the territorial emission estimates (Peters et al., 2012a). Uncertainty is expected to increase for more detailed results, and to decrease with aggregation (Peters et al., 2011b; e.g. the results for Annex B countries will be more accurate than the sector results for an individual country).

The consumption-based emissions attribution method considers the CO_2 emitted to the atmosphere in the production of products, but not the trade in fossil fuels (coal, oil, gas). It is also possible to account for the carbon trade in fossil fuels (Andrew et al., 2013), but we do not present those data here. Peters et al. (2012a) additionally considered trade in biomass.

The consumption data do not modify the global average terms in Eq. (1) but are relevant to the anthropogenic carbon cycle as they reflect the trade-driven movement of emissions across the Earth's surface in response to human activities. Furthermore, if national and international climate policies continue to develop in an un-harmonised way, then the trends reflected in these data will need to be accommodated by those developing policies.

2.1.3 Growth rate in emissions

We report the annual growth rate in emissions for adjacent years (in percent per year) by calculating the difference between the two years and then comparing to the emissions in the first year: $\left[\frac{E_{FF(t_{0+1})} - E_{FF(t_0)}}{E_{FF(t_0)}}\right] \times 100\,\% \,\mathrm{yr}^{-1}$. This is the simplest method to characterise a 1-year growth compared to the previous year and is widely used. We apply a leap-year adjustment to ensure valid interpretations of annual growth rates. This affects the growth rate by about $0.3\,\%\,\mathrm{yr}^{-1}$ $(1/365)$ and causes growth rates to go up approximately $0.3\,\%$ if the first year is a leap year and down $0.3\,\%$ if the second year is a leap year.

The relative growth rate of E_{FF} over time periods of greater than 1 year can be re-written using its logarithm equivalent as follows:

$$\frac{1}{E_{FF}} \frac{dE_{FF}}{dt} = \frac{d(\ln E_{FF})}{dt}. \qquad (2)$$

Here we calculate relative growth rates in emissions for multi-year periods (e.g. a decade) by fitting a linear trend to $\ln(E_{FF})$ in Eq. (2), reported in percent per year. We fit the logarithm of E_{FF} rather than E_{FF} directly because this method ensures that computed growth rates satisfy Eq. (6). This method differs from previous papers (Canadell et al., 2007; Le Quéré et al., 2009; Raupach et al., 2007) that computed the fit to E_{FF} and divided by average E_{FF} directly, but the difference is very small ($< 0.05\,\%\,\mathrm{yr}^{-1}$) in the case of E_{FF}.

2.1.4 Emissions projections

Energy statistics from BP are normally available around June for the previous year. To gain insight on emission trends for the current year (2016), we provide an assessment of global emissions for E_{FF} by combining individual assessments of emissions for China and the USA (the two biggest emitting countries) and the rest of the world.

We specifically estimate emissions in China because the data indicate a significant departure from the long-term trends in the carbon intensity of the economy used in emissions projections in previous global carbon budgets (e.g. Le Quéré et al., 2015a), resulting from a rapid deceleration in emissions growth against continued growth in economic output. This departure could be temporary (Jackson et al., 2016). Our 2016 estimate for China uses (1) coal consumption estimates from the China Coal Industry Association for January through September (CCIA, 2016), (2) estimated consumption of natural gas (IEW, 2016; NDRC, 2016a) and domestic production plus net imports of petroleum (NDRC, 2016b) for January through July from the National Development and Reform Commission, and (3) production of cement reported for January to September (NBS, 2016). Using these data, we estimate the change in emissions for the corresponding

months in 2016 compared to 2015 assuming a 2 % increase in the energy (and thus carbon) content of coal for 2016 resulting from improvements in the quality of the coal used, in line with the trends reported by the National Bureau of Statistics for recent years. We then assume that the relative changes during the first months will persist throughout the year. The main sources of uncertainty are from the incomplete data on stock changes, the carbon content of coal, and the assumption of persistent behaviour for the rest of the year. These are discussed further in Sect. 3.2.1.

For the USA, we use the forecast of the US Energy Information Administration (EIA) for emissions from fossil fuels (EIA, 2016). This is based on an energy forecasting model which is revised monthly, and takes into account heating degree days, household expenditures by fuel type, energy markets, policies, and other effects. We combine this with our estimate of emissions from cement production using the monthly US cement data from USGS for January–July, assuming changes in cement production over the first seven months apply throughout the year. While the EIA's forecasts for current full-year emissions have on average been revised downwards, only seven such forecasts are available, so we conservatively use the full range of adjustments following revision, and additionally assume symmetrical uncertainty to give $\pm 2.3\,\%$ around the central forecast.

For the rest of the world, we use the close relationship between the growth in GDP and the growth in emissions (Raupach et al., 2007) to project emissions for the current year. This is based on the so-called Kaya identity (also called IPAT identity, the acronym standing for human impact (I) on the environment, which is equal to the product of population (P), affluence (A), and technology (T)), whereby E_{FF} (GtC yr^{-1}) is decomposed by the product of GDP (USD yr^{-1}) and the fossil fuel carbon intensity of the economy (I_{FF}; GtC USD^{-1}) as follows:

$$E_{FF} = GDP \times I_{FF}. \qquad (3)$$

Such product-rule decomposition identities imply that the relative growth rates of the multiplied quantities are additive. Taking a time derivative of Eq. (3) gives

$$\frac{dE_{FF}}{dt} = \frac{d(GDP \times I_{FF})}{dt} \qquad (4)$$

and, applying the rules of calculus,

$$\frac{dE_{FF}}{dt} = \frac{dGDP}{dt} \times I_{FF} + GDP \times \frac{dI_{FF}}{dt}. \qquad (5)$$

Finally, dividing Eq. (5) by Eq. (3) gives

$$\frac{1}{E_{FF}} \frac{dE_{FF}}{dt} = \frac{1}{GDP} \frac{dGDP}{dt} + \frac{1}{I_{FF}} \frac{dI_{FF}}{dt}, \qquad (6)$$

where the left-hand term is the relative growth rate of E_{FF}, and the right-hand terms are the relative growth rates of GDP

and I_{FF}, respectively, which can simply be added linearly to give overall growth rate. The growth rates are reported in percent by multiplying each term by 100. As preliminary estimates of annual change in GDP are made well before the end of a calendar year, making assumptions on the growth rate of I_{FF} allows us to make projections of the annual change in CO_2 emissions well before the end of a calendar year. The I_{FF} is based on GDP in constant PPP (purchasing power parity) from the IEA up to 2013 (IEA/OECD, 2015) and extended using the IMF growth rates for 2014 and 2015 (IMF, 2016). Interannual variability in I_{FF} is the largest source of uncertainty in the GDP-based emissions projections. We thus use the standard deviation of the annual I_{FF} for the period 2006–2015 as a measure of uncertainty, reflecting a $\pm 1\sigma$ as in the rest of the carbon budget. This is $\pm 1.0\% \, yr^{-1}$ for the rest of the world (global emissions minus China and USA).

The 2016 projection for the world is made of the sum of the projections for China, USA, and the rest of the world. The uncertainty is added in quadrature among the three regions. The uncertainty here reflects the best of our expert opinion.

2.2 CO_2 emissions from land use, land-use change, and forestry (E_{LUC})

Land-use-change emissions reported here (E_{LUC}) include CO_2 fluxes from deforestation, afforestation, logging (forest degradation and harvest activity), shifting cultivation (cycle of cutting forest for agriculture and then abandoning), and regrowth of forests following wood harvest or abandonment of agriculture. Only some land management activities are included in our land-use-change emissions estimates (Table 5). Some of these activities lead to emissions of CO_2 to the atmosphere, while others lead to CO_2 sinks. E_{LUC} is the net sum of all anthropogenic activities considered. Our annual estimate for 1959–2010 is from a bookkeeping method (Sect. 2.2.1) primarily based on net forest area change and biomass data from the Forest Resource Assessment (FRA) of the Food and Agriculture Organization (FAO), which are only available at intervals of 5 years. We use the bookkeeping method based on FAO FRA 2010 here (Houghton et al., 2012) and present preliminary results of an update using the FAO FRA 2015 (Houghton and Nassikas, 2016). Interannual variability in emissions due to deforestation and degradation have been coarsely estimated from satellite-based fire activity in tropical forest areas (Sect. 2.2.2; Giglio et al., 2013; van der Werf et al., 2010). The bookkeeping method is used to quantify the E_{LUC} over the time period of the available data, and the satellite-based deforestation fire information to incorporate interannual variability (E_{LUC} flux annual anomalies) from tropical deforestation fires. The satellite-based deforestation and degradation fire emissions estimates are available for years 1997–2015. We calculate the global annual anomaly in deforestation and degradation fire emissions in tropical forest regions for each year, compared to the 1997–2010 period, and add this annual flux anomaly to the E_{LUC}

estimated using the published bookkeeping method that is available up to 2010 only and assumed constant at the 2010 value during the period 2011–2015. We thus assume that all land management activities apart from deforestation and degradation do not vary significantly on a year-to-year basis. Other sources of interannual variability (e.g. the impact of climate variability on regrowth fluxes) are accounted for in S_{LAND}. In addition, we use results from dynamic global vegetation models (see Sect. 2.2.3 and Table 6) that calculate net land-use-change CO_2 emissions in response to land-cover change reconstructions prescribed to each model in order to help quantify the uncertainty in E_{LUC} and to explore the consistency of our understanding. The three methods are described below, and differences are discussed in Sect. 3.2. A discussion of other methods to estimate E_{LUC} was provided in the 2015 update (Le Quéré et al., 2015a; Sect. 2.2.4).

2.2.1 Bookkeeping method

Land-use-change CO_2 emissions are calculated by a bookkeeping method approach (Houghton, 2003) that keeps track of the carbon stored in vegetation and soils before deforestation or other land-use change, and the changes in forest age classes, or cohorts, of disturbed lands after land-use change, including possible forest regrowth after deforestation. The method tracks the CO_2 emitted to the atmosphere immediately during deforestation, and over time due to the follow-up decay of soil and vegetation carbon in different pools, including wood products pools after logging and deforestation. It also tracks the regrowth of vegetation and associated build-up of soil carbon pools after land-use change. It considers transitions between forests, pastures, and cropland; shifting cultivation; degradation of forests where a fraction of the trees is removed; abandonment of agricultural land; and forest management such as wood harvest and, in the USA, fire management. In addition to tracking logging debris on the forest floor, the bookkeeping method tracks the fate of carbon contained in harvested wood products that is eventually emitted back to the atmosphere as CO_2, although a detailed treatment of the lifetime in each product pool is not performed (Earles et al., 2012). Harvested wood products are partitioned into three pools with different turnover times. All fuel wood is assumed burned in the year of harvest ($1.0 \, yr^{-1}$). Pulp and paper products are oxidised at a rate of $0.1 \, yr^{-1}$, timber is assumed to be oxidised at a rate of $0.01 \, yr^{-1}$, and elemental carbon decays at $0.001 \, yr^{-1}$. The general assumptions about partitioning wood products among these pools are based on national harvest data (Houghton, 2003).

The primary land-cover change and biomass data for the bookkeeping method analysis is the Forest Resource Assessment of the FAO which provides statistics on forest-cover change and management at intervals of 5 years (FAO, 2010). The data are based on countries' self-reporting, some of which include satellite data in more recent assessments (Table 4). Changes in land cover other than forest are based

Table 5. Comparison of the processes included in the bookkeeping method and DGVMs in their estimates of E_{LUC} and S_{LAND}. See Table 6 for model references. All models include deforestation and forest regrowth after abandonment of agriculture (or from afforestation activities on agricultural land). Processes relevant for E_{LUC} are only described for the DGVMs used with land-cover change in this study (Fig. 6 top panel).

	Bookkeeping	CABLE	CLASS-CTEM	CLM	DLEM	ISAM	JSBACH	JULES	LPJ-GUESS	LPJ	LPX-Bern	OCN	ORCHIDEE	SDGVM	VISIT
Processes relevant for E_{LUC}															
Wood harvest and forest degradation[a]	yes					yes		no	no	no		yes			
Shifting cultivation	yes[b]					no		no	no	no		no			
Cropland harvest	yes					yes		no	yes	no		yes			
Peat fires	no					no		no	no	no		no			
Processes also relevant for S_{LAND}															
Fire simulation and/or suppression	for US only	no	yes	yes	yes	no	yes	no	yes	yes	yes	no	no	yes	yes
Climate and variability	no	yes	yes	yes	yes	yes	yes	yes	yes	yes	yes	yes	yes	yes	yes
CO_2 fertilisation	no	yes	yes	yes	yes	yes	yes	yes	yes	yes	yes	yes	yes	yes	yes
Carbon–nitrogen interactions, including N deposition	no	yes	no	yes	yes	yes	no	no	yes	no	yes	yes	no	yes[c]	no

[a] Refers to the routine harvest of established managed forests rather than pools of harvested products. [b] Not in the recent update (Houghton and Nassikas, 2016). [c] Very limited. Nitrogen uptake is simulated as a function of soil C, and Vcmax is an empirical function of canopy N. Does not consider N deposition.

on annual, national changes in cropland and pasture areas reported by the FAO Statistics Division (FAOSTAT, 2010). Land-use-change country data are aggregated by regions. The carbon stocks on land (biomass and soils), and their response functions subsequent to land-use change, are based on FAO data averages per land-cover type, per biome, and per region. Similar results were obtained using forest biomass carbon density based on satellite data (Baccini et al., 2012). The bookkeeping method does not include land ecosystems' transient response to changes in climate, atmospheric CO_2, and other environmental factors, and the growth/decay curves are based on contemporary data that will implicitly reflect the effects of CO_2 and climate at that time. Published results from the bookkeeping method are available from 1850 to 2010, with preliminary results available to 2015.

2.2.2 Fire-based interannual variability in E_{LUC}

CO_2 emissions associated with land-use change calculated from satellite-based fire activity in tropical forest areas (van der Werf et al., 2010) provide information on emissions due to tropical deforestation and degradation that are complementary to the bookkeeping approach. They do not provide a direct estimate of E_{LUC} as they do not include non-combustion processes such as respiration, wood harvest, wood products, or forest regrowth. Legacy emissions such

as decomposition from on-ground debris and soils are not included in this method either. However, fire estimates provide some insight in the year-to-year variations in the sub-component of the total E_{LUC} flux that result from immediate CO_2 emissions during deforestation caused, for example, by the interactions between climate and human activity (e.g. there is more burning and clearing of forests in dry years) that are not represented by other methods. The "deforestation fire emissions" assume an important role of fire in removing biomass in the deforestation process and thus can be used to infer gross instantaneous CO_2 emissions from deforestation using satellite-derived data on fire activity in regions with active deforestation. The method requires information on the fraction of total area burned associated with deforestation vs. other types of fires, and this information can be merged with information on biomass stocks and the fraction of the biomass lost in a deforestation fire to estimate CO_2 emissions. The satellite-based deforestation fire emissions are limited to the tropics, where fires result mainly from human activities. Tropical deforestation is the largest and most variable single contributor to E_{LUC}.

Fire emissions associated with deforestation and tropical peat burning are based on the Global Fire Emissions Database (GFED4; accessed July 2016) described in van der Werf et al. (2010) but with updated burned area (Giglio et al., 2013) as well as burned area from relatively small

Table 6. References for the process models and data products included in Figs. 6–8. All models and products are updated with new data to end of year 2015.

Model/data name	Reference	Change from Le Quéré et al. (2015a)
Dynamic global vegetation models		
CABLE	Zhang et al. (2013)	Not applicable (not used in 2015)
CLASS-CTEM	Melton and Arora (2016)	Not applicable (not used in 2015)
CLM	Oleson et al. (2013)	No change
DLEM	Tian et al. (2010)	Not applicable (not used in 2015)
ISAM	Jain et al. (2013)	Updated to account for dynamic phenology and dynamic rooting distribution and depth parameterisations for various ecosystem types as described in El Masri et al. (2015). These parameterisations account for light, water, and nutrient stresses while allocating the assimilated carbon to leaf, stem, and root pools.
JSBACH	Reick et al. (2013)[a]	No change
JULES[b]	Clark et al. (2011)[c]	Updated to code release 4.6 and configuration JULES-C-1.1. This version includes improvements to the seasonal cycle of soil respiration.
LPJ-GUESS	Smith et al. (2014)	Use of CRU-NCEP. Crop representation in LPJ-GUESS was adopted from Olin et al. (2015), applying constant fertiliser rate and area fraction under irrigation, as in Elliott et al. (2015).
LPJ[d]	Sitch et al. (2003)[e]	No change
LPX-Bern	Stocker et al. (2014)[f]	Not applicable (not used in 2015)
OCN	Zaehle and Friend (2010)[g]	Updated to v1.r278. Biological N fixation is now simulated dynamically according to the OPT scheme of Meyerholt et al. (2016).
ORCHIDEE	Krinner et al. (2005)[h]	Updated revision 3687, including a new hydrological scheme with 11 layers and a complete diffusion scheme, a new parameterisation of photosynthesis, an improved scheme for representation of snow, and a new representation of soil albedo based on satellite data.
SDGVM	Woodward et al. (1995)[i]	Not applicable (not used in 2015)
VISIT	Kato et al. (2013)[j]	Updated to use CRU-NCEP shortwave radiation data instead of using internally estimated radiation from CRU cloudiness data.
Data products for land-use-change emissions		
Bookkeeping	Houghton et al. (2012)	No change
Bookkeeping using FAO2015	Houghton and Nassikas (2016)	Not applicable (not used in 2015)
Fire-based emissions	van der Werf et al. (2010)	No change
Ocean biogeochemistry models		
NEMO-PlankTOM5	Buitenhuis et al. (2010)[k]	No change
NEMO-PISCES (IPSL)	Aumont and Bopp (2006)	No change
CCSM-BEC	Doney et al. (2009)	No change
MICOM-HAMOCC (NorESM-OC)	Schwinger et al. (2016)	No change
NEMO-PISCES (CNRM)	Séférian et al. (2013)[l]	No change
CSIRO	Oke et al. (2013)	No change
MITgcm-REcoM2	Hauck et al. (2016)	Nanophytoplankton chlorophyll degradation rate set to 0.1 per day
Data products for ocean CO_2 flux		
Landschützer	Landschützer et al. (2015)	No change
Jena CarboScope	Rödenbeck et al. (2014)	Updated to version oc_1.4 with longer spin-up/down periods both before and after the data-constrained period.
Atmospheric inversions for total CO_2 fluxes (land-use-change + land + ocean CO_2 fluxes)		
CarbonTracker	Peters et al. (2010)	Updated to version CTE2016-FT with minor changes in the inversion setup.
Jena CarboScope	Rödenbeck et al. (2003)	Updated to version s81_v3.8.
CAMS[m]	Chevallier et al. (2005)	Updated to version 15.2 with minor changes in the inversion setup.

[a] See also Goll et al. (2015). [b] Joint UK Land Environment Simulator. [c] See also Best et al. (2011). [d] Lund–Potsdam–Jena. [e] Compared to published version, decreased LPJ wood harvest efficiency so that 50 % of biomass was removed off-site compared to 85 % used in the 2012 budget. Residue management of managed grasslands increased so that 100 % of harvested grass enters the litter pool. [f] Compared to published version: changed several model parameters, due to new tuning with multiple observational constraints. No mechanistic changes. [g] See also Zaehle et al. (2011). [h] Compared to published version: revised parameters values for photosynthetic capacity for boreal forests (following assimilation of FLUXNET data), updated parameters values for stem allocation, maintenance respiration and biomass export for tropical forests (based on literature), and CO_2 down-regulation process added to photosynthesis. [i] See also Woodward and Lomas (2004). Changes from publications include sub-daily light downscaling for calculation of photosynthesis and other adjustments. [j] See also Ito and Inatomi (2012). [k] With no nutrient restoring below the mixed layer depth. [l] Uses winds from Atlas et al. (2011). [m] The CAMS (Copernicus Atmosphere Monitoring Service) v15.2 CO_2 inversion system, initially described by Chevallier et al. (2005), relies on the global tracer transport model LMDZ (see also Supplement of Chevallier, 2015; Hourdin et al., 2006).

fires that are detected by satellite as thermal anomalies but not mapped by the burned-area approach (Randerson et al., 2012). The burned-area information is used as input data in a modified version of the satellite-driven Carnegie–Ames–Stanford Approach (CASA) biogeochemical model to estimate carbon emissions associated with fires, keeping track of what fraction of fire emissions was due to deforestation (see van der Werf et al., 2010). The CASA model uses different assumptions to compute decay functions compared to the bookkeeping method, and does not include historical emissions or regrowth from land-use change prior to the availability of satellite data. Comparing coincident CO emissions and their atmospheric fate with satellite-derived CO concentrations allows for some validation of this approach (e.g. van der Werf et al., 2008). Results from the fire-based method to estimate land-use-change emissions anomalies added to the bookkeeping mean E_{LUC} estimate are available from 1997 to 2015. Our combination of land-use-change CO_2 emissions where the variability in annual CO_2 deforestation emissions is diagnosed from fires assumes that year-to-year variability is dominated by variability in deforestation.

2.2.3 Dynamic global vegetation models (DGVMs)

Land-use-change CO_2 emissions have been estimated using an ensemble of DGVM simulations. New model experiments up to year 2015 have been coordinated by the project "Trends and drivers of the regional-scale sources and sinks of carbon dioxide" (TRENDY; Sitch et al., 2015). We use only models that have estimated land-use-change CO_2 emissions following the TRENDY protocol (see Sect. 2.5.2). Models use their latest configurations, summarised in Tables 5 and 6.

Two sets of simulations were performed with the DGVMs, first forced with historical changes in land-cover distribution, climate, atmospheric CO_2 concentration, and N deposition, and second, as further described below with a time-invariant pre-industrial land-cover distribution, allowing for estimation of, by difference with the first simulation, the dynamic evolution of biomass and soil carbon pools in response to prescribed land-cover change. Because of the limited availability of the land-use forcing (see below), 14 DGVMs performed historical simulations with time-invariant land-cover distribution, but only 5 DGVMs managed to simulate realistic simulations with time varying land-cover change. These latter DGVMs accounted for deforestation and (to some extent) regrowth, the most important components of E_{LUC}, but they do not represent all processes resulting directly from human activities on land (Table 5). All DGVMs represent processes of vegetation growth and mortality, as well as decomposition of dead organic matter associated with natural cycles, and include the vegetation and soil carbon response to increasing atmospheric CO_2 levels and to climate variability and change. In addition, eight models explicitly simulate the coupling of C and N cycles and account for atmospheric N deposition (Table 5), with three of those models used for

land-use-change simulations. The DGVMs are independent of the other budget terms except for their use of atmospheric CO_2 concentration to calculate the fertilisation effect of CO_2 on primary production.

For this global carbon budget, the DGVMs used the HYDE land-use-change data set (Klein Goldewijk et al., 2011), which provides annual, half-degree, fractional data on cropland and pasture. These data are based on annual FAO statistics of change in agricultural area available to 2012 (FAOSTAT, 2010). For the years 2013 to 2015, the HYDE data were extrapolated by country for pastures and cropland separately based on the trend in agricultural area over the previous 5 years. The more comprehensive harmonised land-use data set (Hurtt et al., 2011), which also includes fractional data on primary vegetation and secondary vegetation, as well as all underlying transitions between land-use states, has not been made available yet for this year. Hence, the reduced ensemble of DGVMs that can simulate the LUC flux from the HYDE data set only. The HYDE data are independent of the data set used in the bookkeeping method (Houghton, 2003, and updates), which is based primarily on forest area change statistics (FAO, 2010). The HYDE land-use-change data set does not indicate whether land-use changes occur on forested or non-forested land; it only provides the changes in agricultural areas. Hence, it is implemented differently within each model (e.g. an increased cropland fraction in a grid cell can be at the expense of either grassland or forest, the latter resulting in deforestation; land-cover fractions of the non-agricultural land differ between models). Thus, the DGVM forest area and forest area change over time is not consistent with the Forest Resource Assessment of the FAO forest area data used for the bookkeeping model to calculate E_{LUC}. Similarly, model-specific assumptions are applied to convert deforested biomass or deforested area, and other forest product pools, into carbon in some models (Table 5).

The DGVM runs were forced by either 6-hourly CRU-NCEP or by monthly CRU temperature, precipitation, and cloud cover fields (transformed into incoming surface radiation) based on observations and provided on a $0.5° \times 0.5°$ grid and updated to 2015 (Harris et al., 2014; Viovy, 2016). The forcing data include both gridded observations of climate and global atmospheric CO_2, which change over time (Dlugokencky and Tans, 2016), and N deposition (as used in some models; Table 5). As mentioned before, E_{LUC} is diagnosed in each model by the difference between a model simulation with prescribed historical land-cover change and a simulation with constant, pre-industrial land-cover distribution. Both simulations were driven by changing atmospheric CO_2, climate, and, in some models, N deposition over the period 1860–2015. Using the difference between these two DGVM simulations to diagnose E_{LUC} is not fully consistent with the definition of E_{LUC} in the bookkeeping method (Gasser and Ciais, 2013; Stocker and Joos, 2015). The DGVM approach to diagnose land-use-change CO_2 emissions would be expected to produce systematically higher

Table 7. Comparison of results from the bookkeeping method and budget residuals with results from the DGVMs and inverse estimates for the periods 1960–1969, 1970–1979, 1980–1989, 1990–1999, and 2000–2009, as well as the last decade and last year available. All values are in GtC yr^{-1}. The DGVM uncertainties represent $\pm 1\sigma$ of the decadal or annual (for 2015 only) estimates from the individual models; for the inverse models all three results are given where available.

	Mean (GtC yr^{-1})						
	1960–1969	1970–1979	1980–1989	1990–1999	2000–2009	2006–2015	2015
Land-use-change emissions (E_{LUC})							
Bookkeeping method	1.5 ± 0.5	1.3 ± 0.5	1.4 ± 0.5	1.6 ± 0.5	1.0 ± 0.5	1.0 ± 0.5	1.3 ± 0.5
DGVMs[a]	1.2 ± 0.3	1.2 ± 0.3	1.2 ± 0.2	1.2 ± 0.2	1.1 ± 0.2	1.3 ± 0.3	1.2 ± 0.4
Residual terrestrial sink (S_{LAND})							
Budget residual	1.7 ± 0.7	1.7 ± 0.8	1.6 ± 0.8	2.6 ± 0.8	2.6 ± 0.8	3.1 ± 0.9	1.9 ± 0.9
DGVMs[a]	1.2 ± 0.5	2.2 ± 0.5	1.7 ± 0.6	2.3 ± 0.5	2.8 ± 0.6	2.8 ± 0.7	1.0 ± 1.4
Total land fluxes ($S_{LAND} - E_{LUC}$)							
Budget ($E_{FF} - G_{ATM} - S_{OCEAN}$)	0.2 ± 0.5	0.4 ± 0.6	0.1 ± 0.6	1.0 ± 0.6	1.6 ± 0.6	2.2 ± 0.7	0.6 ± 0.7
DGVMs[a]	-0.2 ± 0.7	1.1 ± 0.5	0.4 ± 0.5	1.1 ± 0.3	1.8 ± 0.4	1.7 ± 0.5	-0.1 ± 1.4
Inversions (CTE2016-FT/Jena CarboScope/CAMS)[b]	–/–/–	–/–/–	–/0.2^b/0.9^b	–/1.0^b/1.9^b	1.5^b/1.6^b/2.5^b	2.2^b/2.3^b/3.4^b	1.9^b/2.6^b/2.6^b

[a] Note that for DGVMs, the mean reported for the total land fluxes is not equal to the difference between the means reported for S_{LAND} and E_{LUC} as a different set of models contributed to these two estimates (see Sect. 2.2.3). [b] Estimates are not corrected for the influence of river fluxes, which would reduce the fluxes by 0.45 GtC yr^{-1} when neglecting the anthropogenic influence on land (Sect. 2.7.2). See Table 6 for model references.

E_{LUC} emissions than the bookkeeping approach if all the parameters of the two approaches were the same, which is not the case (see Sect. 2.5.2).

2.2.4 Uncertainty assessment for E_{LUC}

Differences between the bookkeeping, the addition of fire-based interannual variability to the bookkeeping, and DGVM methods originate from three main sources: the land-cover-change data set, the different approaches used in models, and the different processes represented (Table 5). We examine the results from the DGVMs and of the bookkeeping method to assess the uncertainty in E_{LUC}.

The uncertainties in annual E_{LUC} estimates are examined using the standard deviation across models, which averages 0.3 GtC yr^{-1} from 1959 to 2015 (Table 7). The mean of the multi-model E_{LUC} estimates is consistent with a combination of the bookkeeping method and fire-based emissions (Table 7), with the multi-model mean and bookkeeping method differing by less than 0.5 GtC yr^{-1} over 85 % of the time. Based on this comparison, we determine that an uncertainty of ± 0.5 GtC yr^{-1} provides a semi-quantitative measure of uncertainty for annual emissions and reflects our best value judgement that there is at least 68 % chance ($\pm 1\sigma$) that the true land-use-change emission lies within the given range, for the range of processes considered here. This is consistent with the uncertainty analysis of Houghton et al. (2012), which partly reflects improvements in data on forest area change using data and partly more complete understanding and representation of processes in models.

The uncertainties in the decadal E_{LUC} estimates are also examined using the DGVM ensemble, although they are

likely correlated between decades. The correlations between decades come from (1) common biases in system boundaries (e.g. not counting forest degradation in some models), (2) common definition for the calculation of E_{LUC} from the difference of simulations with and without land-use change (a source of bias vs. the unknown truth), (3) common and uncertain land-cover change input data which also cause a bias (though if a different input data set is used each decade, decadal fluxes from DGVMs may be partly decorrelated), and (4) model structural errors (e.g. systematic errors in biomass stocks). In addition, errors arising from uncertain DGVM parameter values would be random but they are not accounted for in this study, since no DGVM provided an ensemble of runs with perturbed parameters.

Prior to 1959, the uncertainty in E_{LUC} is taken as ± 33 %, which is the ratio of uncertainty to mean from the 1960s in the bookkeeping method (Table 7), the first decade available. This ratio is consistent with the mean standard deviation of DGVMs land-use-change emissions over 1870–1958 (0.32 GtC) over the multi-model mean (0.9 GtC).

2.3 Growth rate in atmospheric CO$_2$ concentration (G_{ATM})

Global growth rate in atmospheric CO$_2$ concentration

The rate of growth of the atmospheric CO$_2$ concentration is provided by the US National Oceanic and Atmospheric Administration Earth System Research Laboratory (NOAA/ESRL; Dlugokencky and Tans, 2016), which is updated from Ballantyne et al. (2012). For the 1959–1980 period, the global growth rate is based on measurements of

atmospheric CO_2 concentration averaged from the Mauna Loa and South Pole stations, as observed by the CO_2 Program at Scripps Institution of Oceanography (Keeling et al., 1976). For the 1980–2015 time period, the global growth rate is based on the average of multiple stations selected from the marine boundary layer sites with well-mixed background air (Ballantyne et al., 2012), after fitting each station with a smoothed curve as a function of time, and averaging by latitude band (Masarie and Tans, 1995). The annual growth rate is estimated by Dlugokencky and Tans (2016) from atmospheric CO_2 concentration by taking the average of the most recent December–January months corrected for the average seasonal cycle and subtracting this same average 1 year earlier. The growth rate in units of $ppm\,yr^{-1}$ is converted to units of $GtC\,yr^{-1}$ by multiplying by a factor of $2.12\,GtC\,ppm^{-1}$ (Ballantyne et al., 2012) for consistency with the other components.

The uncertainty around the annual growth rate based on the multiple stations data set ranges between 0.11 and $0.72\,GtC\,yr^{-1}$, with a mean of $0.61\,GtC\,yr^{-1}$ for 1959–1979 and $0.19\,GtC\,yr^{-1}$ for 1980–2015, when a larger set of stations were available (Dlugokencky and Tans, 2016). It is based on the number of available stations, and thus takes into account both the measurement errors and data gaps at each station. This uncertainty is larger than the uncertainty of $\pm 0.1\,GtC\,yr^{-1}$ reported for decadal mean growth rate by the IPCC because errors in annual growth rate are strongly anti-correlated in consecutive years leading to smaller errors for longer timescales. The decadal change is computed from the difference in concentration 10 years apart based on a measurement error of 0.35 ppm. This error is based on offsets between NOAA/ESRL measurements and those of the World Meteorological Organization World Data Centre for Greenhouse Gases (NOAA/ESRL, 2015) for the start and end points (the decadal change uncertainty is the $\sqrt{(2(0.35\,ppm)^2)}(10\,yr)^{-1}$ assuming that each yearly measurement error is independent). This uncertainty is also used in Table 8.

The contribution of anthropogenic CO and CH_4 is neglected from the global carbon budget (see Sect. 2.7.1). We assign a high confidence to the annual estimates of G_{ATM} because they are based on direct measurements from multiple and consistent instruments and stations distributed around the world (Ballantyne et al., 2012).

In order to estimate the total carbon accumulated in the atmosphere since 1750 or 1870, we use an atmospheric CO_2 concentration of 277 ± 3 or 288 ± 3 ppm, respectively, based on a cubic spline fit to ice core data (Joos and Spahni, 2008). The uncertainty of ± 3 ppm (converted to $\pm 1\sigma$) is taken directly from the IPCC's assessment (Ciais et al., 2013). Typical uncertainties in the growth rate in atmospheric CO_2 concentration from ice core data are ± 1–$1.5\,GtC$ per decade as evaluated from the Law Dome data (Etheridge et al., 1996)

for individual 20-year intervals over the period from 1870 to 1960 (Bruno and Joos, 1997).

2.4   Ocean CO_2 sink

Estimates of the global ocean CO_2 sink are based on a combination of a mean CO_2 sink estimate for the 1990s from observations, as well as a trend and variability in the ocean CO_2 sink for 1959–2015 from seven global ocean biogeochemistry models. We use two observation-based estimates of S_{OCEAN} available for recent decades to provide a qualitative assessment of confidence in the reported results.

2.4.1   Observation-based estimates

A mean ocean CO_2 sink of $2.2 \pm 0.4\,GtC\,yr^{-1}$ for the 1990s was estimated by the IPCC (Denman et al., 2007) based on indirect observations and their spread: ocean–land CO_2 sink partitioning from observed atmospheric O_2/N_2 concentration trends (Manning and Keeling, 2006), an oceanic inversion method constrained by ocean biogeochemistry data (Mikaloff Fletcher et al., 2006), and a method based on penetration timescale for CFCs (McNeil et al., 2003). This is comparable with the sink of $2.0 \pm 0.5\,GtC\,yr^{-1}$ estimated by Khatiwala et al. (2013) for the 1990s, and with the sink of 1.9 to $2.5\,GtC\,yr^{-1}$ estimated from a range of methods for the period 1990–2009 (Wanninkhof et al., 2013), with uncertainties ranging from ± 0.3 to $\pm 0.7\,GtC\,yr^{-1}$. The most direct way for estimating the observation-based ocean sink is from the product of (sea–air pCO_2 difference) $\times$ (gas transfer coefficient). Estimates based on sea–air pCO_2 are fully consistent with indirect observations (Wanninkhof et al., 2013), but their uncertainty is larger mainly due to difficulty in capturing complex turbulent processes in the gas transfer coefficient (Sweeney et al., 2007) and because of uncertainties in the pre-industrial river outgas of CO_2 (Jacobson et al., 2007).

The two observation-based estimates (Landschützer et al., 2015; Rödenbeck et al., 2014) used here compute the ocean CO_2 sink and its variability using interpolated measurements of surface ocean fugacity of CO_2 (pCO_2 corrected for the non-ideal behaviour of the gas; Pfeil et al., 2013). The measurements were from the Surface Ocean CO_2 Atlas version 4, which is an update of version 3 (Bakker et al., 2016) and contains data to 2015 (see data attribution Table 1a). In contrast to last year's global carbon budget, where preliminary data were used for the past year, data used here are fully quality-controlled following standard SOCAT procedures. The SOCAT v4 were mapped using a data-driven diagnostic method (Rödenbeck et al., 2013) and a combined self-organising map and feed-forward neural network (Landschützer et al., 2014). The global observation-based estimates were adjusted to remove a background (not part of the anthropogenic ocean flux) ocean source of CO_2 to the atmosphere of $0.45\,GtC\,yr^{-1}$ from river input to the ocean (Jacobson et al., 2007) in order to make them comparable to

Table 8. Decadal mean in the five components of the anthropogenic CO_2 budget for the periods 1960–1969, 1970–1979, 1980–1989, 1990–1999, and 2000–2009, as well as the last decade and last year available. All values are in GtC yr^{-1}. All uncertainties are reported as $\pm 1\sigma$. A data set containing data for each year during 1959–2014 is available at http://cdiac.ornl.gov/GCP/carbonbudget/2015/. Please follow the terms of use and cite the original data sources as specified in the data set.

	Mean (GtC yr^{-1})		
	1960–1969	1970–1979	1980–1989	1990–1999	2000–2009	2006–2015	2015
Emissions							
Fossil fuels and industry (E_{FF})	3.1 ± 0.2	4.7 ± 0.2	5.5 ± 0.3	6.3 ± 0.3	8.0 ± 0.4	9.3 ± 0.5	9.9 ± 0.5
Land-use-change emissions (E_{LUC})	1.5 ± 0.5	1.3 ± 0.5	1.4 ± 0.5	1.6 ± 0.5	1.0 ± 0.5	1.0 ± 0.5	1.3 ± 0.5
Partitioning							
Growth rate in atmospheric CO_2 concentration (G_{ATM})	1.7 ± 0.1	2.8 ± 0.1	3.4 ± 0.1	3.1 ± 0.1	4.0 ± 0.1	4.5 ± 0.1	6.3 ± 0.2
Ocean sink (S_{OCEAN})	1.2 ± 0.5	1.5 ± 0.5	1.9 ± 0.5	2.2 ± 0.5	2.3 ± 0.5	2.6 ± 0.5	3.0 ± 0.5
Residual terrestrial sink (S_{LAND})	1.7 ± 0.7	1.7 ± 0.8	1.6 ± 0.8	2.6 ± 0.8	2.6 ± 0.8	3.1 ± 0.9	1.9 ± 0.9

S_{OCEAN}, which only represents the annual uptake of anthropogenic CO_2 by the ocean. Several other data-based products are available, but they show large discrepancies with observed variability that need to be resolved. Here we used the two data products that had the best fit to observations for their representation of tropical and global variability (Rödenbeck et al., 2015).

We use the data-based product of Khatiwala et al. (2009) updated by Khatiwala et al. (2013) to estimate the anthropogenic carbon accumulated in the ocean during 1765–1958 (60.2 GtC) and 1870–1958 (47.5 GtC), and assume an oceanic uptake of 0.4 GtC for 1750–1765 (for which time no data are available) based on the mean uptake during 1765–1770. The estimate of Khatiwala et al. (2009) is based on regional disequilibrium between surface pCO_2 and atmospheric CO_2, and a Green's function utilising transient ocean tracers like CFCs and ^{14}C to ascribe changes through time. It does not include changes associated with changes in ocean circulation, temperature, and climate, but these are thought to be small over the time period considered here (Ciais et al., 2013). The uncertainty in cumulative uptake of ± 20 GtC (converted to $\pm 1\sigma$) is taken directly from the IPCC's review of the literature (Rhein et al., 2013), or about $\pm 30\%$ for the annual values (Khatiwala et al., 2009).

2.4.2   Global ocean biogeochemistry models

The trend in the ocean CO_2 sink for 1959–2015 is computed using a combination of seven global ocean biogeochemistry models (Table 6). The models represent the physical, chemical, and biological processes that influence the surface ocean concentration of CO_2 and thus the air-sea CO_2 flux. The models are forced by meteorological reanalysis and atmospheric CO_2 concentration data available for the entire time

period. Models do not include the effects of anthropogenic changes in nutrient supply, which could lead to an increase in the ocean sink of up to about 0.3 GtC yr^{-1} over the industrial period (Duce et al., 2008). They compute the air-sea flux of CO_2 over grid boxes of 1 to 4° in latitude and longitude. The ocean CO_2 sink for each model is normalised to the observations by dividing the annual model values by their modelled average over 1990–1999 and multiplying this by the observation-based estimate of 2.2 GtC yr^{-1} (obtained from Manning and Keeling, 2006; McNeil et al., 2003; Mikaloff Fletcher et al., 2006). The ocean CO_2 sink for each year (t) in GtC yr^{-1} is therefore

$$S_{OCEAN}(t) = \frac{1}{n} \sum_{m=1}^{m=n} \frac{S_{OCEAN}^m(t)}{S_{OCEAN}^m(1990\text{–}1999)} \times 2.2, \qquad (7)$$

where n is the number of models. This normalisation ensures that the ocean CO_2 sink for the global carbon budget is based on observations, whereas the trends and annual values in CO_2 sinks are from model estimates. The normalisation based on a ratio assumes that if models over or underestimate the sink in the 1990s, it is primarily due to the process of diffusion, which depends on the gradient of CO_2. Thus, a ratio is more appropriate than an offset as it takes into account the time dependence of CO_2 gradients in the ocean. The mean uncorrected ocean CO_2 sink from the models for 1990–1999 ranges between 1.7 and 2.4 GtC yr^{-1}, with a multi-model mean of 2.0 GtC yr^{-1}.

2.4.3   Uncertainty assessment for S_{OCEAN}

The uncertainty around the mean ocean sink of anthropogenic CO_2 was quantified by Denman et al. (2007) for the 1990s (see Sect. 2.4.1). To quantify the uncertainty around

annual values, we examine the standard deviation of the normalised model ensemble. We use further information from the two data-based products to assess the confidence level. The average standard deviation of the normalised ocean model ensemble is $0.16\,\text{GtC}\,\text{yr}^{-1}$ during 1980–2010 (with a maximum of 0.33), but it increases as the model ensemble goes back in time, with a standard deviation of $0.22\,\text{GtC}\,\text{yr}^{-1}$ across models in the 1960s. We estimate that the uncertainty in the annual ocean CO_2 sink is about $\pm 0.5\,\text{GtC}\,\text{yr}^{-1}$ from the fractional uncertainty in the data uncertainty of $\pm 0.4\,\text{GtC}\,\text{yr}^{-1}$ and standard deviation across models of up to $\pm 0.33\,\text{GtC}\,\text{yr}^{-1}$, reflecting both the uncertainty in the mean sink from observations during the 1990s (Denman et al., 2007; Sect. 2.4.1) and in the interannual variability as assessed by models.

We examine the consistency between the variability in the model-based and the data-based products to assess confidence in S_{OCEAN}. The interannual variability of the ocean fluxes (quantified as the standard deviation) of the two data-based estimates for 1986–2015 (where they overlap) is $\pm 0.34\,\text{GtC}\,\text{yr}^{-1}$ (Rödenbeck et al., 2014) and $\pm 0.41\,\text{GtC}\,\text{yr}^{-1}$ (Landschützer et al., 2015), compared to $\pm 0.29\,\text{GtC}\,\text{yr}^{-1}$ for the normalised model ensemble. The standard deviation includes a component of trend and decadal variability in addition to interannual variability, and their relative influence differs across estimates. The phase is generally consistent between estimates, with a higher ocean CO_2 sink during El Niño events. The annual data-based estimates correlate with the ocean CO_2 sink estimated here with a correlation of $r = 0.71$ (0.51 to 0.77 for individual models), and $r = 0.81$ (0.66 to 0.79) for the data-based estimates of Rödenbeck et al. (2014) and Landschützer et al. (2015), respectively (simple linear regression), with their mutual correlation at 0.65. The agreement is better for decadal variability than for interannual variability. The use of annual data for the correlation may reduce the strength of the relationship because the dominant source of variability associated with El Niño events is less than one year. We assess a medium confidence level to the annual ocean CO_2 sink and its uncertainty because they are based on multiple lines of evidence, and the results are consistent in that the interannual variability in the model and data-based estimates are all generally small compared to the variability in the growth rate of atmospheric CO_2 concentration.

2.5 Terrestrial CO_2 sink

The difference between, on the one hand, fossil fuel (E_{FF}) and land-use-change emissions (E_{LUC}) and, on the other hand, the growth rate in atmospheric CO_2 concentration (G_{ATM}) and the ocean CO_2 sink (S_{OCEAN}) is attributable to the net sink of CO_2 in terrestrial vegetation and soils (S_{LAND}), within the given uncertainties (Eq. 1). Thus, this sink can be estimated as the residual of the other terms in the mass balance budget, as well as directly calculated using DGVMs. The residual land sink (S_{LAND}) is thought to be in part because of the fertilising effect of rising atmospheric CO_2 on plant growth, N deposition, and effects of climate change such as the lengthening of the growing season in northern temperate and boreal areas. S_{LAND} does not include gross land sinks directly resulting from land-use change (e.g. regrowth of vegetation) as these are estimated as part of the net land-use flux (E_{LUC}). System boundaries make it difficult to exactly attribute CO_2 fluxes on land between S_{LAND} and E_{LUC} (Erb et al., 2013), and by design most of the uncertainties in our method are allocated to S_{LAND} for those processes that are poorly known or represented in models.

2.5.1 Residual of the budget

For 1959–2015, the terrestrial carbon sink was estimated from the residual of the other budget terms by rearranging Eq. (1):

$$S_{\text{LAND}} = E_{\text{FF}} + E_{\text{LUC}} - (G_{\text{ATM}} + S_{\text{OCEAN}}). \tag{8}$$

The uncertainty in S_{LAND} is estimated annually from the root sum of squares of the uncertainty in the right-hand terms assuming the errors are not correlated. The uncertainty averages to $\pm 0.8\,\text{GtC}\,\text{yr}^{-1}$ over 1959–2015 (Table 7). S_{LAND} estimated from the residual of the budget includes, by definition, all the missing processes and potential biases in the other components of Eq. (8).

2.5.2 DGVMs

A comparison of the residual calculation of S_{LAND} in Eq. (8) with estimates from DGVMs as used to estimate E_{LUC} in Sect. 2.2.3, but here excluding the effects of changes in land cover (using a constant pre-industrial land-cover distribution), provides an independent estimate of the consistency of S_{LAND} with our understanding of the functioning of the terrestrial vegetation in response to CO_2 and climate variability (Table 7). As described in Sect. 2.2.3, the DGVM runs that exclude the effects of changes in land cover include all climate variability and CO_2 effects over land, but they do not include reductions in CO_2 sink capacity associated with human activity directly affecting changes in vegetation cover and management, which by design is allocated to E_{LUC}. This effect has been estimated to have led to a reduction in the terrestrial sink by $0.5\,\text{GtC}\,\text{yr}^{-1}$ since 1750 (Gitz and Ciais, 2003). The models in this configuration estimate the mean and variability of S_{LAND} based on atmospheric CO_2 and climate, and thus both terms can be compared to the budget residual. We apply three criteria for minimum model realism by including only those models with (1) steady state after spin-up; (2) where available, net land fluxes ($S_{\text{LAND}} - E_{\text{LUC}}$) that are a carbon sink over the 1990s as constrained by global atmospheric and oceanic observations (Keeling and Manning, 2014; Wanninkhof et al., 2013); and (3) where available, global E_{LUC} that is a carbon source over the 1990s.

Fourteen models met criteria (1), and five of the models that provided E_{LUC} met all three criteria.

The standard deviation of the annual CO_2 sink across the DGVMs' averages to ± 0.8 GtC yr^{-1} for the period 1959 to 2015. The model mean, over different decades, correlates with the budget residual with $r = 0.68$ (0.51 to $r = 0.77$ for individual models). The standard deviation is similar to that of the five model ensembles presented in Le Quéré et al. (2009), but the correlation is improved compared to $r = 0.54$ obtained in the earlier study. The DGVM results suggest that the sum of our knowledge on annual CO_2 emissions and their partitioning is plausible (see Sect. 4), and provide insight on the underlying processes and regional breakdown. However, as the standard deviation across the DGVMs (0.8 GtC yr^{-1} on average) is of the same magnitude as the combined uncertainty due to the other components (E_{FF}, E_{LUC}, G_{ATM}, S_{OCEAN}; Table 7), the DGVMs do not provide further reduction of uncertainty in the annual terrestrial CO_2 sink compared to the residual of the budget (Eq. 8). Yet, DGVM results are largely independent of the residual of the budget, and it is worth noting that the residual method and ensemble mean DGVM results are consistent within their respective uncertainties. We attach a medium confidence level to the annual land CO_2 sink and its uncertainty because the estimates from the residual budget and averaged DGVMs match well within their respective uncertainties, and the estimates based on the residual budget are primarily dependent on E_{FF} and G_{ATM}, both of which are well constrained.

2.6 The atmospheric perspective

The worldwide network of atmospheric measurements can be used with atmospheric inversion methods to constrain the location of the combined total surface CO_2 fluxes from all sources, including fossil and land-use-change emissions and land and ocean CO_2 fluxes. The inversions assume E_{FF} to be well known, and they solve for the spatial and temporal distribution of land and ocean fluxes from the residual gradients of CO_2 between stations that are not explained by emissions. Inversions used atmospheric CO_2 data to the end of 2015 (including preliminary values in some cases), and three atmospheric CO_2 inversions (Table 6) to infer the total CO_2 flux over land regions, and the distribution of the total land and ocean CO_2 fluxes for the mid- to high-latitude Northern Hemisphere (30–90° N), tropics (30° S–30° N) and mid- to high-latitude region of the Southern Hemisphere (30–90° S). We focus here on the largest and most consistent sources of information and use these estimates to comment on the consistency across various data streams and process-based estimates.

Atmospheric inversions

The three inversion systems used in this release are the CarbonTracker (Peters et al., 2010), the Jena CarboScope (Rö-denbeck, 2005), and CAMS (Chevallier et al., 2005). See Table 6 for version numbers. They are based on the same Bayesian inversion principles that interpret the same, for the most part, observed time series (or subsets thereof), but use different methodologies that represent some of the many approaches used in the field. This mainly concerns the time resolution of the estimates (i.e. weekly or monthly), spatial breakdown (i.e. grid size), assumed correlation structures, and mathematical approach. The details of these approaches are documented extensively in the references provided. Each system uses a different transport model, which was demonstrated to be a driving factor behind differences in atmospheric-based flux estimates, and specifically their global distribution (Stephens et al., 2007).

The three inversions use atmospheric CO_2 observations from various flask and in situ networks. They prescribe spatial and global E_{FF} that can vary from that presented here. The CarbonTracker and CAMS inversions prescribed the same global E_{FF} as in Sect. 2.1.1, during 2010–2015 for CarbonTracker and during 1979–2015 in CAMS. The Jena CarboScope inversion uses E_{FF} from EDGAR (2011) v4.2. Different spatial and temporal distributions of E_{FF} were prescribed in each inversion.

Given their prescribed E_{FF}, each inversion estimates natural fluxes from a similar set of surface CO_2 measurement stations, and CarbonTracker additionally uses two sites of aircraft CO_2 vertical profiles over the Amazon and Siberia, regions where surface observations are sparse. The atmospheric transport models of each inversion are TM5 for CarbonTracker, TM3 for Jena CarboScope, and LMDZ for CAMS. These three models are based on the same ECMWF wind fields. The three inversions use different prior natural fluxes, which partly influences their optimised fluxes. CAMS assumes that the prior land flux is zero on the annual mean in each grid cell of the transport model, so that any sink or source on land is entirely reflecting the information brought by atmospheric measurements. CarbonTracker simulates a small prior sink on land from the SIBCASA model that results from regrowth following fire disturbances of an otherwise net zero biosphere. Jena CarboScope assumes a prior sink on land as well from the LPJ model. Inversion results for the sum of natural ocean and land fluxes (Fig. 8) are more constrained in the Northern Hemisphere (NH) than in the tropics, because of the higher measurement stations density in the NH.

Finally, results from atmospheric inversions include the natural CO_2 fluxes from rivers (which need to be taken into account to allow comparison to other sources) and chemical oxidation of reactive carbon-containing gases (which are neglected here). These inverse estimates are not truly independent of the other estimates presented here as the atmospheric observations include a set of observations used to estimate the global growth rate in atmospheric CO_2 concentration (Sect. 2.3). However, they provide new information on the regional distribution of fluxes.

We focus the analysis on two known strengths of the inverse approach: the derivation of the year-to-year changes in total land fluxes ($S_{LAND} - E_{LUC}$) consistent with the whole network of atmospheric observations, and the spatial breakdown of land and ocean fluxes ($S_{LAND} - E_{LUC} + S_{OCEAN}$) across large regions of the globe. The spatial breakdown is discussed in Sect. 3.1.3.

2.7 Processes not included in the global carbon budget

2.7.1 Contribution of anthropogenic CO and CH_4 to the global carbon budget

Anthropogenic emissions of CO and CH_4 to the atmosphere are eventually oxidised to CO_2 and thus are part of the global carbon budget. These contributions are omitted in Eq. (1), but an attempt is made in this section to estimate their magnitude and identify the sources of uncertainty. Anthropogenic CO emissions are from incomplete fossil fuel and biofuel burning and deforestation fires. The main anthropogenic emissions of fossil CH_4 that matter for the global carbon budget are the fugitive emissions of coal, oil, and gas upstream sectors (see below). These emissions of CO and CH_4 contribute a net addition of fossil carbon to the atmosphere.

In our estimate of E_{FF} we assumed (Sect. 2.1.1) that all the fuel burned is emitted as CO_2; thus, CO anthropogenic emissions and their atmospheric oxidation into CO_2 within a few months are already counted implicitly in E_{FF} and should not be counted twice (same for E_{LUC} and anthropogenic CO emissions by deforestation fires). Anthropogenic emissions of fossil CH_4 are not included in E_{FF}, because these fugitive emissions are not included in the fuel inventories. Yet they contribute to the annual CO_2 growth rate after CH_4 gets oxidised into CO_2. Anthropogenic emissions of fossil CH_4 represent 15 % of total CH_4 emissions (Kirschke et al., 2013) that is 0.061 GtC yr^{-1} for the past decade. Assuming steady state, these emissions are all converted to CO_2 by OH oxidation and thus explain 0.06 GtC yr^{-1} of the global CO_2 growth rate in the past decade, or 0.07–0.1 GtC yr^{-1} using the higher CH_4 emissions reported recently (Schwietzke et al., 2016).

Other anthropogenic changes in the sources of CO and CH_4 from wildfires, biomass, wetlands, ruminants, or permafrost changes are similarly assumed to have a small effect on the CO_2 growth rate.

2.7.2 Anthropogenic carbon fluxes in the land to ocean aquatic continuum

The approach used to determine the global carbon budget considers only anthropogenic CO_2 emissions and their partitioning among the atmosphere, ocean, and land. In this analysis, the land and ocean reservoirs that take up anthropogenic CO_2 from the atmosphere are conceived as independent carbon storage repositories. This approach omits the fact that carbon is continuously displaced from the land to the ocean

through the land–ocean aquatic continuum (LOAC) comprising freshwaters, estuaries, and coastal areas (Bauer et al., 2013; Regnier et al., 2013). A significant fraction of this lateral carbon flux is entirely "natural" and is thus a steady-state component of the pre-industrial carbon cycle. However, changes in environmental conditions and land-use change have caused an increase in the lateral transport of carbon into the LOAC – a perturbation that is relevant for the global carbon budget presented here.

The results of the analysis of Regnier et al. (2013) can be summarised in two points of relevance for the anthropogenic CO_2 budget. First, the anthropogenic perturbation has increased the organic carbon export from terrestrial ecosystems to the hydrosphere at a rate of 1.0 ± 0.5 GtC yr^{-1}, mainly owing to enhanced carbon export from soils. Second, this exported anthropogenic carbon is partly respired through the LOAC, partly sequestered in sediments along the LOAC and, to a lesser extent, transferred in the open ocean where it may accumulate. The increase in storage of land-derived organic carbon in the LOAC and open ocean combined is estimated by Regnier et al. (2013) at 0.65 ± 0.35 GtC yr^{-1}. The implication of a substantial LOAC carbon accumulation is that S_{LAND} corresponds to carbon sequestered both in land ecosystems and in LOAC. We do not attempt to separate these two storage components in our study focused on S_{LAND}.

3 Results

3.1 Global carbon budget averaged over decades and its variability

The global carbon budget averaged over the last decade (2006–2015) is shown in Fig. 2. For this time period, 91 % of the total emissions ($E_{FF} + E_{LUC}$) were caused by fossil fuels and industry, and 9 % by land-use change. The total emissions were partitioned among the atmosphere (44 %), ocean (26 %), and land (30 %). All components except land-use-change emissions have grown since 1959 (Figs. 3 and 4), with important interannual variability in the growth rate in atmospheric CO_2 concentration and in the land CO_2 sink (Fig. 4) and some decadal variability in all terms (Table 8).

3.1.1 CO_2 emissions

Global CO_2 emissions from fossil fuels and industry have increased every decade from an average of 3.1 ± 0.2 GtC yr^{-1} in the 1960s to an average of 9.3 ± 0.5 GtC yr^{-1} during 2006–2015 (Table 8 and Fig. 5). The growth rate in these emissions decreased between the 1960s and the 1990s, with 4.5 % yr^{-1} in the 1960s (1960–1969), 2.8 % yr^{-1} in the 1970s (1970–1979), 1.9 % yr^{-1} in the 1980s (1980–1989), and 1.1 % yr^{-1} in the 1990s (1990–1999). After this period, the growth rate began increasing again in the 2000s at an average growth rate of 3.5 % yr^{-1}, decreasing to 1.8 % yr^{-1}
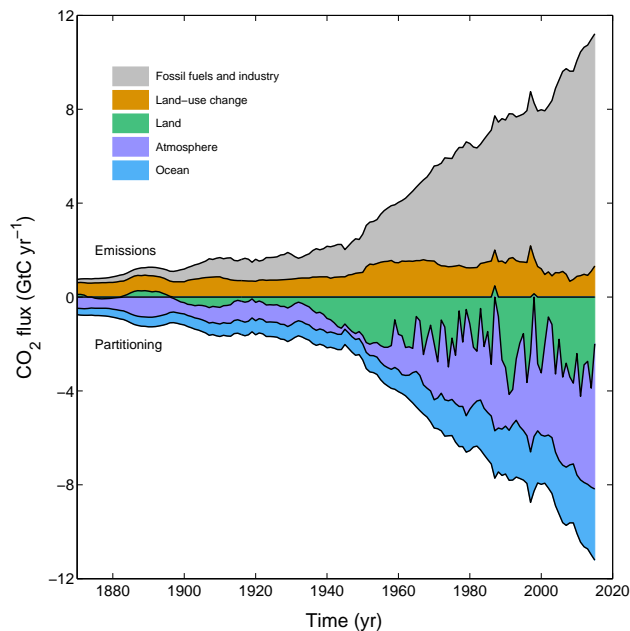
Figure 3. Combined components of the global carbon budget illustrated in Fig. 2 as a function of time, for emissions from fossil fuels and industry (E_{FF}; grey) and emissions from land-use change (E_{LUC}; brown), as well as their partitioning among the atmosphere (G_{ATM}; purple), land (S_{LAND}; green), and oceans (S_{OCEAN}; dark blue). All time series are in GtC yr^{-1}. G_{ATM} and S_{OCEAN} (and by construction also S_{LAND}) prior to 1959 are based on different methods. The primary data sources for fossil fuels and industry are from Boden and Andres (2016), with uncertainty of about ±5 % (±1σ); land-use-change emissions are from Houghton et al. (2012) with uncertainties of about ±30 %; growth rate in atmospheric CO_2 concentration prior to 1959 is from Joos and Spahni (2008) with uncertainties of about ±1–1.5 GtC decade^{-1} or ±0.1–0.15 GtC yr^{-1} (Bruno and Joos, 1997), and from Dlugokencky and Tans (2016) from 1959 with uncertainties of about ± 0.2 GtC yr^{-1}; the ocean sink prior to 1959 is from Khatiwala et al. (2013) with uncertainty of about ± 30%, and from this study from 1959 with uncertainties of about ±0.5 GtC yr^{-1}; and the residual land sink is obtained by difference (Eq. 8), resulting in uncertainties of about ±50 % prior to 1959 and ±0.8 GtC yr^{-1} after that. See the text for more details of each component and their uncertainties.

for the last decade (2006–2015). In contrast, CO_2 emissions from land-use change have remained relatively constant at around 1.3 ± 0.5 GtC yr^{-1} during 1960–2015. A decrease in emissions from land-use change is suggested between the 1990s and 2000s by the combination of bookkeeping and fire-based emissions used here (Table 7), but it is highly uncertain due to uncertainty in the underlying land-cover-change data. This decrease is not found in the current ensemble of the DGVMs (Fig. 6), which are otherwise consistent with the bookkeeping method within their respective uncertainty (Table 7). The decrease is also not found in the study of tropical deforestation of Achard et al. (2014), where the fluxes in the 1990s were similar to those of the 2000s and
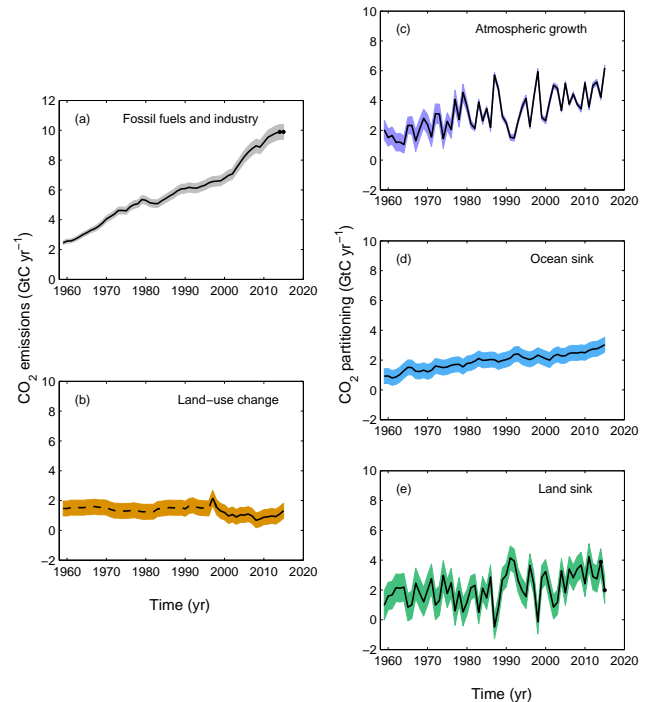

Figure 4. Components of the global carbon budget and their uncertainties as a function of time, presented individually for **(a)** emissions from fossil fuels and industry (E_{FF}), **(b)** emissions from land-use change (E_{LUC}), **(c)** growth rate in atmospheric CO_2 concentration (G_{ATM}), **(d)** the ocean CO_2 sink (S_{OCEAN}; positive indicates a flux from the atmosphere to the ocean), and **(e)** the land CO_2 sink (S_{LAND}; positive indicates a flux from the atmosphere to the land). All time series are in GtC yr^{-1} with the uncertainty bounds representing ±1σ in shaded colour. Data sources are as in Fig. 3. The black dots in **(a, e)** show values for 2014 and 2015 that originate from a different data set to the remainder of the data, while the dashed line in **(b)** highlights the start of satellite data use to estimate the interannual variability and extend the series in time (see text).

outside our uncertainty range. A new study based on FAO data to 2015 (Federici et al., 2015) suggests that E_{LUC} decreased during 2011–2015 compared to 2001–2010.

3.1.2 Partitioning among the atmosphere, ocean, and land

Emissions are partitioned among the atmosphere, ocean, and land (Eq. 1). The growth rate in atmospheric CO_2 level increased from 1.7 ± 0.1 GtC yr^{-1} in the 1960s to 4.5 ± 0.1 GtC yr^{-1} during 2006–2015 with important decadal variations (Table 8). Both ocean and land CO_2 sinks increased roughly in line with the atmospheric increase, but with significant decadal variability on land (Table 8). The ocean CO_2 sink increased from 1.2 ± 0.5 GtC yr^{-1} in the 1960s to 2.6 ± 0.5 GtC yr^{-1} during 2006–2015, with interannual variations of the order of a few tenths of GtC yr^{-1}
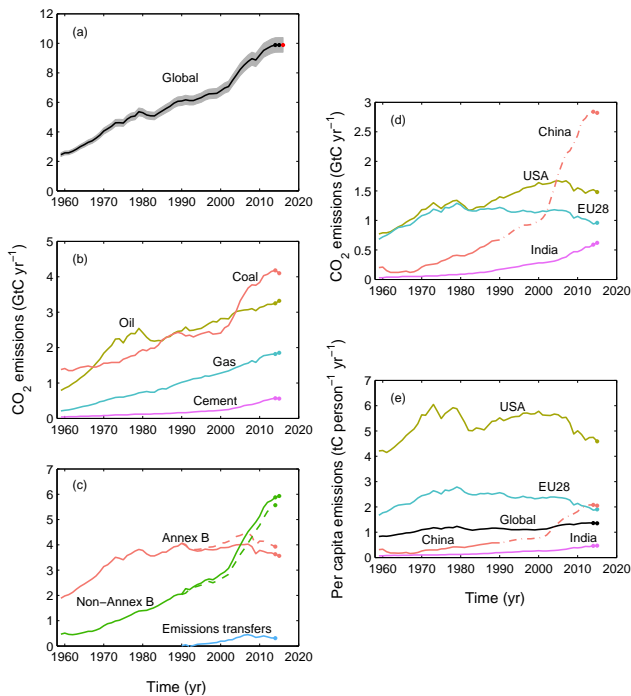
Figure 5. CO_2 emissions from fossil fuels and industry for **(a)** the globe, including an uncertainty of $\pm 5\%$ (grey shading), the emissions extrapolated using BP energy statistics (black dots), and the emissions projection for year 2016 based on GDP projection (red dot). **(b)** Global emissions by fuel type, including coal (salmon), oil (olive), gas (turquoise), and cement (purple), and excluding gas flaring which is small (0.6 % in 2013). **(c)** Territorial (solid line) and consumption (dashed line) emissions for the countries listed in Annex B of the Kyoto Protocol (salmon lines; mostly advanced economies with emissions limitations) vs. non-Annex B countries (green lines); also shown are the emissions transfer from non-Annex B to Annex B countries (light-blue line). **(d)** Territorial CO_2 emissions for the top three country emitters (USA – olive; China – salmon; India – purple) and for the European Union (EU; turquoise for the 28 member states of the EU as of 2012). **(e)** Per capita emissions for the top three country emitters and the EU (all colours as in panel **(d)**) and the world (black). In **(b–e)**, the dots show the data that were extrapolated from BP energy statistics for 2014 and 2015. All time series are in $GtC\,yr^{-1}$ except the per capita emissions **(e)**, which are in tonnes of carbon per person per year $(tC\,person^{-1}\,yr^{-1})$. Territorial emissions are primarily from Boden and Andres (2016) except for national data for the USA and EU28 for 1990–2014, which are reported by the countries to the UNFCCC as detailed in the text, and for China from 1990, which are estimated here from BP energy statistics (the latter shown as a dash-dot line); consumption-based emissions are updated from Peters et al. (2011a). See Sect. 2.1.1 for details of the calculations and data sources.

generally showing an increased ocean sink during El Niño events (i.e. 1982–1983, 1997–1998, 2015–2016) (Fig. 7; Rödenbeck et al., 2014). Although there is some coherence between the ocean models and data products and among data products regarding the mean, decadal variability, and trend, the ocean models and data products show poor agreement for interannual variability (Sect. 2.4.3 and Fig. 7). As shown in Fig. 7, the two data products and most model estimates produce a mean CO_2 sink for the 1990s that is below the mean assessed by the IPCC from indirect (but arguably more reliable) observations (Denman et al., 2007; Sect. 2.4.1). This discrepancy suggests we may need to reassess estimates of the mean ocean carbon sinks, with some implications for the cumulative carbon budget (Landschützer et al., 2016).

The residual terrestrial CO_2 sink increased from $1.7 \pm 0.7\,GtC\,yr^{-1}$ in the 1960s to $3.1 \pm 0.9\,GtC\,yr^{-1}$ during 2006–2015, with important interannual variations of up to $2\,GtC\,yr^{-1}$ generally showing a decreased land sink during El Niño events, overcompensating for the increase in ocean sink and accounting for the enhanced growth rate in atmospheric CO_2 concentration during El Niño events. The high uptake anomaly around year 1991 is thought to be caused by the effect of the volcanic eruption of Mount Pinatubo on climate and is not generally reproduced by the DGVMs, but it is assigned to the land by the two inverse systems that include this period (Fig. 6). The larger land CO_2 sink during 2006–2015 compared to the 1960s is reproduced by all the DGVMs in response to combined atmospheric CO_2 increase, climate, and variability, consistent with the budget residual and reflecting a common knowledge of the processes (Table 7). The DGVM ensemble mean of $2.8 \pm 0.7\,GtC\,yr^{-1}$ also reproduces the observed mean for the period 2006–2015 calculated from the budget residual (Table 7).

The total CO_2 fluxes on land ($S_{LAND} - E_{LUC}$) constrained by the atmospheric inversions show in general very good agreement with the global budget estimate, as expected given the strong constrains of G_{ATM} and the small relative uncertainty assumed on S_{OCEAN} and E_{FF} by inversions. The total land flux is of similar magnitude for the decadal average, with estimates for 2006–2015 from the three inversions of 2.2, 2.3, and $3.4\,GtC\,yr^{-1}$ compared to $2.1 \pm 0.7\,GtC\,yr^{-1}$ for the total flux computed with the carbon budget from other terms in Eq. (1) (Table 7). The total land sink from the three inversions is 1.8, 1.8, and $3.0\,GtC\,yr^{-1}$ when including a mean river flux adjustment of $0.45\,GtC\,yr^{-1}$, though the exact adjustment is in fact smaller because the anthropogenic contribution to river fluxes is only a fraction of the total river flux (Sect. 2.7.2). The interannual variability in the inversions also matched the residual-based S_{LAND} closely (Fig. 6). The total land flux from the DGVM multi-model mean also compares well with the estimate from the carbon budget and atmospheric inversions, with a decadal mean of $1.7 \pm 0.5\,GtC\,yr^{-1}$ (Table 7; 2006–2015), although individual models differ by several GtC for some years (Fig. 6).

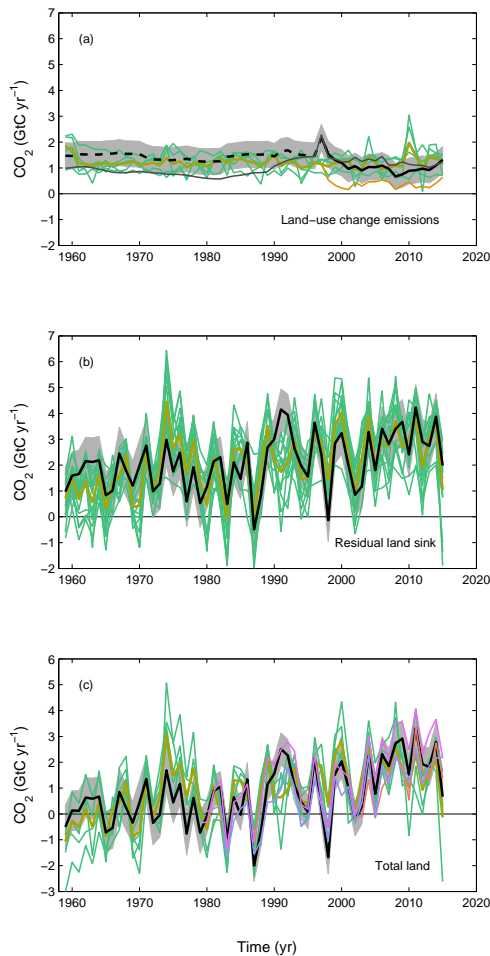**Figure 6.** CO_2 exchanges between the atmosphere and the terrestrial biosphere. **(a)** Comparison of the global carbon budget values of CO_2 emissions from land-use change (E_{LUC}; black with $\pm 1\sigma$ uncertainty in grey shading), with CO_2 emissions from land-use change showing individual DGVM results (green) and the multimodel mean (olive), as well as fire-based results (orange); land-use-change data prior to 1997 (dashed black) highlights the pre-satellite years; preliminary results using the FAO FRA 2015 (Houghton and Nassikas, 2016) are also shown in dark grey. **(b)** Land CO_2 sink (S_{LAND}; black with uncertainty in grey shading) showing individual DGVM results (green) and multi-model mean (olive). **(c)** Total land CO_2 fluxes (**b–a**; black with uncertainty in grey shading), from DGVM results (green) and the multi-model mean (olive), and atmospheric inversions Chevallier et al. (2005; CAMSv15.2) in purple; Rödenbeck et al. (2003; Jena CarboScope, s81_v3.8) in violet; Peters et al. (2010; Carbon Tracker, CTE2016-FT) in salmon; and the carbon balance from Eq. (1) (black). Five DGVMs are plotted in **(a)** and 14 in **(b, c)**; see Table 5 for the list and Table 6 for the description. In **(c)** the inversions were corrected for the pre-industrial land sink of CO_2 from river input by removing a sink of $0.45\,\mathrm{GtC\,yr^{-1}}$ (Jacobson et al., 2007). This correction does not take into account the anthropogenic contribution to river fluxes (see Sect. 2.7.2).
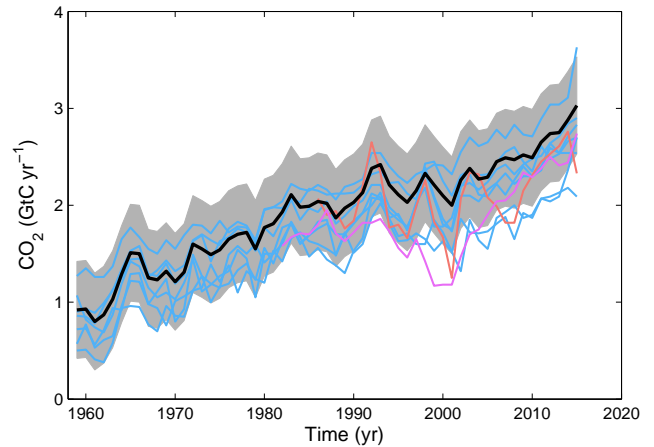

Figure 7. Comparison of the anthropogenic atmosphere–ocean CO_2 flux showing the budget values of S_{OCEAN} (black; with $\pm 1\sigma$ uncertainty in grey shading), individual ocean models before normalisation (blue), and the two ocean data-based products (Rödenbeck et al. (2014) in salmon and Landschützer et al. (2015) in purple; see Table 6). Both data-based products were adjusted for the pre-industrial ocean source of CO_2 from river input to the ocean, which is not present in the models, by adding a sink of $0.45\,\mathrm{GtC\,yr^{-1}}$ (Jacobson et al., 2007), to make them comparable to S_{OCEAN}. This adjustment does not take into account the anthropogenic contribution to river fluxes (see Sect. 2.7.2).

3.1.3 Regional distribution

Figure 8 shows the partitioning of the total surface fluxes excluding emissions from fossil fuels and industry ($S_{LAND} + S_{OCEAN} - E_{LUC}$) according to the process models in the ocean and on land, as well as to the three atmospheric inversions. The total surface fluxes provide information on the regional distribution of those fluxes by latitude bands (Fig. 8). The global mean CO_2 fluxes from process models for 2006–2015 is $4.2 \pm 0.6\,\mathrm{GtC\,yr^{-1}}$. This is comparable to the fluxes of $4.8 \pm 0.5\,\mathrm{GtC\,yr^{-1}}$ inferred from the remainder of the carbon budget ($E_{FF} - G_{ATM}$ in Eq. 1; Table 8) within their respective uncertainties. The total CO_2 fluxes from the three inversions range between 4.6 and $4.9\,\mathrm{GtC\,yr^{-1}}$, consistent with the carbon budget as expected from the constraints on the inversions.

In the south (south of 30° S), the atmospheric inversions and process models all suggest a CO_2 sink for 2006–2015 of between 1.2 and $1.6\,\mathrm{GtC\,yr^{-1}}$ (Fig. 8), although the details of the interannual variability are not fully consistent across methods. The interannual variability in the south is low because of the dominance of ocean area with low variability compared to land areas.

In the tropics (30° S–30° N), both the atmospheric inversions and process models suggest the carbon balance in this region is close to neutral over the past decade, with fluxes for 2006–2015 ranging between −0.5 and +0.6 $\mathrm{GtC\,yr^{-1}}$. Both the process-based models and the inversions consistently al-
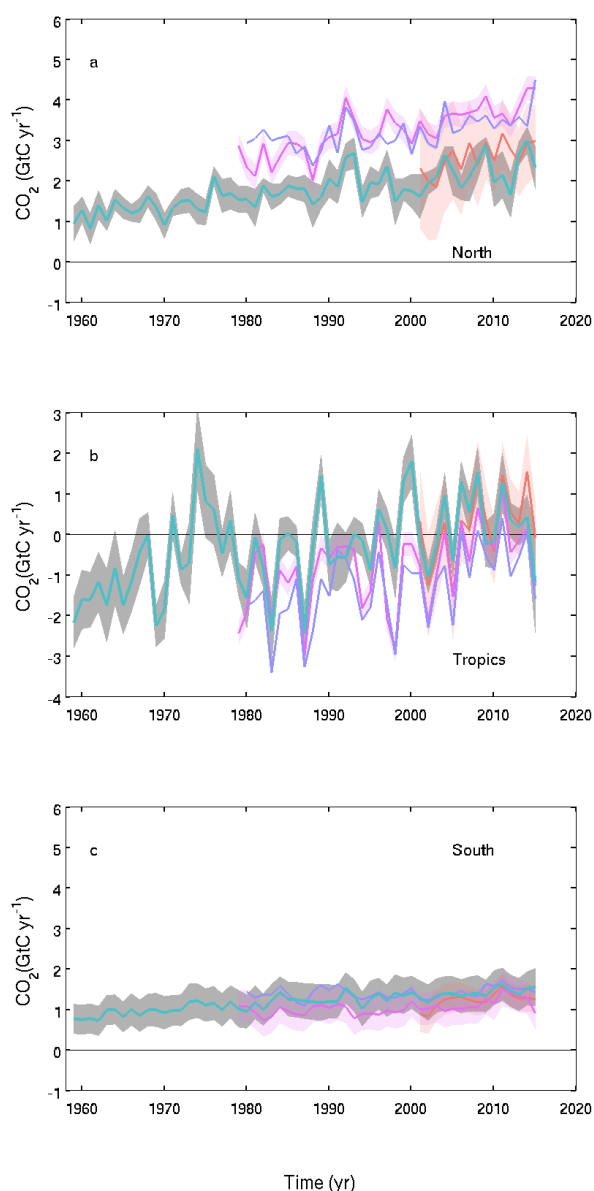
Figure 8. CO_2 fluxes between the atmosphere and the surface ($S_{OCEAN} + S_{LAND} - E_{LUC}$) by latitude bands for the **(a)** north (north of 30° N), **(b)** tropics (30° S–30° N), and **(c)** south (south of 30° S). Estimates from the combination of the multi-model means for the land and oceans are shown (turquoise) with $\pm 1\sigma$ of the model ensemble (in grey). Results from the three atmospheric inversions are shown from Chevallier et al. (2005; CAMSv15.2) in purple, Rödenbeck et al. (2003; Jena CarboScope, s81_v3.8) in blue, and Peters et al. (2010; CarbonTracker, CTE2016-FT) in salmon; see Table 6. Where available, the uncertainty in the inversions is also shown.

locate more year-to-year variability in CO_2 fluxes to the tropics compared to the north (north of 30° N; Fig. 8), this variability being dominated by land fluxes.

In the north (north of 30° N), the inversions and process models are not in agreement on the magnitude of the CO_2

sink with the ensemble mean of the process models suggesting a total Northern Hemisphere sink for 2006–2015 of 2.3 ± 0.4 GtC yr^{-1}, while the three inversions estimate a sink of 2.7, 3.8, and 3.8 GtC yr^{-1}. The mean difference can only partly be explained by the influence of river fluxes, which is seen by the inversions but not included in the process models, as this flux in the Northern Hemisphere would be less than 0.45 GtC yr^{-1}, particularly when only the anthropogenic contribution to river fluxes is accounted for. The CarbonTracker inversion is close to the one standard deviation of the process models for the mean sink during their overlap period. CAMS and Jena CarboScope give a higher sink in the north than the process models, and a correspondingly higher source in the tropics. Differences between CarbonTracker and CAMS, Jena CarboScope may be related to differences in inter-hemispheric mixing time of their transport models, and other inversion settings. Differences between the mean fluxes of CAMS, Jena CarboScope, and the ensemble of process models cannot be explained easily. They could reflect a bias either in these two inversions or in missing processes or biases in the process models, such as the lack of adequate parameterisations for forest management in the north and for forest degradation emissions in tropics for the DGVMs.

The estimated contribution of the north and its uncertainty from process models is sensitive both to the ensemble of process models used and to the specifics of each inversion. All three inversions show substantial differences in variability and/or trend, and one inversion shows a substantial difference in the mean Northern Hemisphere sink.

3.2 Global carbon budget for year 2015

3.2.1 CO_2 emissions

Global CO_2 emissions from fossil fuels and industry remained nearly constant at 9.9 ± 0.5 GtC in 2015 (Fig. 5), distributed among coal (41 %), oil (34 %), gas (19 %), cement (5.6 %), and gas flaring (0.7 %). Compared to the previous year, emissions from coal and cement decreased by −1.8 and −1.9 %, respectively, while emissions from oil and gas increased by 1.9 and 1.7 %, respectively. Due to lack of data, gas flaring in 2014 and 2015 is assumed the same as 2013.

Growth in emissions in 2015 was not statistically different from zero, at 0.06 % higher than in 2014, in stark contrast with the decadal average of 1.8 % yr^{-1} (2006–2015). Growth in 2015 is in the range of our projection change of −0.6 [−1.6 to +0.5] % made last year (Le Quéré et al., 2015a) based on national emissions projections for China and the USA, and projections of gross domestic product corrected for I_{FF} improvements for the rest of the world. However, the specific projection for 2015 for China made last year (likely range of −4.6 to −1.1 %) was for a larger decrease in emissions than realised (−0.7 %). This is due to lower decline in coal production in the last 4 months of the year compared to January–August and to improvements in

energy content of coal through improvements in the quality of the coal used which were at the top of the range of improvements considered in our projection.

In 2015, the largest contributions to global CO_2 emissions were from China (29 %), the USA (15 %), the EU (28 member states; 10 %), and India (6.3 %). The percentages are the fraction of the global emissions including bunker fuels (3.2 %). These four regions account for 59 % of global emissions. Growth rates for these countries from 2014 to 2015 were -0.7 % (China), -2.6 % (USA), $+1.4$ % (EU28), and $+5.2$ % (India). The per capita CO_2 emissions in 2015 were 1.3 tC person^{-1} yr^{-1} for the globe, and were 4.6 (USA), 2.1 (China), 1.9 (EU28), and 0.5 tC person^{-1} yr^{-1} (India) for the four highest emitting countries (Fig. 5e).

Territorial emissions in Annex B countries decreased by -0.2 % yr^{-1} on average during 1990–2014. Trends observed for consumption emissions were less monotonic, with 0.8 % yr^{-1} growth over 1990–2007 and a -1.5 % yr^{-1} decrease over 2007–2014 (Fig. 5c). In non-Annex B countries during 1990–2014, territorial emissions have grown at 4.7 % yr^{-1}, while consumption emissions have grown at 4.4 % yr^{-1}. In 1990, 65 % of global territorial emissions were emitted in Annex B countries (33 % in non-Annex B, and 2 % in bunker fuels used for international shipping and aviation), while in 2014 this had reduced to 37 % (60 % in non-Annex B, and 3 % in bunker fuels). In terms of consumption emissions this split was 67 % in 1990 and 41 % in 2014 (33 to 59 % in non-Annex B). The difference between territorial and consumption emissions (the net emission transfer via international trade) from non-Annex B to Annex B countries has increased from near zero in 1990 to 0.3 GtC yr^{-1} around 2005 and remained relatively stable afterwards until the last year available (2014; Fig. 5). The increase in net emission transfers of 0.30 GtC yr^{-1} between 1990 and 2014 compares with the emission reduction of 0.4 GtC yr^{-1} in Annex B countries. These results show the importance of net emission transfer via international trade from non-Annex B to Annex B countries, as well as the stabilisation of emissions transfers when averaged over Annex B countries during the past decade. In 2014, the biggest emitters from a consumption perspective were China (25 % of the global total), USA (16 %), EU28 (12 %), and India (5 %).

Based on fire activity, the global CO_2 emissions from land-use change are estimated as 1.3 ± 0.5 GtC in 2015, slightly above the 2006–2015 average of 1.0 ± 0.5 GtC yr^{-1}. The slight rise in E_{LUC} in 2015 is consistent with estimates of peat fires in Asia based on atmospheric data (Yin et al., 2016). However, the estimated annual variability is not generally consistent between methods, except that all methods estimate that variability in E_{LUC} is small relative to the variability from S_{LAND} (Fig. 6a). This could be partly due to the design of the DGVM experiments, which use flux differences between simulations with and without land-cover change, and thus their variability may differ due to, for example, fires in forest regions where the contemporary forest

cover is smaller than pre-industrial cover used in the "without land-cover change" runs.

3.2.2 Partitioning among the atmosphere, ocean, and land

The growth rate in atmospheric CO_2 concentration was 6.3 ± 0.2 GtC in 2015 (2.97 ± 0.09 ppm; Fig. 4; Dlugokencky and Tans, 2016). This is well above the 2006–2015 average of 4.5 ± 0.1 GtC yr^{-1} and reflects the large interannual variability in the growth rate of atmospheric CO_2 concentration associated with El Niño and La Niña events.

The ocean CO_2 sink was 3.0 ± 0.5 GtC yr^{-1} in 2015, an increase of 0.15 GtC yr^{-1} over 2015 according to ocean models. Five of the seven ocean models produce an increase in the ocean CO_2 sink in 2015 compared to 2014, with near-zero changes in the last two models (Fig. 7). However, the two data products disagree over changes in the last year, with a decrease of -0.4 GtC yr^{-1} found in Rödenbeck et al. (2014) and an increase of 0.3 GtC yr^{-1} found in Landschützer et al. (2015). Thus, there is no overall consistency in the annual change in the ocean CO_2 sink, although there is an indication of increasing convergence among products for the assessment of multi-year changes, as suggested by the time-series correlations reported in Sect. 2.4.3 (see also Landschützer et al., 2015). An increase in the ocean CO_2 sink in 2015 would be consistent with the observed El Niño conditions and continued rising atmospheric CO_2. All estimates suggest an ocean CO_2 sink for 2015 that is larger than their 2006–2015 average.

The terrestrial CO_2 sink calculated as the residual from the carbon budget was 1.9 ± 0.9 GtC in 2015, well below the 3.1 ± 0.9 GtC yr^{-1} averaged over 2006–2015 (Fig. 4), and reflecting the onset of the El Niño conditions in the second half of 2015. The DGVM mean produces a sink of 1.0 ± 1.4 GtC in 2015, also well below the 2006–2015 average (Table 7). Both models and inversions suggest that the lower sink in 2015 primarily originated in the tropics (Fig. 8).

3.3 Emission projections and the global carbon budget for year 2016

3.3.1 CO_2 emissions

Using separate projections for China, the USA, and the rest of the world as described in Sect. 2.1.4, we project a continued low growth in global CO_2 emissions from fossil fuels and cement production in 2016 of $+0.5$ % (range of -0.7 to $+2.1$ %) from 2015 levels (Table 9), or $+0.2$ % (-1.0 to $+1.8$ %) after adjusting for leap year (see Sect. 2.1.3). Our method is imprecise and contains several assumptions that could influence the results beyond the given range, and as such is indicative only. Within the given assumptions, global emissions remain nearly constant at 9.9 ± 0.5 GtC (36.4 ± 1.8 GtCO$_2$) in 2016, but they are still 63% above

Table 9. Actual CO_2 emissions from fossil fuels and industry (E_{FF}) compared to projections made the previous year based on world GDP (IMF October 2015) and the fossil fuel intensity of GDP (I_{FF}) based on subtracting the CO_2 and GDP growth rates. The "Actual" values are the latest estimate available and the "Projected" value for 2016 refers to those presented in this paper. No correction for leap years is applied (Sect. 2.1.3).

	E_{FF}		GDP		I_{FF}	
	Projected	Actual	Projected	Actual	Projected	Actual
2009[a]	−2.8 %	−1.1 %	−1.1 %	−0.05 %	−1.7 %	−1.1 %
2010[b]	> 3 %	5.7 %	4.8 %	5.4 %	> −1.7 %	+0.3 %
2011[c]	3.1 ± 1.5 %	4.1 %	4.0 %	4.2 %	−0.9 ± 1.5 %	−0.2 %
2012[d]	2.6 %[i] (1.9 to 3.5)	1.7 %	3.3 %	3.5 %	−0.7 %	−1.8 %
2013[e]	2.1 % (1.1 to 3.1)	1.1 %	2.9 %	3.3 %	−0.8 %	−2.2 %
2014[f]	2.5 % (1.3 to 3.5)	0.8 %	3.3 %	3.0 %	−0.7 %	−2.6 %

Change in method

	E_{FF}		E_{FF} (China)		E_{FF} (USA)		E_{FF} (rest of world)	
	Projected	Actual	Projected	Actual	Projected	Actual	Projected	Actual
2015[g]	−0.6 % (−1.6 to 0.5)	0.05 %	−3.9 % (−4.6 to −1.1)	−0.7 %	−1.5 % (−5.5 to 0.3)	−2.6 %	1.2 % (−0.2 to 2.6)	1.2 %
2016[h]	+0.5 %[i] (−1.7 to +2.1)	–	−0.2 %[i] (−3.5 to +1.6)	–	−1.4 %[i] (−3.7 to +0.9)	–	+1.3 %[i] (−0.2 to +2.8)	–

[a] Le Quéré et al. (2009). [b] Friedlingstein et al. (2010). [c] Peters et al. (2013). [d] Le Quéré et al. (2013). [e] Le Quéré et al. (2014). [f] Friedlingstein et al. (2014) and Le Quéré et al. (2015b). [g] Jackson et al. (2016) and Le Quéré et al. (2015a). [h] This study. [i] These numbers are not adjusted for leap years (see Sect. 2.1.3 for leap-year adjustments).

emissions in 1990. The drivers of the trends in E_{FF} are discussed elsewhere (Peters et al., 2016).

For China, the expected change based on available data during January to July or September (see Sect. 2.1.4) is for an increase in emissions of −0.2 % (range of −3.5 to +1.6 %) in 2016 compared to 2015, or −0.5 % (range of −3.8 to +1.3 %) after adjusting for leap year (see Sect. 2.1.3). This is based on estimated decreases in coal consumption (−1.8 %) and estimated growth in apparent oil (+4.0 %) and natural gas (+7.2 %) consumption and in cement production (+2.6 %). The uncertainty range considers the spread between different data sources, as well as differences between July/August and end-of-year data observed in 2014 and 2015. The estimated reduction in coal consumption also incorporates an assumed 2 % increase in the energy density of coal – based on increases in the last 2 years, which are assumed to continue given production limits in 2016 that are likely to affect production of low-quality coal more – and the uncertainty range also reflects uncertainty in this figure.

For the USA, the EIA emissions projection for 2016 combined with cement data from USGS gives a decrease of −1.4 % (range of −3.7 to +0.9 %) compared to 2015, or −1.7 % (range of −4.0 to +0.6 %) after adjusting for leap year (see Sect. 2.1.3).

For the rest of the world, the expected growth for 2016 of +1.3 % (range of −0.2 to +2.8 %), or +1.0 % (range of −0.4 to +2.5 %) after adjusting for leap year (see Sect. 2.1.3). This is computed using the GDP projection for the world excluding China and the USA of 2.5 % made by the IMF (IMF, 2016) and a decrease in I_{FF} of −1.2 % yr^{-1}, which is the average from 2006 to 2015. The uncertainty range is based on the standard deviation of the interannual variability in I_{FF} during 2006–2015 of ±1.0 % yr^{-1} and our estimate of uncertainty in the IMF's GDP forecast of ±0.5 %.

3.3.2 Partitioning among the atmosphere, ocean, and land

The growth in atmospheric CO_2 concentration (G_{ATM}) was projected to be high again in 2016, at 6.7 ± 1.1 GtC (3.15 ± 0.53 ppm) for the Mauna Loa station (Betts et al., 2016). Growth at Mauna Loa is closely correlated with the global growth ($r = 0.95$ for 1959–2015). Therefore, the global growth rate in atmospheric CO_2 concentration is also expected to be high in 2016. In the 8-month period between December 2015 and August 2016, the observed global growth in atmospheric CO_2 concentration was already 2.3 ppm (Dlugokencky and Tans, 2016) after seasonal adjustment, supporting the projection of Betts et al. (2016). Even with a return to El Niño neutral or possible emerging La Niña conditions for the second half of 2016, positive growth in atmospheric CO_2 would still be expected during the last

4 months of the year because of the continuing persistent emissions. For example, during the transitions from El Niño to La Niña of 1986–1987, 1998–1999, and 2010–2011, atmospheric CO_2 growth of 0.3, 0.6, and 0.9 ppm, respectively, was observed in the last 4 months of the year.

Combining projected E_{FF} and G_{ATM} suggests a total for the combined land and ocean ($S_{LAND} + S_{OCEAN} - E_{LUC}$) of about 3 GtC only. S_{OCEAN} was 3.0 GtC in 2015 and is expected to slightly increase in 2016 from a delayed response to El Niño conditions (Feely et al., 1999). E_{LUC} was 1.3 GtC in 2015, above the decadal mean average of 1.0 GtC yr^{-1}, and is expected to return to average or below average in 2016 based on fire activity related to land management so far (up to August). Hence, for 2016, the residual land sink S_{LAND} is expected to be well below its 2006–2015 average and approximately balance E_{LUC}. This is consistent with our understanding of the response of the terrestrial vegetation to El Niño conditions and increasing atmospheric CO_2 concentrations, though the uncertainties in G_{ATM} and of the partitioning among S_{LAND} and S_{OCEAN} are substantial.

3.4 Cumulative emissions

Cumulative emissions for 1870–2015 were 410 ± 20 GtC for E_{FF}, and 145 ± 50 GtC for E_{LUC} based on the bookkeeping method of Houghton et al. (2012) for 1870–1996 and a combination with fire-based emissions for 1997–2015 as described in Sect. 2.2 (Table 10). The cumulative emissions are rounded to the nearest 5 GtC. The total cumulative emissions from fossil and land-use change for 1870–2015 are 555 ± 55 GtC. These emissions were partitioned among the atmosphere (235 ± 5 GtC based on atmospheric measurements in ice cores of 288 ppm (Sect. 2.3; Joos and Spahni, 2008) and recent direct measurements of 399.1 ppm (Dlugokencky and Tans, 2016), ocean (160 ± 20 GtC using Khatiwala et al. , 2013, prior to 1959 and Table 8 otherwise), and land (160 ± 60 GtC by the difference).

Cumulative emissions for the early period 1750–1869 were 3 GtC for E_{FF} and about 45 GtC for E_{LUC} (rounded to nearest 5), of which 10 GtC was emitted in the period 1850–1870 (Houghton et al., 2012) and 30 GtC in the period 1750–1850 based on the average of four publications (22 GtC by Pongratz et al., 2009; 15 GtC by van Minnen et al., 2009; 64 GtC by Shevliakova et al., 2009; and 24 GtC by Zaehle et al., 2011). The growth rate in atmospheric CO_2 concentration during that time was about 25 GtC, and the ocean uptake about 20 GtC, implying a land uptake of 5 GtC. These numbers have large relative uncertainties but balance within the limits of our understanding.

Cumulative emissions for 1750–2015 based on the sum of the two periods above (before rounding to the nearest 5 GtC) were 410 ± 20 GtC for E_{FF}, and 190 ± 65 GtC for E_{LUC}, for a total of 600 ± 70 GtC, partitioned among the atmosphere (260 ± 5 GtC), ocean (175 ± 20 GtC), and land (165 ± 70 GtC).

Cumulative emissions through to year 2016 can be estimated based on the 2016 projections of E_{FF} (Sect. 3.2), the largest contributor, and assuming a constant E_{LUC} of 1.0 GtC (average of last decade). For 1870–2016, these are 565 ± 55 GtC (2075 ± 205 GtCO$_2$) for total emissions, with about 75 % contribution from E_{FF} (420 ± 20 GtC) and about 25 % contribution from E_{LUC} (150 ± 50 GtC). Cumulative emissions since year 1870 are higher than the emissions of 515 [445 to 585] GtC reported in the IPCC (Stocker et al., 2013) because they include an additional 55 GtC from emissions in 2012–2016 (mostly from E_{FF}). The uncertainty presented here ($\pm 1\sigma$) is smaller than the range of 90 % used by IPCC, but both estimates overlap within their uncertainty ranges.

4 Discussion

Each year when the global carbon budget is published, each component for all previous years is updated to take into account corrections that are the result of further scrutiny and verification of the underlying data in the primary input data sets. The updates have generally been relatively small and focused on the most recent years, except for land-use change, where they are more significant but still generally within the provided uncertainty range (Fig. 9). The difficulty in accessing land-cover change data to estimate E_{LUC} is the key problem to providing continuous records of emissions in this sector. Current FAO estimates are based on statistics reported at the country level and are not spatially explicit. Advances in satellite recovery of land-cover change could help to keep track of land-use change through time (Achard et al., 2014; Harris et al., 2012). Revisions in E_{LUC} for the 2008/2009 budget were the result of the release of FAO 2010, which contained a major update to forest cover change for the period 2000–2005 and provided the data for the following 5 years to 2010 (Fig. 9b). The differences this year could be attributable to both the different data and the different methods. Comparison of global carbon budget components released annually by GCP since 2006 show that update differences were highest at 0.82 GtC yr^{-1} for the growth rate in atmospheric CO_2 concentration (from a one-off correction back to year 1979), 0.24 GtC yr^{-1} for fossil fuels and industry, and 0.52 GtC yr^{-1} for the ocean CO_2 sink (from a change from one to multiple models; Fig. 9d). The update for the residual land CO_2 sink was also large (Fig. 9e), with a maximum value of 0.83 GtC yr^{-1}, directly reflecting revisions in other terms of the budget.

Our capacity to constrain the global carbon budget can be evaluated by adding the five components of Eq. (1) using DGVM estimates for S_{LAND}, thus using largely independent estimates for each component (Fig. 10). This residual global budget represents all the carbon unaccounted currently. Figure 10 shows that the mean global residual is close to zero, and there is no trend over the entire time period. However,

Table 10. Cumulative CO_2 emissions for different time periods in gigatonnes of carbon (GtC). We also provide the 1850–2005 time period used in a number of model evaluation publications. All uncertainties are reported as $\pm 1\sigma$. All values are rounded to the nearest 5 GtC as in Stocker et al. (2013), reflecting the limits of our capacity to constrain cumulative estimates. Thus, some columns will not exactly balance because of rounding errors.

Units of GtC	1750–2015	1850–2005	1870–2015	1870–2016
Emissions				
Fossil fuels and industry (E_{FF})	410 ± 20	320 ± 15	410 ± 20	420 ± 20*
Land-use-change emissions (E_{LUC})	190 ± 65	150 ± 55	145 ± 50	150 ± 50*
Total emissions	600 ± 70	470 ± 55	555 ± 55	565 ± 55*
Partitioning				
Growth rate in atmospheric CO_2 concentration (G_{ATM})	260 ± 5	195 ± 5	235 ± 5	
Ocean sink (S_{OCEAN})	175 ± 20	160 ± 20	160 ± 20	
Residual terrestrial sink (S_{LAND})	165 ± 70	115 ± 60	160 ± 60	

* The extension to year 2016 uses the emissions projections for fossil fuels and industry for 2016 (Sect. 3.2) and assumes a constant E_{LUC} flux (Sect. 2.2).

it also highlights periods of multiple years where the sum of the estimates differs significantly from zero. These include an unaccounted flux from the surface to the atmosphere (or underestimated emissions) during 1973–1979 and 1997–2001 and an unaccounted sink from the atmosphere to the surface (or overestimated emissions) during 1961–1965 and 1990–1992. This unaccounted variability could come from errors in our estimates of the five components of Equation (1; Li et al., 2016), or from missing factors in the global carbon budget, including but not limited to those discussed in Sect. 2.7. This unaccounted variability limits our ability to verify reported emissions and limits our confidence in the underlying processes regulating the carbon cycle feedbacks with climate change.

Another semi-independent way to evaluate the results is provided through the comparison with the atmospheric inversions and their regional breakdown. The comparison shows a first-order consistency between inversions and process models but with substantial discrepancies, particularly for the allocation of the mean sink between the tropics and the Northern Hemisphere. Understanding these discrepancies and further analysis of regional carbon budgets would provide additional information to quantify and improve our estimates, as has been shown by the project REgional Carbon Cycle Assessment and Processes (RECCAP; Canadell et al., 2012).

Annual estimates of each component of the global carbon budgets have their limitations, some of which could be improved with better data and/or better understanding of carbon dynamics. The primary limitations involve resolving fluxes on annual timescales and providing updated estimates for recent years for which data-based estimates are not yet available or only beginning to emerge. Of the various terms in the global budget, only the burning of fossil fuels and the growth rate in atmospheric CO_2 concentration terms are based primarily on empirical inputs supporting annual estimates in this carbon budget. While these models represent the current state of the art, they provide only simulated changes in primary carbon budget components. For example, the decadal trends in global ocean uptake and the interannual variations associated with the El Niño–Southern Ocean Oscillation (ENSO) are not directly constrained by observations, although many of the processes controlling these trends are sufficiently well known that the model-based trends still have value as benchmarks for further validation. Data-based products for the ocean CO_2 sink provide new ways to evaluate the model results, and could be used directly as data become more rapidly available and methods for creating such products improve. However, there are still large discrepancies among data-based estimates, in large part due to the lack of routine data sampling, which precludes their direct use for now (Rödenbeck et al., 2015). Estimates of land-use emissions and their year-to-year variability have even larger uncertainty, and much of the underlying data are not available as an annual update. Efforts are underway to work with annually available satellite area change data or FAO reported data in combination with fire data and modelling to provide annual updates for future budgets.

Our approach also depends on the reliability of the energy and land-cover change statistics provided at the country level, which are potentially subject to biases. Thus, it is critical to develop multiple ways to estimate the carbon balance at the global and regional level, including estimates from the inversion of atmospheric CO_2 concentration, the use of other oceanic and atmospheric tracers, and the compilation of emissions using alternative statistics (e.g. sectors). It is also important to challenge the consistency of information across observational streams, for example to contrast the coherence of temperature trends with those of CO_2 sink trends. Multiple approaches ranging from global to regional scale would greatly help increase confidence and reduce uncertainty in CO_2 emissions and their fate.
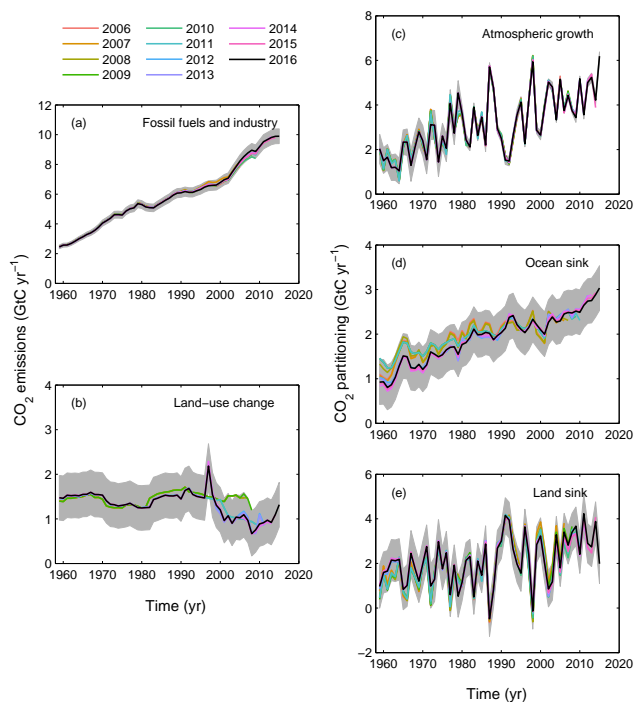
Figure 9. Comparison of global carbon budget components released annually by GCP since 2006. CO_2 emissions from **(a)** fossil fuels and industry (E_{FF}) and **(b)** land-use change (E_{LUC}), as well as their partitioning among **(c)** the atmosphere (G_{ATM}), **(d)** the ocean (S_{OCEAN}), and **(e)** the land (S_{LAND}). See legend for the corresponding years, and Table 3 for references. The budget year corresponds to the year when the budget was first released. All values are in $GtC\,yr^{-1}$. Grey shading shows the uncertainty bounds representing $\pm 1\sigma$ of the current global carbon budget.

5 Data availability

The data presented here are made available in the belief that their wide dissemination will lead to greater understanding and new scientific insights into how the carbon cycle works, how humans are altering it, and how we can mitigate the resulting human-driven climate change. The free availability of these data does not constitute permission for publication of the data. For research projects, if the data are essential to the work, or if an important result or conclusion depends on the data, co-authorship may need to be considered. Full contact details and information on how to cite the data are given at the top of each page in the accompanying database and are summarised in Table 2.

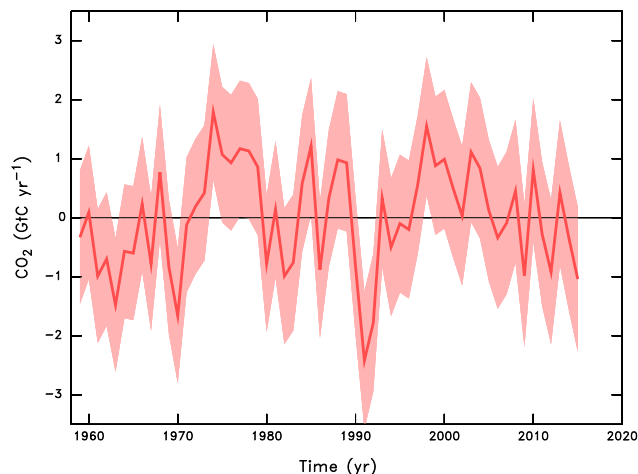The accompanying database includes two Excel files organised in the following spreadsheets (accessible with the free viewer http://www.microsoft.com/en-us/download/details.aspx?id=10).

Figure 10. Unaccounted carbon in the global carbon budget ($GtC\,yr^{-1}$). This is calculated as the sum of G_{ATM} plus S_{OCEAN} minus E_{FF} and E_{LUC} as described in Fig. 4, plus S_{LAND} as estimated with the ensemble of DGVMs as in Fig. 6b. Therefore, the unaccounted carbon represents the fluxes that are missing after accounting for all known processes as quantified in available estimates (see discussion). The uncertainty is the annual uncertainty for the five terms as described in the text, added in quadrature. Positive values indicate an unaccounted surface-to-atmosphere flux of CO_2 or an underestimation of the emissions.

File Global_Carbon_Budget_2016v1.0.xlsx includes the following:

1. Summary

2. The global carbon budget (1959–2015)

3. Global CO_2 emissions from fossil fuels and cement production by fuel type, and the per capita emissions (1959–2015)

4. CO_2 emissions from land-use change from the individual methods and models (1959–2015)

5. Ocean CO_2 sink from the individual ocean models and data products (1959–2015)

6. Terrestrial residual CO_2 sink from the DGVMs (1959–2015)

7. Additional information on the carbon balance prior to 1959 (1750–2015)

File National_Carbon_Emissions_2016v1.0.xlsx includes the following:

1. Summary

2. Territorial country CO_2 emissions from fossil fuels and industry (1959–2015) from CDIAC, extended to 2015 using BP data

3. Territorial country CO_2 emissions from fossil fuels and industry (1959–2015) from CDIAC with UNFCCC data overwritten where available, extended to 2015 using BP data

4. Consumption country CO_2 emissions from fossil fuels and industry and emissions transfer from the international trade of goods and services (1990–2014) using CDIAC/UNFCCC data (worksheet 3 above) as reference

5. Emissions transfers (consumption minus territorial emissions; 1990–2014)

6. Country definitions

7. Details of disaggregated countries

8. Details of aggregated countries

National emissions data are also available from the Global Carbon Atlas (http://globalcarbonatlas.org).

6 Conclusions

The estimation of global CO_2 emissions and sinks is a major effort by the carbon cycle research community that requires a combination of measurements and compilation of statistical estimates and results from models. The delivery of an annual carbon budget serves two purposes. First, there is a large demand for up-to-date information on the state of the anthropogenic perturbation of the climate system and its underpinning causes. A broad stakeholder community relies on the data sets associated with the annual carbon budget, including scientists, policy makers, businesses, journalists, and the broader society increasingly engaged in adapting to and mit-

igating human-driven climate change. Second, over the last decade we have seen unprecedented changes in the human and biophysical environments (e.g. increase in the growth of fossil fuel emissions, ocean temperatures, and strength of the land sink), which call for more frequent assessments of the state of the planet and, by implication, a better understanding of the future evolution of the carbon cycle. Both the ocean and the land surface presently remove a large fraction of anthropogenic emissions. Any significant change in the function of carbon sinks is of great importance to climate policy-making, as they affect the excess carbon dioxide remaining in the atmosphere and therefore the compatible emissions for any climate stabilisation target. Better constraints of carbon cycle models against contemporary data sets raise the capacity for the models to become more accurate at future projections.

This all requires more frequent, robust, and transparent data sets and methods that can be scrutinised and replicated. After 11 annual releases from the GCP, the effort is growing and the traceability of the methods has become increasingly complex. Here, we have documented in detail the data sets and methods used to compile the annual updates of the global carbon budget, explained the rationale for the choices made and the limitations of the information, and finally highlighted the need for additional information where gaps exist.

This paper via "living data" will help to keep track of new budget updates. The evolution over time of the carbon budget is now a key indicator of the anthropogenic perturbation of the climate system, and its annual delivery joins a set of other climate indicators to monitor the evolution of human-induced climate change, such as the annual updates on the global surface temperature, sea level rise, and minimum Arctic sea ice extent.

Appendix A

Table A1. Attribution of fCO_2 measurements for year 2015 included in addition to SOCAT v4 (Bakker et al., 2016) to inform ocean data products.

Vessel	Start date yyyy-mm-dd	End date yyyy-mm-dd	Regions	No. of samples	Principal investigators	DOI (if available)/comment
Atlantic Companion	2015-03-03	2015-03-10	North Atlantic	8496	Steinhoff, T.; Becker, M.; Körtzinger, A.	doi:10.3334/CDIAC/OTG.VOS_Atlantic_Companion_Line_2015
Atlantic Companion	2015-03-30	2015-04-07	North Atlantic	9265	Steinhoff, T.; Becker, M.; Körtzinger, A.	doi:10.3334/CDIAC/OTG.VOS_Atlantic_Companion_Line_2015
Aurora Australis	2014-12-05	2015-01-24	Southern Ocean	41 463	Tilbrook, B.	doi:10.3334/CDIAC/OTG.VOS_AA_2014
Benguela Stream	2015-01-08	2015-01-14	North Atlantic, Tropical Atlantic	4664	Schuster, U.; Jones, S.D.; Watson, A.J.	doi:10.3334/CDIAC/OTG.VOS_BENGUELA_STREAM_2015
Benguela Stream	2015-02-05	2015-02-12	North Atlantic, Tropical Atlantic	4056	Schuster, U.; Jones, S.D.; Watson, A.J.	doi:10.3334/CDIAC/OTG.VOS_BENGUELA_STREAM_2015
Benguela Stream	2015-02-22	2015-03-01	North Atlantic, Tropical Atlantic	6158	Schuster, U.; Jones, S.D.; Watson, A.J.	doi:10.3334/CDIAC/OTG.VOS_BENGUELA_STREAM_2015
Benguela Stream	2015-04-30	2015-05-07	North Atlantic, Tropical Atlantic	6125	Schuster, U.; Jones, S.D.; Watson, A.J.	doi:10.3334/CDIAC/OTG.VOS_BENGUELA_STREAM_2015
Benguela Stream	2015-05-17	2015-05-24	North Atlantic, Tropical Atlantic	6152	Schuster, U.; Jones, S.D.; Watson, A.J.	doi:10.3334/CDIAC/OTG.VOS_BENGUELA_STREAM_2015
Benguela Stream	2015-05-27	2015-06-04	North Atlantic, Tropical Atlantic	6116	Schuster, U.; Jones, S.D.; Watson, A.J.	doi:10.3334/CDIAC/OTG.VOS_BENGUELA_STREAM_2015
Benguela Stream	2015-06-24	2015-07-02	North Atlantic, Tropical Atlantic	6538	Schuster, U.; Jones, S.D.; Watson, A.J.	doi:10.3334/CDIAC/OTG.VOS_BENGUELA_STREAM_2015
Benguela Stream	2015-07-11	2015-07-19	North Atlantic, Tropical Atlantic	6220	Schuster, U.; Jones, S.D.; Watson, A.J.	doi:10.3334/CDIAC/OTG.VOS_BENGUELA_STREAM_2015
Benguela Stream	2015-07-22	2015-07-30	North Atlantic, Tropical Atlantic	6534	Schuster, U.; Jones, S.D.; Watson, A.J.	doi:10.3334/CDIAC/OTG.VOS_BENGUELA_STREAM_2015
Benguela Stream	2015-08-08	2015-08-16	North Atlantic, Tropical Atlantic	6727	Schuster, U.; Jones, S.D.; Watson, A.J.	doi:10.3334/CDIAC/OTG.VOS_BENGUELA_STREAM_2015
Benguela Stream	2015-08-19	2015-08-27	North Atlantic, Tropical Atlantic	6811	Schuster, U.; Jones, S.D.; Watson, A.J.	doi:10.3334/CDIAC/OTG.VOS_BENGUELA_STREAM_2015
Cap Blanche	2015-03-28	2015-04-10	Tropical Pacific, Southern Ocean	6117	Cosca C.; Feely R.; Alin S.	doi:10.3334/CDIAC/OTG.VOS_CAP_BLANCHE_2015
Cap Blanche	2015-09-30	2015-10-12	Tropical Pacific, Southern Ocean	5582	Cosca C.; Feely R.; Alin S.	doi:10.3334/CDIAC/OTG.VOS_CAP_BLANCHE_2015
Cap Blanche	2015-11-20	2015-12-04	Tropical Pacific, Southern Ocean	6677	Cosca C.; Feely R.; Alin S.	doi:10.3334/CDIAC/OTG.VOS_CAP_BLANCHE_2015
Cap San Lorenzo	2015-02-28	2015-03-12	North Atlantic, Tropical Atlantic	5699	Lefèvre, N., Diverrès D.	
Cap San Lorenzo	2015-03-31	2015-04-06	Tropical Atlantic	2654	Lefèvre, N., Diverrès D.	
Cap San Lorenzo	2015-04-28	2015-05-07	North Atlantic, Tropical Atlantic	4335	Lefèvre, N., Diverrès D.	
Cap San Lorenzo	2015-06-20	2015-07-01	North Atlantic, Tropical Atlantic	5833	Lefèvre, N., Diverrès D.	
Cap San Lorenzo	2015-07-29	2015-08-04	North Atlantic	2934	Lefèvre, N., Diverrès D.	
Colibri	2015-02-26	2015-03-10	North Atlantic, Tropical Atlantic	4615	Lefèvre, N., Diverrès D.	
Colibri	2015-03-12	2015-03-23	North Atlantic, Tropical Atlantic	5561	Lefèvre, N., Diverrès D.	
Colibri	2015-05-26	2015-06-04	North Atlantic, Tropical Atlantic	3683	Lefèvre, N., Diverrès D.	
Colibri	2015-06-07	2015-06-18	North Atlantic, Tropical Atlantic	5613	Lefèvre, N., Diverrès D.	
Equinox	2015-02-24	2015-03-06	Tropical Atlantic	3563	Wanninkhof, R.; Pierrot, D.; Barbero, L.	doi:10.3334/CDIAC/OTG.VOS_EQNX_2015
Equinox	2015-03-07	2015-03-11	Tropical Atlantic	1588	Wanninkhof, R.; Pierrot, D.; Barbero, L.	doi:10.3334/CDIAC/OTG.VOS_EQNX_2015
Equinox	2015-03-19	2015-03-27	Tropical Atlantic	2694	Wanninkhof, R.; Pierrot, D.; Barbero, L.	doi:10.3334/CDIAC/OTG.VOS_EQNX_2015
Equinox	2015-03-27	2015-04-06	Tropical Atlantic	3607	Wanninkhof, R.; Pierrot, D.; Barbero, L.	doi:10.3334/CDIAC/OTG.VOS_EQNX_2015
Equinox	2015-04-06	2015-04-17	Tropical Atlantic	3750	Wanninkhof, R.; Pierrot, D.; Barbero, L.	doi:10.3334/CDIAC/OTG.VOS_EQNX_2015
Equinox	2015-04-17	2015-04-27	Tropical Atlantic	3611	Wanninkhof, R.; Pierrot, D.; Barbero, L.	doi:10.3334/CDIAC/OTG.VOS_EQNX_2015
Equinox	2015-04-28	2015-05-11	North Atlantic, Tropical Atlantic	5151	Wanninkhof, R.; Pierrot, D.; Barbero, L.	doi:10.3334/CDIAC/OTG.VOS_EQNX_2015
Equinox	2015-05-11	2015-05-21	North Atlantic	2323	Wanninkhof, R.; Pierrot, D.; Barbero, L.	doi:10.3334/CDIAC/OTG.VOS_EQNX_2015
Equinox	2015-05-21	2015-06-02	North Atlantic	3565	Wanninkhof, R.; Pierrot, D.; Barbero, L.	doi:10.3334/CDIAC/OTG.VOS_EQNX_2015
Equinox	2015-06-02	2015-06-04	North Atlantic	484	Wanninkhof, R.; Pierrot, D.; Barbero, L.	doi:10.3334/CDIAC/OTG.VOS_EQNX_2015
Explorer of the Seas	2014-12-27	2015-01-04	Tropical Atlantic	2804	Wanninkhof, R.; Pierrot, D.; Barbero, L.	doi:10.3334/CDIAC/OTG.VOS_EXP2014
Explorer of the Seas	2015-01-04	2015-01-09	Tropical Atlantic	1698	Wanninkhof, R.; Pierrot, D.; Barbero, L.	doi:10.3334/CDIAC/OTG.VOS_EXP2015
Explorer of the Seas	2015-01-09	2015-01-18	Tropical Atlantic	3176	Wanninkhof, R.; Pierrot, D.; Barbero, L.	doi:10.3334/CDIAC/OTG.VOS_EXP2015
Explorer of the Seas	2015-01-18	2015-01-24	Tropical Atlantic	2058	Wanninkhof, R.; Pierrot, D.; Barbero, L.	doi:10.3334/CDIAC/OTG.VOS_EXP2015
Explorer of the Seas	2015-01-24	2015-01-29	Tropical Atlantic	1587	Wanninkhof, R.; Pierrot, D.; Barbero, L.	doi:10.3334/CDIAC/OTG.VOS_EXP2015

Table A1. Continued.

Vessel	Start date yyyy-mm-dd	End date yyyy-mm-dd	Regions	No. of samples	Principal investigators	DOI (if available)/comment
Explorer of the Seas	2015-01-29	2015-02-07	Tropical Atlantic	3176	Wanninkhof, R.; Pierrot, D.; Barbero, L.	doi:10.3334/CDIAC/OTG.VOS_EXP2015
Explorer of the Seas	2015-02-07	2015-02-12	Tropical Atlantic	1707	Wanninkhof, R.; Pierrot, D.; Barbero, L.	doi:10.3334/CDIAC/OTG.VOS_EXP2015
Explorer of the Seas	2015-02-12	2015-02-15	Tropical Atlantic	1289	Wanninkhof, R.; Pierrot, D.; Barbero, L.	doi:10.3334/CDIAC/OTG.VOS_EXP2015
F.G. Walton Smith	2015-01-12	2015-01-14	Tropical Atlantic	816	Millero, F.; Wanninkhof, R.	
F.G. Walton Smith	2015-04-09	2015-04-10	Tropical Atlantic	613	Millero, F.; Wanninkhof, R.	
F.G. Walton Smith	2015-04-13	2015-04-17	Tropical Atlantic	2078	Millero, F.; Wanninkhof, R.	
F.G. Walton Smith	2015-04-22	2015-05-02	Tropical Atlantic	3514	Millero, F.; Wanninkhof, R.	
F.G. Walton Smith	2015-05-07	2015-05-20	Tropical Atlantic	6523	Millero, F.; Wanninkhof, R.	
F.G. Walton Smith	2015-05-26	2015-05-27	Tropical Atlantic	684	Millero, F.; Wanninkhof, R.	
F.G. Walton Smith	2015-06-01	2015-06-05	Tropical Atlantic	2038	Millero, F.; Wanninkhof, R.	
F.G. Walton Smith	2015-06-10	2015-06-27	Tropical Atlantic	7319	Millero, F.; Wanninkhof, R.	
F.G. Walton Smith	2015-07-14	2015-07-15	Tropical Atlantic	689	Millero, F.; Wanninkhof, R.	
F.G. Walton Smith	2015-07-27	2015-08-01	Tropical Atlantic	2258	Millero, F.; Wanninkhof, R.	
F.G. Walton Smith	2015-08-22	2015-09-04	Tropical Atlantic	6600	Millero, F.; Wanninkhof, R.	
F.G. Walton Smith	2015-09-21	2015-09-25	Tropical Atlantic	2096	Millero, F.; Wanninkhof, R.	
F.G. Walton Smith	2015-09-28	2015-10-02	Tropical Atlantic	1990	Millero, F.; Wanninkhof, R.	
F.G. Walton Smith	2015-10-27	2015-11-06	North Atlantic, Tropical Atlantic	3896	Millero, F.; Wanninkhof, R.	
F.G. Walton Smith	2015-11-10	2015-11-11	Tropical Atlantic	271	Millero, F.; Wanninkhof, R.	
F.G. Walton Smith	2015-11-16	2015-11-20	Tropical Atlantic	82	Millero, F.; Wanninkhof, R.	
G.O. Sars	2015-01-17	2015-02-10	North Atlantic	9661	Lauvset, S.K.	
G.O. Sars	2015-04-12	2015-04-25	North Atlantic	11 719	Lauvset, S.K.; Skjelvan, I.	
G.O. Sars	2015-04-29	2015-05-01	North Atlantic	2939	Lauvset, S.K.; Skjelvan, I.	
G.O. Sars	2015-07-05	2015-07-14	North Atlantic	8921	Lauvset, S.K.; Skjelvan, I.	
G.O. Sars	2015-07-21	2015-08-13	North Atlantic	20 088	Lauvset, S.K.; Skjelvan, I.	
G.O. Sars	2015-08-18	2015-09-05	North Atlantic	18 076	Lauvset, S.K.; Skjelvan, I.	
G.O. Sars	2015-09-12	2015-09-25	North Atlantic	11 327	Lauvset, S.K.; Skjelvan, I.	
G.O. Sars	2015-09-30	2015-10-14	Arctic, North Atlantic	13 610	Lauvset, S.K.; Skjelvan, I.	
G.O. Sars	2015-10-27	2015-11-03	North Atlantic	6937	Lauvset, S.K.; Skjelvan, I.	
Gordon Gunter	2015-03-04	2015-03-14	Tropical Atlantic	4678	Wanninkhof, R.; Pierrot, D.; Barbero, L.	doi:10.3334/CDIAC/OTG.COAST_GU2015_UW
Gordon Gunter	2015-03-18	2015-04-02	Tropical Atlantic	5015	Wanninkhof, R.; Pierrot, D.; Barbero, L.	doi:10.3334/CDIAC/OTG.COAST_GU2015_UW
Gordon Gunter	2015-04-15	2015-04-27	North Atlantic, Tropical Atlantic	4334	Wanninkhof, R.; Pierrot, D.; Barbero, L.	doi:10.3334/CDIAC/OTG.COAST_GU2015_UW
Gordon Gunter	2015-05-16	2015-06-05	North Atlantic	9118	Wanninkhof, R.; Pierrot, D.; Barbero, L.	doi:10.3334/CDIAC/OTG.COAST_GU2015_UW
Gordon Gunter	2015-06-09	2015-06-12	North Atlantic	1031	Wanninkhof, R.; Pierrot, D.; Barbero, L.	doi:10.3334/CDIAC/OTG.COAST_GU2015_UW
Gordon Gunter	2015-06-19	2015-07-03	North Atlantic	5688	Wanninkhof, R.; Pierrot, D.; Barbero, L.	doi:10.3334/CDIAC/OTG.COAST_GU2015_UW
Gordon Gunter	2015-07-08	2015-07-24	North Atlantic, Tropical Atlantic	7293	Wanninkhof, R.; Pierrot, D.; Barbero, L.	doi:10.3334/CDIAC/OTG.COAST_GU2015_UW
Gordon Gunter	2015-07-30	2015-08-16	Tropical Atlantic	7434	Wanninkhof, R.; Pierrot, D.; Barbero, L.	doi:10.3334/CDIAC/OTG.COAST_GU2015_UW
Gordon Gunter	2015-08-23	2015-09-06	Tropical Atlantic	6452	Wanninkhof, R.; Pierrot, D.; Barbero, L.	doi:10.3334/CDIAC/OTG.COAST_GU2015_UW
Gordon Gunter	2015-09-14	2015-09-28	Tropical Atlantic	6111	Wanninkhof, R.; Pierrot, D.; Barbero, L.	doi:10.3334/CDIAC/OTG.COAST_GU2015_UW
Gulf Challenger	2015-03-13	2015-03-13	North Atlantic	1148	Vandemark, D.; Salisbury, J.; Hunt, C.	doi:10.3334/CDIAC/otg.TSM_UNH_GOM
Gulf Challenger	2015-06-05	2015-06-05	North Atlantic	1071	Vandemark, D.; Salisbury, J.; Hunt, C.	doi:10.3334/CDIAC/otg.TSM_UNH_GOM
Gulf Challenger	2015-08-26	2015-08-26	North Atlantic	1127	Vandemark, D.; Salisbury, J.; Hunt, C.	doi:10.3334/CDIAC/otg.TSM_UNH_GOM
Gulf Challenger	2015-10-07	2015-10-07	North Atlantic	1078	Vandemark, D.; Salisbury, J.; Hunt, C.	doi:10.3334/CDIAC/otg.TSM_UNH_GOM
Gulf Challenger	2015-11-18	2015-11-18	North Atlantic	960	Vandemark, D.; Salisbury, J.; Hunt, C.	doi:10.3334/CDIAC/otg.TSM_UNH_GOM
Healy	2015-07-14	2015-07-24	Arctic, North Pacific	4121	Sutherland, S.C.; Newberger, T.; Takahashi, T.	doi:10.3334/CDIAC/OTG.VOS_Healy_Lines_2015
Healy	2015-08-11	2015-10-21	Arctic, North Pacific	27 033	Sutherland, S.C.; Newberger, T.; Takahashi, T.	doi:10.3334/CDIAC/OTG.VOS_Healy_Lines_2015
Healy	2015-10-26	2015-10-28	North Pacific	960	Sutherland, S.C.; Newberger, T.; Takahashi, T.	doi:10.3334/CDIAC/OTG.VOS_Healy_Lines_2015
Henry B. Bigelow	2015-03-12	2015-03-21	North Atlantic	3525	Wanninkhof, R.; Pierrot, D.; Barbero, L.	doi:10.3334/CDIAC/OTG.AOML_BIGELOW_ECOAST_2015
Henry B. Bigelow	2015-03-23	2015-04-03	North Atlantic	5059	Wanninkhof, R.; Pierrot, D.; Barbero, L.	doi:10.3334/CDIAC/OTG.AOML_BIGELOW_ECOAST_2015
Henry B. Bigelow	2015-04-07	2015-04-23	North Atlantic	6155	Wanninkhof, R.; Pierrot, D.; Barbero, L.	doi:10.3334/CDIAC/OTG.AOML_BIGELOW_ECOAST_2015
Henry B. Bigelow	2015-04-27	2015-05-07	North Atlantic	4638	Wanninkhof, R.; Pierrot, D.; Barbero, L.	doi:10.3334/CDIAC/OTG.AOML_BIGELOW_ECOAST_2015
Henry B. Bigelow	2015-05-19	2015-06-03	North Atlantic	6456	Wanninkhof, R.; Pierrot, D.; Barbero, L.	doi:10.3334/CDIAC/OTG.AOML_BIGELOW_ECOAST_2015
Henry B. Bigelow	2015-06-11	2015-06-19	North Atlantic	3839	Wanninkhof, R.; Pierrot, D.; Barbero, L.	doi:10.3334/CDIAC/OTG.AOML_BIGELOW_ECOAST_2015
Henry B. Bigelow	2015-06-24	2015-07-02	North Atlantic	3401	Wanninkhof, R.; Pierrot, D.; Barbero, L.	doi:10.3334/CDIAC/OTG.AOML_BIGELOW_ECOAST_2015
Henry B. Bigelow	2015-07-27	2015-08-07	North Atlantic	5265	Wanninkhof, R.; Pierrot, D.; Barbero, L.	doi:10.3334/CDIAC/OTG.AOML_BIGELOW_ECOAST_2015

www.earth-syst-sci-data.net/8/605/2016/

Earth Syst. Sci. Data, 8, 605–649, 2016

Table A1. Continued.

Vessel	Start date yyyy-mm-dd	End date yyyy-mm-dd	Regions	No. of samples	Principal investigators	DOI (if available)/comment
Henry B. Bigelow	2015-08-12	2015-08-21	North Atlantic	4315	Wanninkhof, R.; Pierrot, D.; Barbero, L.	doi:10.3334/CDIAC/OTG.AOML_BIGELOW_ECOAST_2015
Henry B. Bigelow	2015-09-01	2015-09-17	North Atlantic	7836	Wanninkhof, R.; Pierrot, D.; Barbero, L.	doi:10.3334/CDIAC/OTG.AOML_BIGELOW_ECOAST_2015
Henry B. Bigelow	2015-09-23	2015-09-30	North Atlantic	3382	Wanninkhof, R.; Pierrot, D.; Barbero, L.	doi:10.3334/CDIAC/OTG.AOML_BIGELOW_ECOAST_2015
Henry B. Bigelow	2015-10-07	2015-10-22	North Atlantic	7186	Wanninkhof, R.; Pierrot, D.; Barbero, L.	doi:10.3334/CDIAC/OTG.AOML_BIGELOW_ECOAST_2015
Henry B. Bigelow	2015-10-27	2015-11-06	North Atlantic	4472	Wanninkhof, R.; Pierrot, D.; Barbero, L.	doi:10.3334/CDIAC/OTG.AOML_BIGELOW_ECOAST_2015
Henry B. Bigelow	2015-11-12	2015-11-17	North Atlantic	2402	Wanninkhof, R.; Pierrot, D.; Barbero, L.	doi:10.3334/CDIAC/OTG.AOML_BIGELOW_ECOAST_2015
Laurence M. Gould	2014-12-30	2015-02-07	Southern Ocean	7302	Sweeney, C.; Takahashi, T.; Newberger, T.; Sutherland, S.C.; Munro, D.R.	doi:10.3334/CDIAC/OTG.VOS_LM_GOULD_2014
Laurence M. Gould	2015-02-14	2015-03-16	Southern Ocean	9450	Sweeney, C.; Takahashi, T.; Newberger, T.; Sutherland, S.C.; Munro, D.R.	doi:10.3334/CDIAC/OTG.VOS_LM_GOULD_2015
Laurence M. Gould	2015-03-21	2015-04-03	Southern Ocean	2602	Sweeney, C.; Takahashi, T.; Newberger, T.; Sutherland, S.C.; Munro, D.R.	doi:10.3334/CDIAC/OTG.VOS_LM_GOULD_2015
Laurence M. Gould	2015-04-08	2015-05-11	Southern Ocean	7691	Sweeney, C.; Takahashi, T.; Newberger, T.; Sutherland, S.C.; Munro, D.R.	doi:10.3334/CDIAC/OTG.VOS_LM_GOULD_2015
Laurence M. Gould	2015-05-16	2015-06-16	Southern Ocean	9497	Sweeney, C.; Takahashi, T.; Newberger, T.; Sutherland, S.C.; Munro, D.R.	doi:10.3334/CDIAC/OTG.VOS_LM_GOULD_2015
Laurence M. Gould	2015-06-21	2015-06-30	Southern Ocean	2379	Sweeney, C.; Takahashi, T.; Newberger, T.; Sutherland, S.C.; Munro, D.R.	doi:10.3334/CDIAC/OTG.VOS_LM_GOULD_2015
Marcus G. Langseth	2015-04-13	2015-04-22	North Atlantic	1948	Sutherland, S.C.; Newberger, T.; Takahashi, T.; Sweeney, C.	doi:10.3334/CDIAC/OTG.VOS_MG_LANGSETH_LINES_2015
Marcus G. Langseth	2015-06-01	2015-06-23	North Atlantic	8608	Sutherland, S.C.; Newberger, T.; Takahashi, T.; Sweeney, C.	doi:10.3334/CDIAC/OTG.VOS_MG_LANGSETH_LINES_2015
Marcus G. Langseth	2015-07-31	2015-09-12	North Atlantic	14 519	Sutherland, S.C.; Newberger, T.; Takahashi, T.; Sweeney, C.	doi:10.3334/CDIAC/OTG.VOS_MG_LANGSETH_LINES_2015
Marion Dufresne	2015-01-07	2015-02-06	Indian Ocean, Southern Ocean	4529	Metzl, N.; Lo Monaco, C.	doi:10.3334/CDIAC/OTG.VOS_OISO_24
Mooring	2014-03-07	2015-03-22	Tropical Atlantic	3048	Sutton, A.; Sabine, C.; Manzello, D.; Musielewicz, S.; Maenner, S.; Dietrich, C.; Bott, R.; Osborne, J.	doi:10.3334/CDIAC/OTG.CHEECA_80W_25N
Mooring	2014-03-07	2015-04-03	Tropical Pacific	3129	Sutton, A.; Sabine, C.; Maenner, S.; Musielewicz, S.; Bott, R.; Osborne, J.	doi:10.3334/CDIAC/otg.TSM_Stratus_85W_20S
Mooring	2014-05-02	2015-04-28	North Pacific	2630	Sutton, A.; Sabine, C.; Send, U.; Ohman, M.; Musielewicz, S.; Maenner, S.; Dietrich, C.; Bott, R.; Osborne, J.	doi:10.3334/CDIAC/OTG.TSM_CCE2_121W_34N
Mooring	2014-05-06	2015-01-27	North Pacific	2122	Mathis, J.; Monacci, N.; Musielewicz, S.; Maenner, S.	doi:10.3334/CDIAC/OTG.TSM_Southeast_AK_56N_134W
Mooring	2014-05-24	2015-05-06	Tropical Pacific	2447	Sutton, A.; Sabine, C.; De Carlo, E.; Musielewicz, S.; Maenner, S.; Dietrich, C.; Bott, R.; Osborne, J.	doi:10.3334/CDIAC/OTG.TSM_Kaneohe_158W_21N
Mooring	2014-07-21	2015-07-07	North Atlantic	2796	Sutton, A.; Sabine, C.; Andersson, A.; Bates, N.; Musielewicz, S.; Maenner, S.; Dietrich, C.; Bott, R.; Osborne, J.	doi:10.3334/CDIAC/OTG.TSM_Crescent_64W_32N
Mooring	2014-10-06	2015-01-07	North Atlantic	741	Sutton, A.; Sabine, C.; Maenner, S.; Musielewicz, S.; Bott, R.; Osborne, J.	doi:10.3334/CDIAC/OTG.TSM_Hog_Reef_64W_32N
Nathaniel B. Palmer	2015-01-06	2015-01-18	Southern Ocean	4320	Sutherland, S.C.; Newberger, T.; Takahashi, T.; Sweeney, C.	doi:10.3334/CDIAC/OTG.VOS_PALMER_2015
Nathaniel B. Palmer	2015-01-23	2015-03-14	Southern Ocean	17 383	Sutherland, S.C.; Newberger, T.; Takahashi, T.; Sweeney, C.	doi:10.3334/CDIAC/OTG.VOS_PALMER_2015
Nathaniel B. Palmer	2015-03-27	2015-04-28	Southern Ocean	10 623	Sutherland, S.C.; Newberger, T.; Takahashi, T.; Sweeney, C.	doi:10.3334/CDIAC/OTG.VOS_PALMER_2015
Nathaniel B. Palmer	2015-05-12	2015-05-28	Southern Ocean	5654	Sutherland, S.C.; Newberger, T.; Takahashi, T.; Sweeney, C.	doi:10.3334/CDIAC/OTG.VOS_PALMER_2015
Nathaniel B. Palmer	2015-08-05	2015-08-28	Southern Ocean	7528	Sutherland, S.C.; Newberger, T.; Takahashi, T.; Sweeney, C.	doi:10.3334/CDIAC/OTG.VOS_PALMER_2015
Nathaniel B. Palmer	2015-09-08	2015-10-18	Southern Ocean, Tropical Atlantic	13 871	Sutherland, S.C.; Newberger, T.; Takahashi, T.; Sweeney, C.	doi:10.3334/CDIAC/OTG.VOS_PALMER_2015
New Century 2	2014-12-12	2015-01-12	North Pacific, Tropical Pacific	3221	Nakaoka, S.	doi:10.3334/CDIAC/OTG.VOS_New_Century_2_2014
New Century 2	2015-03-16	2015-03-31	North Pacific	1343	Nakaoka, S.	doi:10.3334/CDIAC/OTG.VOS_New_Century_2_2015
New Century 2	2015-04-01	2015-04-14	North Pacific	1417	Nakaoka, S.	doi:10.3334/CDIAC/OTG.VOS_New_Century_2_2015
New Century 2	2015-04-16	2015-05-03	North Pacific	1668	Nakaoka, S.	doi:10.3334/CDIAC/OTG.VOS_New_Century_2_2015
New Century 2	2015-05-04	2015-05-17	North Pacific	1616	Nakaoka, S.	doi:10.3334/CDIAC/OTG.VOS_New_Century_2_2015
New Century 2	2015-05-20	2015-06-04	North Pacific	1569	Nakaoka, S.	doi:10.3334/CDIAC/OTG.VOS_New_Century_2_2015

Table A1. Continued.

Vessel	Start date yyyy-mm-dd	End date yyyy-mm-dd	Regions	No. of samples	Principal investigators	DOI (if available)/comment
New Century 2	2015-06-05	2015-06-21	North Pacific	1545	Nakaoka, S.	doi:10.3334/CDIAC/OTG.VOS_New_Century_2_2015
New Century 2	2015-06-23	2015-07-07	North Pacific	1376	Nakaoka, S.	doi:10.3334/CDIAC/OTG.VOS_New_Century_2_2015
New Century 2	2015-07-07	2015-07-20	North Pacific	1440	Nakaoka, S.	doi:10.3334/CDIAC/OTG.VOS_New_Century_2_2015
New Century 2	2015-07-23	2015-08-07	North Pacific	1538	Nakaoka, S.	doi:10.3334/CDIAC/OTG.VOS_New_Century_2_2015
New Century 2	2015-08-09	2015-08-21	North Pacific	1460	Nakaoka, S.	doi:10.3334/CDIAC/OTG.VOS_New_Century_2_2015
New Century 2	2015-08-26	2015-09-24	North Pacific, Tropical Pacific	2422	Nakaoka, S.	doi:10.3334/CDIAC/OTG.VOS_New_Century_2_2015
New Century 2	2015-09-24	2015-10-23	North Atlantic, North Pacific, Tropical Atlantic, Tropical Pacific	3157	Nakaoka, S.	doi:10.3334/CDIAC/OTG.VOS_New_Century_2_2015
Nuka Arctica	2015-10-21	2015-11-08	North Atlantic	5318	Omar, A.; Olsen, A.; Johannessen, T.	
Nuka Arctica	2015-12-01	2015-12-21	North Atlantic	10 558	Omar, A.; Olsen, A.; Johannessen, T.	
Polarstern	2014-12-03	2015-01-31	Southern Ocean	58 046	van Heuven, S.; Hoppema, M.	doi:10.3334/CDIAC/OTG.OA_VOS_POLARSTERN_2014
Polarstern	2015-05-19	2015-06-27	Arctic, North Atlantic	39 056	van Heuven, S.; Hoppema, M.	doi:10.3334/CDIAC/OTG.OA_VOS_POLARSTERN_2015
Polarstern	2015-06-29	2015-08-14	Arctic, North Atlantic	20 164	van Heuven, S.; Hoppema, M.	doi:10.3334/CDIAC/OTG.OA_VOS_POLARSTERN_2015
Polarstern	2015-08-18	2015-10-11	Arctic, North Atlantic	43 709	van Heuven, S.; Hoppema, M.	doi:10.3334/CDIAC/OTG.OA_VOS_POLARSTERN_2015
Polarstern	2015-10-30	2015-12-01	North Atlantic, Southern Ocean, Tropical Atlantic	27 178	van Heuven, S.; Hoppema, M.	doi:10.3334/CDIAC/OTG.OA_VOS_POLARSTERN_2015
Ronald H. Brown	2015-01-15	2015-01-29	North Pacific, Tropical Pacific	4855	Wanninkhof, R.; Pierrot, D.; Barbero, L.	doi:10.3334/CDIAC/OTG.VOS_RB_2015
Ronald H. Brown	2015-01-30	2015-02-12	North Pacific	5365	Wanninkhof, R.; Pierrot, D.; Barbero, L.	doi:10.3334/CDIAC/OTG.VOS_RB_2015
Ronald H. Brown	2015-03-01	2015-03-30	Tropical Pacific	13 576	Wanninkhof, R.; Pierrot, D.; Barbero, L.	doi:10.3334/CDIAC/OTG.VOS_RB_2015
Ronald H. Brown	2015-04-10	2015-05-12	Tropical Pacific	15 021	Wanninkhof, R.; Pierrot, D.; Barbero, L.	doi:10.3334/CDIAC/OTG.VOS_RB_2015
Ronald H. Brown	2015-05-25	2015-06-24	North Pacific, Tropical Pacific	13 690	Wanninkhof, R.; Pierrot, D.; Barbero, L.	doi:10.3334/CDIAC/OTG.VOS_RB_2015
Ronald H. Brown	2015-07-14	2015-07-31	North Pacific	5862	Wanninkhof, R.; Pierrot, D.; Barbero, L.	doi:10.3334/CDIAC/OTG.VOS_RB_2015
Ronald H. Brown	2015-08-06	2015-08-21	Arctic, North Pacific	6365	Wanninkhof, R.; Pierrot, D.; Barbero, L.	doi:10.3334/CDIAC/OTG.VOS_RB_2015
Ronald H. Brown	2015-08-22	2015-09-04	Arctic, North Pacific	6298	Wanninkhof, R.; Pierrot, D.; Barbero, L.	doi:10.3334/CDIAC/OTG.VOS_RB_2015
Ronald H. Brown	2015-11-22	2015-12-18	Tropical Pacific	10 838	Wanninkhof, R.; Pierrot, D.; Barbero, L.	doi:10.3334/CDIAC/OTG.VOS_RB_2015
S.A. Agulhas II	2014-12-08	2015-02-16	Southern Ocean	23 342	Monteiro, P.M.S.; Joubert, W.R.; Gregor, L.	doi:10.3334/CDIAC/OTG.VOS_SA_Agulhas_II_2015
S.A. Agulhas II	2015-07-23	2015-08-12	Southern Ocean	16 271	Monteiro, P.M.S.; Joubert, W.R.; Gregor, L.	doi:10.3334/CDIAC/OTG.VOS_SA_Agulhas_II_2015
S.A. Agulhas II	2015-09-04	2015-10-06	Southern Ocean	12 371	Monteiro, P.M.S.; Joubert, W.R.; Gregor, L.	doi:10.3334/CDIAC/OTG.VOS_SA_Agulhas_II_2015
Simon Stevin	2015-06-01	2015-06-01	North Atlantic	445	Gkritzalis, T.; Cattrijsse, A.	
Simon Stevin	2015-06-04	2015-06-04	North Atlantic	909	Gkritzalis, T.; Cattrijsse, A.	
Simon Stevin	2015-06-08	2015-06-08	North Atlantic	440	Gkritzalis, T.; Cattrijsse, A.	
Simon Stevin	2015-06-23	2015-06-23	North Atlantic	749	Gkritzalis, T.; Cattrijsse, A.	
Simon Stevin	2015-06-24	2015-06-24	North Atlantic	1234	Gkritzalis, T.; Cattrijsse, A.	
Simon Stevin	2015-06-25	2015-06-25	North Atlantic	787	Gkritzalis, T.; Cattrijsse, A.	
Simon Stevin	2015-06-30	2015-06-30	North Atlantic	425	Gkritzalis, T.; Cattrijsse, A.	
Simon Stevin	2015-07-02	2015-07-02	North Atlantic	154	Gkritzalis, T.; Cattrijsse, A.	
Simon Stevin	2015-07-06	2015-07-06	North Atlantic	168	Gkritzalis, T.; Cattrijsse, A.	
Simon Stevin	2015-07-10	2015-07-10	North Atlantic	357	Gkritzalis, T.; Cattrijsse, A.	
Simon Stevin	2015-07-13	2015-07-13	North Atlantic	223	Gkritzalis, T.; Cattrijsse, A.	
Simon Stevin	2015-07-14	2015-07-14	North Atlantic	54	Gkritzalis, T.; Cattrijsse, A.	
Simon Stevin	2015-07-15	2015-07-15	North Atlantic	477	Gkritzalis, T.; Cattrijsse, A.	
Simon Stevin	2015-07-16	2015-07-16	North Atlantic	465	Gkritzalis, T.; Cattrijsse, A.	
Simon Stevin	2015-07-22	2015-07-22	North Atlantic	87	Gkritzalis, T.; Cattrijsse, A.	
Simon Stevin	2015-07-23	2015-07-23	North Atlantic	428	Gkritzalis, T.; Cattrijsse, A.	
Simon Stevin	2015-07-24	2015-07-24	North Atlantic	299	Gkritzalis, T.; Cattrijsse, A.	
Simon Stevin	2015-07-31	2015-07-31	North Atlantic	401	Gkritzalis, T.; Cattrijsse, A.	
Simon Stevin	2015-08-03	2015-08-03	North Atlantic	394	Gkritzalis, T.; Cattrijsse, A.	
Simon Stevin	2015-08-04	2015-08-04	North Atlantic	412	Gkritzalis, T.; Cattrijsse, A.	
Simon Stevin	2015-08-07	2015-08-07	Tropical Atlantic	463	Gkritzalis, T.; Cattrijsse, A.	
Simon Stevin	2015-08-10	2015-08-10	North Atlantic	479	Gkritzalis, T.; Cattrijsse, A.	
Simon Stevin	2015-08-12	2015-08-12	North Atlantic	341	Gkritzalis, T.; Cattrijsse, A.	
Simon Stevin	2015-08-17	2015-08-17	North Atlantic	439	Gkritzalis, T.; Cattrijsse, A.	
Simon Stevin	2015-08-18	2015-08-18	North Atlantic	414	Gkritzalis, T.; Cattrijsse, A.	
Simon Stevin	2015-08-19	2015-08-19	North Atlantic	470	Gkritzalis, T.; Cattrijsse, A.	
Simon Stevin	2015-08-21	2015-08-21	North Atlantic	401	Gkritzalis, T.; Cattrijsse, A.	
Simon Stevin	2015-08-24	2015-08-24	North Atlantic	450	Gkritzalis, T.; Cattrijsse, A.	
Simon Stevin	2015-08-27	2015-08-27	North Atlantic	373	Gkritzalis, T.; Cattrijsse, A.	
Simon Stevin	2015-08-28	2015-08-28	North Atlantic	455	Gkritzalis, T.; Cattrijsse, A.	
Simon Stevin	2015-09-02	2015-09-02	North Atlantic	961	Gkritzalis, T.; Cattrijsse, A.	
Simon Stevin	2015-09-03	2015-09-03	North Atlantic	450	Gkritzalis, T.; Cattrijsse, A.	
Simon Stevin	2015-09-04	2015-09-04	North Atlantic	307	Gkritzalis, T.; Cattrijsse, A.	
Simon Stevin	2015-09-08	2015-09-08	North Atlantic	464	Gkritzalis, T.; Cattrijsse, A.	

www.earth-syst-sci-data.net/8/605/2016/

Earth Syst. Sci. Data, 8, 605–649, 2016

Table A1. Continued.

Vessel	Start date yyyy-mm-dd	End date yyyy-mm-dd	Regions	No. of samples	Principal investigators	DOI (if available)/comment
Simon Stevin	2015-09-09	2015-09-09	North Atlantic	436	Gkritzalis, T.; Cattrijsse, A.	
Simon Stevin	2015-09-10	2015-09-10	North Atlantic	469	Gkritzalis, T.; Cattrijsse, A.	
Simon Stevin	2015-09-11	2015-09-11	North Atlantic	443	Gkritzalis, T.; Cattrijsse, A.	
Simon Stevin	2015-09-15	2015-09-15	North Atlantic	729	Gkritzalis, T.; Cattrijsse, A.	
Simon Stevin	2015-09-16	2015-09-16	North Atlantic	1081	Gkritzalis, T.; Cattrijsse, A.	
Simon Stevin	2015-09-21	2015-09-21	North Atlantic	366	Gkritzalis, T.; Cattrijsse, A.	
Simon Stevin	2015-09-25	2015-09-25	North Atlantic	454	Gkritzalis, T.; Cattrijsse, A.	
Simon Stevin	2015-09-28	2015-09-28	North Atlantic	440	Gkritzalis, T.; Cattrijsse, A.	
Simon Stevin	2015-09-29	2015-09-29	North Atlantic	701	Gkritzalis, T.; Cattrijsse, A.	
Simon Stevin	2015-09-30	2015-09-30	North Atlantic	850	Gkritzalis, T.; Cattrijsse, A.	
Simon Stevin	2015-10-05	2015-10-05	North Atlantic	453	Gkritzalis, T.; Cattrijsse, A.	
Simon Stevin	2015-10-06	2015-10-06	North Atlantic	491	Gkritzalis, T.; Cattrijsse, A.	
Simon Stevin	2015-10-07	2015-10-07	North Atlantic	423	Gkritzalis, T.; Cattrijsse, A.	
Simon Stevin	2015-10-08	2015-10-08	North Atlantic	437	Gkritzalis, T.; Cattrijsse, A.	
Simon Stevin	2015-10-10	2015-10-10	North Atlantic	488	Gkritzalis, T.; Cattrijsse, A.	
Simon Stevin	2015-10-11	2015-10-11	North Atlantic	448	Gkritzalis, T.; Cattrijsse, A.	
Simon Stevin	2015-10-20	2015-10-20	North Atlantic	435	Gkritzalis, T.; Cattrijsse, A.	
Simon Stevin	2015-10-21	2015-10-21	North Atlantic	319	Gkritzalis, T.; Cattrijsse, A.	
Simon Stevin	2015-11-01	2015-11-01	North Atlantic	387	Gkritzalis, T.; Cattrijsse, A.	
Simon Stevin	2015-11-04	2015-11-04	North Atlantic	272	Gkritzalis, T.; Cattrijsse, A.	
Simon Stevin	2015-11-05	2015-11-05	North Atlantic	415	Gkritzalis, T.; Cattrijsse, A.	
Simon Stevin	2015-11-06	2015-11-06	North Atlantic	114	Gkritzalis, T.; Cattrijsse, A.	
Simon Stevin	2015-11-12	2015-11-12	North Atlantic	202	Gkritzalis, T.; Cattrijsse, A.	
Simon Stevin	2015-12-07	2015-12-07	North Atlantic	217	Gkritzalis, T.; Cattrijsse, A.	
Simon Stevin	2015-12-08	2015-12-08	North Atlantic	336	Gkritzalis, T.; Cattrijsse, A.	
Simon Stevin	2015-12-09	2015-12-09	North Atlantic	156	Gkritzalis, T.; Cattrijsse, A.	
Soyo Maru	2015-05-08	2015-05-11	North Pacific, Tropical Pacific	3972	Ono, T.	
Soyo Maru	2015-08-01	2015-08-07	North Pacific	8354	Ono, T.	
Soyo Maru	2015-10-26	2015-11-03	North Pacific	10759	Ono, T.	
Tangaroa	2015-01-28	2015-03-10	Southern Ocean	34868	Currie, K.	doi:10.3334/CDIAC/OTG.VOS_Tangaroa_2015
Tangaroa	2015-03-27	2015-04-14	Southern Ocean	15297	Currie, K.	doi:10.3334/CDIAC/OTG.VOS_Tangaroa_2015
Tangaroa	2015-04-17	2015-04-22	Southern Ocean	4797	Currie, K.	doi:10.3334/CDIAC/OTG.VOS_Tangaroa_2015
Tangaroa	2015-04-23	2015-04-30	Southern Ocean	5791	Currie, K.	doi:10.3334/CDIAC/OTG.VOS_Tangaroa_2015
Tangaroa	2015-05-04	2015-05-21	Southern Ocean	12051	Currie, K.	doi:10.3334/CDIAC/OTG.VOS_Tangaroa_2015
Tangaroa	2015-05-23	2015-06-01	Southern Ocean	7985	Currie, K.	doi:10.3334/CDIAC/OTG.VOS_Tangaroa_2015
Tangaroa	2015-07-04	2015-08-02	Southern Ocean	26898	Currie, K.	doi:10.3334/CDIAC/OTG.VOS_Tangaroa_2015
Tangaroa	2015-08-04	2015-08-26	Southern Ocean	18553	Currie, K.	doi:10.3334/CDIAC/OTG.VOS_Tangaroa_2015
Tangaroa	2015-09-05	2015-09-24	Southern Ocean	12776	Currie, K.	doi:10.3334/CDIAC/OTG.VOS_Tangaroa_2015
Tangaroa	2015-09-26	2015-10-04	Tropical Pacific	7207	Currie, K.	doi:10.3334/CDIAC/OTG.VOS_Tangaroa_2014
Tangaroa	2015-10-13	2015-10-25	Southern Ocean	10658	Currie, K.	doi:10.3334/CDIAC/OTG.VOS_Tangaroa_2015
Trans Future 5	2015-01-10	2015-01-24	North Pacific, Southern Ocean, Tropical Pacific	1507	Nojiri, Y.	doi:10.3334/CDIAC/OTG.VOS_TF5_2015
Trans Future 5	2015-01-31	2015-02-10	North Pacific, Tropical Pacific	1179	Nojiri, Y.	doi:10.3334/CDIAC/OTG.VOS_TF5_2015
Trans Future 5	2015-02-11	2015-02-24	Southern Ocean, Tropical Pacific	922	Nojiri, Y.	doi:10.3334/CDIAC/OTG.VOS_TF5_2015
Trans Future 5	2015-02-25	2015-03-08	North Pacific, Southern Ocean, Tropical Pacific	1379	Nojiri, Y.	doi:10.3334/CDIAC/OTG.VOS_TF5_2015
Trans Future 5	2015-03-14	2015-03-24	North Pacific, Tropical Pacific	1083	Nojiri, Y.	doi:10.3334/CDIAC/OTG.VOS_TF5_2015
Trans Future 5	2015-04-25	2015-05-05	North Pacific, Tropical Pacific	1090	Nakaoka, S.	doi:10.3334/CDIAC/OTG.VOS_TF5_2015
Trans Future 5	2015-05-06	2015-05-20	Southern Ocean, Tropical Pacific	913	Nakaoka, S.	doi:10.3334/CDIAC/OTG.VOS_TF5_2015
Trans Future 5	2015-05-21	2015-06-01	North Pacific, Southern Ocean, Tropical Pacific	1381	Nakaoka, S.	doi:10.3334/CDIAC/OTG.VOS_TF5_2015
Trans Future 5	2015-06-06	2015-06-15	North Pacific, Tropical Pacific	1138	Nakaoka, S.	doi:10.3334/CDIAC/OTG.VOS_TF5_2015
Trans Future 5	2015-06-16	2015-06-28	Southern Ocean, Tropical Pacific	911	Nakaoka, S.	doi:10.3334/CDIAC/OTG.VOS_TF5_2015
Trans Future 5	2015-06-29	2015-07-12	North Pacific, Southern Ocean, Tropical Pacific	1431	Nakaoka, S.	doi:10.3334/CDIAC/OTG.VOS_TF5_2015
Trans Future 5	2015-07-18	2015-07-30	North Pacific, Tropical Pacific	1112	Nakaoka, S.	doi:10.3334/CDIAC/OTG.VOS_TF5_2015
Trans Future 5	2015-07-30	2015-08-11	Southern Ocean, Tropical Pacific	884	Nakaoka, S.	doi:10.3334/CDIAC/OTG.VOS_TF5_2015
Trans Future 5	2015-08-12	2015-08-24	North Pacific, Southern Ocean, Tropical Pacific	1400	Nakaoka, S.	doi:10.3334/CDIAC/OTG.VOS_TF5_2015
Trans Future 5	2015-09-26	2015-10-07	North Pacific, Tropical Pacific	811	Nakaoka, S.	doi:10.3334/CDIAC/OTG.VOS_TF5_2015
Trans Future 5	2015-10-07	2015-10-19	Southern Ocean, Tropical Pacific	889	Nakaoka, S.	doi:10.3334/CDIAC/OTG.VOS_TF5_2015
Trans Future 5	2015-10-21	2015-11-01	North Pacific, Southern Ocean, Tropical Pacific	1427	Nakaoka, S.	doi:10.3334/CDIAC/OTG.VOS_TF5_2015
Wakataka Maru	2015-06-30	2015-07-04	North Pacific	6356	Kuwata, A.; Tadokoro, K., Ono, T.	
Wakataka Maru	2015-07-11	2015-07-21	North Pacific	14479	Kuwata, A.; Tadokoro, K., Ono, T.	
Wakataka Maru	2015-07-29	2015-08-05	North Pacific	9773	Kuwata, A.; Tadokoro, K., Ono, T.	
Wakataka Maru	2015-09-30	2015-10-15	North Pacific	15111	Kuwata, A.; Tadokoro, K., Ono, T.	

Appendix B

Table B1. Funding supporting the production of the various components of the global carbon budget (see also acknowledgements).

Funder and grant number (where relevant)	Author initials
Australia, Integrated Marine Observing System and Antarctic Climate and Ecosystems CRC	BT
European Commission (EC) Copernicus Atmosphere Monitoring Service, European Centre for Medium-Range Weather Forecasts (ECMWF)	FC
EC H2020 (AtlantOS; grant no. 633211)	NL, AO
EC H2020 (CRESCENDO; grant no. 641816)	CD, RS, OA, PF
EC H2020 European Research Council (ERC) (QUINCY; grant no. 647204).	SZ
EC H2020 ERC Synergy grant (IMBALANCE-P; grant no. ERC-2013-SyG-610028)	PC
France, BNP Paribas Foundation grant to support the Global Carbon Atlas	PC
French Institut National des Sciences de l'Univers (INSU) and Institut Paul Emile Victor (IPEV) for OISO cruises	NM
French Institut de recherche pour le développement (IRD)	NL
German Federal Ministry of Education and Research (grant no. 01LK1224I ICOS-D)	MH
German Research Foundation's Emmy Noether Programme (grant no. PO1751/1-1)	JN
German Max Planck Society	CR, SZ
Germany, Federal Ministry of Education and Research (BMBF)	AK
Germany, Helmholtz Postdoc Programme (Initiative and Networking Fund of the Helmholtz Association)	JH
Japan Ministry of Agriculture, Forestry and Fisheries (MAFF)	OT
Japan Ministry of Environment	SN
Japan Ministry of Environment (grant no. ERTDF S-10)	EK
NASA LCLUC programme (grant no. NASA NNX14AD94G)	AJ
New Zealand National Institute of Water and Atmospheric Research (NIWA) Core Funding	KC
Norway Research Council (grant no. 229752)	AMO
Norway Research Council (grant no. 569980)	GPP, RMA, JIK
Norway Research Council (project EVA; grant no. 229771)	JS
Norwegian Environment Agency (grant no. 16078007)	IS
Research Fund – Flanders (FWO; formerly Hercules Foundation)	TG
South Africa Council for Scientific and Industrial Research (CSIR)	PMSM
UK Natural Environment Research Council (RAGANRAoCC; grant no. NE/K002473/1)	US
UK Newton Fund through the Met Office Climate Science for Service Partnership Brazil (CSSP Brazil)	AJW
US Department of Agriculture, National Institute of Food and Agriculture (grant no. 2015-67003-23485)	DL
US Department of Energy (grant no. DE-FC03-97ER62402/A010)	DL
US Department of Energy, Biological and Environmental Research Program, Office of Science (grant no. DE-AC05-00OR22725)	APW
US Department of Commerce, NOAA's Climate Observation Division of the Climate Program Office	SRA, AJS
US Department of Energy, Office of Science and BER programme (grant no. DOE DE-SC0016323)	AJ
US National Science Foundation (grant no. AGS-1048827)	SD
US National Science Foundation (grant no. AOAS-1543457)	DRM
US National Science Foundation (grant no. AOAS-1341647)	DRM
US NOAA's Climate Observation Division of the Climate Program Office (grant no. N8R1SE3P00); US NOAA's Ocean Acidification Program (grant no. N8R3CEAP00)	DP, LB
US National Science Foundation (grant no. NSF AGS 12-43071)	AJ
Computing resources	
GENCI (Grand Équipement National de Calcul Intensif; allocation t2016012201), France	FC
Météo-France/DSI supercomputing centre	RS
Netherlands Organisation for Scientific Research (NWO) (SH-312-14)	IvdL-L
Norwegian Metacenter for Computational Science (NOTUR, project nn2980k) and the Norwegian Storage Infrastructure (NorStore, project ns2980k)	JS
UEA High Performance Computing Cluster, UK	OA, CLQ

www.earth-syst-sci-data.net/8/605/2016/

Earth Syst. Sci. Data, 8, 605–649, 2016

References

Achard, F., Beuchle, R., Mayaux, P., Stibig, H. J., Bodart, C., Brink, A., Carboni, S., Desclée, B., Donnay, F., and Eva, H.: Determination of tropical deforestation rates and related carbon losses from 1990 to 2010, Glob. Change Biol., 20, 2540–2554, 2014.

Andres, R., Boden, T., and Higdon, D.: A new evaluation of the uncertainty associated with CDIAC estimates of fossil fuel carbon dioxide emission, Tellus B, 66, 23616, doi:10.3402/tellusb.v66.23616, 2014.

Andres, R. J., Fielding, D. J., Marland, G., Boden, T. A., Kumar, N., and Kearney, A. T.: Carbon dioxide emissions from fossil fuel use, 1751–1950, Tellus, 51, 759–765, 1999.

Andres, R. J., Boden, T. A., Bréon, F.-M., Ciais, P., Davis, S., Erickson, D., Gregg, J. S., Jacobson, A., Marland, G., Miller, J., Oda, T., Olivier, J. G. J., Raupach, M. R., Rayner, P., and Treanton, K.: A synthesis of carbon dioxide emissions from fossil-fuel combustion, Biogeosciences, 9, 1845–1871, doi:10.5194/bg-9-1845-2012, 2012.

Andrew, R. M. and Peters, G. P.: A multi-region input-output table based on the Global Trade Analysis Project Database (GTAP-MRIO), Economic Systems Research, 25, 99–121, 2013.

Andrew, R. M., Davis, S. J., and Peters, G. P.: Climate policy and dependence on traded carbon, Environ. Res. Lett., 8, 34011, doi:10.1088/1748-9326/8/3/034011, 2013.

Archer, D., Eby, M., Brovkin, V., Ridgwell, A., Cao, L., Mikolajewicz, U., Caldeira, K. M., K., Munhoven, G., Montenegro, A., and Tokos, K.: Atmospheric Lifetime of Fossil Fuel Carbon Dioxide, Annu. Rev. Earth Planet. Sc., 37, 117-134, 2009.

Atlas, R., Hoffman, R. N., Ardizzone, J., Leidner, S. M., Jusem, J. C., Smith, D. K., and Gombos, D.: A cross-calibrated, multiplatform ocean surface wind velocity product for meteorological and oceanographic applications, B. Am. Meteorol. Soc., 92, 157–174, 2011.

Aumont, O. and Bopp, L.: Globalizing results from ocean in situ iron fertilization studies, Global Biogeochem. Cyc., 20, GB2017, doi:10.1029/2005GB002591, 2006.

Baccini, A., Goetz, S. J., Walker, W. S., Laporte, N. T., Sun, M., Sulla-Menashe, D., Hackler, J., Beck, P. S. A., Dubayah, R., Friedl, M. A., Samanta, S., and Houghton, R. A.: Estimated carbon dioxide emissions from tropical deforestation improved by carbon-density maps, Nature Climate Change, 2, 182–186, 2012.

Bakker, D. C. E., Pfeil, B., Landa, C. S., Metzl, N., O'Brien, K. M., Olsen, A., Smith, K., Cosca, C., Harasawa, S., Jones, S. D., Nakaoka, S.-I., Nojiri, Y., Schuster, U., Steinhoff, T., Sweeney, C., Takahashi, T., Tilbrook, B., Wada, C., Wanninkhof, R., Alin, S. R., Balestrini, C. F., Barbero, L., Bates, N. R., Bianchi, A. A., Bonou, F., Boutin, J., Bozec, Y., Burger, E. F., Cai, W.-J., Castle, R. D., Chen, L., Chierici, M., Currie, K., Evans, W., Featherstone, C., Feely, R. A., Fransson, A., Goyet, C., Greenwood, N., Gregor, L., Hankin, S., Hardman-Mountford, N. J., Harlay, J., Hauck, J., Hoppema, M., Humphreys, M. P., Hunt, C. W., Huss, B., Ibánhez, J. S. P., Johannessen, T., Keeling, R., Kitidis, V., Körtzinger, A., Kozyr, A., Krasakopoulou, E., Kuwata, A., Landschützer, P., Lauvset, S. K., Lefèvre, N., Lo Monaco, C., Manke, A., Mathis, J. T., Merlivat, L., Millero, F. J., Monteiro, P. M. S., Munro, D. R., Murata, A., Newberger, T., Omar, A. M., Ono, T., Paterson, K., Pearce, D., Pierrot, D., Robbins, L. L., Saito, S., Salisbury, J., Schlitzer, R., Schneider, B., Schweitzer, R., Sieger, R., Skjelvan, I., Sullivan, K. F., Sutherland, S. C., Sutton, A. J., Tadokoro, K., Telszewski, M., Tuma, M., van Heuven, S. M. A. C., Vandemark, D., Ward, B., Watson, A. J., and Xu, S.: A multi-decade record of high-quality $f CO_2$ data in version 3 of the Surface Ocean CO_2 Atlas (SOCAT), Earth Syst. Sci. Data, 8, 383–413, doi:10.5194/essd-8-383-2016, 2016.

Ballantyne, A. P., Alden, C. B., Miller, J. B., Tans, P. P., and White, J. W. C.: Increase in observed net carbon dioxide uptake by land and oceans during the last 50 years, Nature, 488, 70–72, 2012.

Ballantyne, A. P., Andres, R., Houghton, R., Stocker, B. D., Wanninkhof, R., Anderegg, W., Cooper, L. A., DeGrandpre, M., Tans, P. P., Miller, J. B., Alden, C., and White, J. W. C.: Audit of the global carbon budget: estimate errors and their impact on uptake uncertainty, Biogeosciences, 12, 2565–2584, doi:10.5194/bg-12-2565-2015, 2015.

Bauer, J. E., Cai, W.-J., Raymond, P. A., Bianchi, T. S., Hopkinson, C. S., and Regnier, P. A. G.: The changing carbon cycle of the coastal ocean, Nature, 504, 61–70, 2013.

Best, M. J., Pryor, M., Clark, D. B., Rooney, G. G., Essery, R. L. H., Ménard, C. B., Edwards, J. M., Hendry, M. A., Porson, A., Gedney, N., Mercado, L. M., Sitch, S., Blyth, E., Boucher, O., Cox, P. M., Grimmond, C. S. B., and Harding, R. J.: The Joint

UK Land Environment Simulator (JULES), model description – Part 1: Energy and water fluxes, Geosci. Model Dev., 4, 677–699, doi:10.5194/gmd-4-677-2011, 2011.

Betts, R. A., Jones, C. D., Knight, J. R., Keeling, R. F., and Kennedy, J. J.: El Nino and a record CO_2 rise, Nature Climate Change, 6, 806–810, 2016.

Boden, T. A. and Andres, R. J.: Global, Regional, and National Fossil-Fuel CO_2 Emissions, available at: http://cdiac.ornl.gov/trends/emis/overview_2013.html (last access: April 2016), Oak Ridge National Laboratory, US Department of Energy, Oak Ridge, Tenn., USA, 2016.

BP: Change in methodology for calculating CO_2 emissions from energy use, available at: http://www.bp.com/content/dam/bp/pdf/energy-economics/statistical-review-2016/bp-statistical-review-of-world-energy-2016-carbon-emissions-methodology.pdf (last access: September 2016), 2016a.

BP: Statistical Review of World Energy 2016, available at: https://www.bp.com/content/dam/bp/pdf/energy-economics/statistical-review-2016/bp-statistical-review-of-world-energy-2016-full-report.pdf (last access: June 2016), 2016b.

Bruno, M. and Joos, F.: Terrestrial carbon storage during the past 200 years: A monte carlo analysis of CO_2 data from ice core and atmospheric measurements, Global Biogeochem. Cy., 11, 111–124, 1997.

Buitenhuis, E. T., Rivkin, R. B., Sailley, S., and Le Quéré, C.: Biogeochemical fluxes through microzooplankton, Global Biogeochem. Cy., 24, GB4015, doi:10.1029/2009gb003601, 2010.

Canadell, J., Ciais, P., Sabine, C., and Joos, F. (Eds.): REgional Carbon Cycle Assessment and Processes (RECCAP), Biogeosciences, http://www.biogeosciences.net/special_issue107.html, 2012.

Canadell, J. G., Le Quéré, C., Raupach, M. R., Field, C. B., Buitenhuis, E. T., Ciais, P., Conway, T. J., Gillett, N. P., Houghton, R. A., and Marland, G.: Contributions to accelerating atmospheric CO_2 growth from economic activity, carbon intensity, and efficiency of natural sinks, P. Natl. Acad. Sci. USA, 104, 18866–18870, 2007.

CCIA: China Coal Industry Association, 2016 First Three Quarters of Economic Operation of Coal, available at: http://www.coalchina.org.cn/detail/16/10/25/00000007/content.html, last access: 29 October 2016 (in Chinese).

Chevallier, F.: On the statistical optimality of CO_2 atmospheric inversions assimilating CO_2 column retrievals, Atmos. Chem. Phys., 15, 11133–11145, doi:10.5194/acp-15-11133-2015, 2015.

Chevallier, F., Fisher, M., Peylin, P., Serrar, S., Bousquet, P., Bréon, F.-M., Chédin, A., and Ciais, P.: Inferring CO_2 sources and sinks from satellite observations: Method and application to TOVS data, J. Geophys. Res., 110, D24309, doi:10.1029/2005JD006390, 2005.

Ciais, P., Sabine, C., Govindasamy, B., Bopp, L., Brovkin, V., Canadell, J., Chhabra, A., DeFries, R., Galloway, J., Heimann, M., Jones, C., Le Quéré, C., Myneni, R., Piao, S., and Thornton, P.: Chapter 6: Carbon and Other Biogeochemical Cycles, in: Climate Change 2013 The Physical Science Basis, edited by: Stocker, T., Qin, D., and Platner, G.-K., Cambridge University Press, Cambridge, 2013.

Clark, D. B., Mercado, L. M., Sitch, S., Jones, C. D., Gedney, N., Best, M. J., Pryor, M., Rooney, G. G., Essery, R. L. H., Blyth, E., Boucher, O., Harding, R. J., Huntingford, C., and Cox, P. M.: The Joint UK Land Environment Simulator (JULES), model description – Part 2: Carbon fluxes and vegetation dynamics, Geosci. Model Dev., 4, 701–722, doi:10.5194/gmd-4-701-2011, 2011.

Davis, S. J. and Caldeira, K.: Consumption-based accounting of CO_2 emissions, P. Natl. Acad. Sci. USA, 107, 5687–5692, 2010.

Denman, K. L., Brasseur, G., Chidthaisong, A., Ciais, P., Cox, P. M., Dickinson, R. E., Hauglustaine, D., Heinze, C., Holland, E., Jacob, D., Lohmann, U., Ramachandran, S., da Silva Dias, P. L., Wofsy, S. C., and Zhang, X.: Couplings Between Changes in the Climate System and Biogeochemistry, in: Climate Change 2007: The Physical Science Basis. Contribution of Working Group I to the Fourth Assessment Report of the Intergovernmental Panel on Climate Change, edited by: Solomon, S., Qin, D., Manning, M., Chen, Z., Marquis, M., Averyt, K. B., Tignor, M., and Miller, H. L., Cambridge University Press, Cambridge, UK and New York, USA, 2007.

Dietzenbacher, E., Pei, J. S., and Yang, C. H.: Trade, production fragmentation, and China's carbon dioxide emissions, J. Environ. Econ. Manag., 64, 88–101, 2012.

Dlugokencky, E. and Tans, P.: Trends in atmospheric carbon dioxide, National Oceanic & Atmospheric Administration, Earth System Research Laboratory (NOAA/ESRL), available at: http://www.esrl.noaa.gov/gmd/ccgg/trends/global.html, last access: 28 October 2016.

Doney, S. C., Lima, I., Feely, R. A., Glover, D. M., Lindsay, K., Mahowald, N., Moore, J. K., and Wanninkhof, R.: Mechanisms governing interannual variability in upper-ocean inorganic carbon system and air–sea CO_2 fluxes: Physical climate and atmospheric dust, Deep-Sea Res. Pt. II, 56, 640–655, 2009.

Duce, R. A., LaRoche, J., Altieri, K., Arrigo, K. R., Baker, A. R., Capone, D. G., Cornell, S., Dentener, F., Galloway, J., Ganeshram, R. S., Geider, R. J., Jickells, T., Kuypers, M. M., Langlois, R., Liss, P. S., Liu, S. M., Middelburg, J. J., Moore, C. M., Nickovic, S., Oschlies, A., Pedersen, T., Prospero, J., Schlitzer, R., Seitzinger, S., Sorensen, L. L., Uematsu, M., Ulloa, O., Voss, M., Ward, B., and Zamora, L.: Impacts of atmospheric anthropogenic nitrogen on the open ocean, Science, 320, 893–897, 2008.

Durant, A. J., Le Quéré, C., Hope, C., and Friend, A. D.: Economic value of improved quantification in global sources and sinks of carbon dioxide, Philos. T. Roy. Soc. A, 369, 1967–1979, doi:10.1098/rsta.2011.0002, 2011.

Earles, J. M., Yeh, S., and Skog, K. E.: Timing of carbon emissions from global forest clearance, Nature Climate Change, 2, 682–685, 2012.

EDGAR: Global Emissions EDGAR v4.2 (November 2011), available at: http://edgar.jrc.ec.europa.eu/overview.php?v=42 (last access: October 2016), 2011.

EIA: US Energy Information Administration, Short-Term Energy and Winter Fuels Outlook, available at: http://www.eia.gov/forecasts/steo/outlook.cfm, last access: October 2016.

Elliott, J., Müller, C., Deryng, D., Chryssanthacopoulos, J., Boote, K. J., Büchner, M., Foster, I., Glotter, M., Heinke, J., Iizumi, T., Izaurralde, R. C., Mueller, N. D., Ray, D. K., Rosenzweig, C., Ruane, A. C., and Sheffield, J.: The Global Gridded Crop Model Intercomparison: data and modeling protocols for Phase 1 (v1.0),

www.earth-syst-sci-data.net/8/605/2016/

Earth Syst. Sci. Data, 8, 605–649, 2016

Geosci. Model Dev., 8, 261–277, doi:10.5194/gmd-8-261-2015, 2015.

El Masri, B., Shu, S., and Jain, A. K.: Implementation of a dynamic rooting depth and phenology into a land surface model: Evaluation of carbon, water, and energy fluxes in the high latitude ecosystems, Agr. Forest Meteorol., 211–212, 85–99, 2015.

Erb, K.-H., Kastner, T., Luyssaert, S., Houghton, R. A., Kuemmerle, T., Olofsson, P., and Haberl, H.: Bias in the attribution of forest carbon sinks, Nature Climate Change, 3, 854–856, 2013.

Etheridge, D. M., Steele, L. P., Langenfelds, R. L., and Francey, R. J.: Natural and anthropogenic changes in atmospheric CO_2 over the last 1000 years from air in Antarctic ice and firn, J. Geophys. Res., 101, 4115–4128, 1996.

FAO: Global Forest Resource Assessment 2010, 378 pp., Food and Agriculture Organization of the United Nations, Rome, Italy 2010.

FAOSTAT: Food and Agriculture Organization Statistics Division, available at: http://faostat.fao.org/ (last access: October 2012), 2010.

Federici, S., Tubiello, F. N., Salvatore, M., Jacobs, H., and Schmidhuber, J.: New estimates of CO_2 forest emissions and removals: 1990–2015, Forest Ecol. Manage., 352, 89–98, 2015.

Feely, R. A., Wanninkhof, R., Takahashi, T., and Tans, P.: Influence of El Nino on the equatorial Pacific contribution to atmospheric CO_2 accumulation, Nature, 398, 597–601, 1999.

Francey, R. J., Trudinger, C. M., van der Schoot, M., Law, R. M., Krummel, P. B., Langenfelds, R. L., Steele, L. P., Allison, C. E., Stavert, A. R., Andres, R. J., and Rodenbeck, C.: Reply to "Anthropogenic CO_2 emissions", Nature Climate Change, 3, 604–604, 2013.

Friedlingstein, P., Houghton, R. A., Marland, G., Hackler, J., Boden, T. A., Conway, T. J., Canadell, J. G., Raupach, M. R., Ciais, P., and Le Quéré, C.: Update on CO_2 emissions, Nat. Geosci., 3, 811–812, 2010.

Friedlingstein, P., Andrew, R. M., Rogelj, J., Peters, G. P., Canadell, J. G., Knutti, R., Luderer, G., Raupach, M. R., Schaeffer, M., van Vuuren, D. P., and Le Quéré, C.: Persistent growth of CO_2 emissions and implications for reaching climate targets, Nat. Geosci., 7, 709–715, doi:10.1038/ngeo2248, 2014.

Gasser, T. and Ciais, P.: A theoretical framework for the net land-to-atmosphere CO_2 flux and its implications in the definition of "emissions from land-use change", Earth Syst. Dynam., 4, 171–186, doi:10.5194/esd-4-171-2013, 2013.

GCP: The Global Carbon Budget 2007, available at: http://www.globalcarbonproject.org/carbonbudget/archive.htm (last access: 7 November 2016), 2007.

Giglio, L., Randerson, J., and van der Werf, G.: Analysis of daily, monthly, and annual burned area using the fourth-generation global fire emissions database (GFED4), J. Geophys. Res.-Biogeo., 118, 317–328, doi:10.1002/jgrg.20042, 2013.

Gitz, V. and Ciais, P.: Amplifying effects of land-use change on future atmospheric CO_2 levels, Global Biogeochem. Cy., 17, 1024, doi:10.1029/2002GB001963, 2003.

Goll, D. S., Brovkin, V., Liski, J., Raddatz, T., Thum, T., and Todd-Brown, K. E. O.: Strong dependence of CO_2 emissions from anthropogenic land cover change on initial land cover and soil carbon parametrization, Global Biogeochem. Cy., 29, 1511–1523, doi:10.1002/2014gb004988, 2015.

Gonzalez-Gaya, B., Fernandez-Pinos, M. C., Morales, L., Mejanelle, L., Abad, E., Pina, B., Duarte, C. M., Jimenez, B., and Dachs, J.: High atmosphere-ocean exchange of semivolatile aromatic hydrocarbons, Nat. Geosci., 9, 438–442, doi:10.1038/ngeo2714, 2016.

Gregg, J. S., Andres, R. J., and Marland, G.: China: Emissions pattern of the world leader in CO_2 emissions from fossil fuel consumption and cement production, Geophys. Res. Lett., 35, L08806, doi:10.1029/2007GL032887, 2008.

Harris, I., Jones, P. D., Osborn, T. J., and Lister, D. H.: Updated high-resolution grids of monthly climatic observations – the CRU TS3.10 Dataset, Int. J. Climatol., 34, 623–642, 2014.

Harris, N., Brown, S., and Hagen, S. C.: Baseline map of carbon emissions from deforestation in tropical regions, Science, 336, 1573–1576, 2012.

Hauck, J., Köhler, P., Wolf-Gladrow, D., and Völker, C.: Iron fertilisation and century-scale effects of open ocean dissolution of olivine in a simulated CO_2 removal experiment, Environ. Res. Lett., 11, 024007, doi:10.1088/1748-9326/11/2/024007, 2016.

Hertwich, E. G. and Peters, G. P.: Carbon Footprint of Nations: A Global, Trade-Linked Analysis, Environ. Sci. Tech., 43, 6414–6420, doi:10.1021/es803496a, 2009.

Houghton, R. A.: Revised estimates of the annual net flux of carbon to the atmosphere from changes in land use and land management 1850–2000, Tellus B, 55, 378–390, 2003.

Houghton, R. A. and Nassikas, A. A.: Global and regional fluxes of carbon from land use and land-cover change 1850–2015, Global Biogeochem. Cy., submitted, 2016.

Houghton, R. A., House, J. I., Pongratz, J., van der Werf, G. R., DeFries, R. S., Hansen, M. C., Le Quéré, C., and Ramankutty, N.: Carbon emissions from land use and land-cover change, Biogeosciences, 9, 5125–5142, doi:10.5194/bg-9-5125-2012, 2012.

Hourdin, F., Musat, I., Bony, S., Braconnot, P., Codron, F., Dufresne, J.-L., Fairhead, L., Filiberti, M.-A., Freidlingstein, P., Grandpeix, J.-Y., Krinner, G., LeVan, P., Li, Z.-X., and Lott, F.: The LMDZ4 general circulation model: climate performance and sensitivity to parametrized physics with emphasis on tropical convection, Clim. Dynam., 27, 787–813, doi:10.1007/s00382-006-0158-0, 2006.

Hurtt, G. C., Chini, L. P., Frolking, S., Betts, R. A., Feddema, J., Fischer, G., Fisk, J. P., Hibbard, K., Houghton, R. A., Janetos, A., Jones, C. D., Kindermann, G., Kinoshita, T., Goldewijk, K. K., Riahi, K., Shevliakova, E., Smith, S., Stehfest, E., Thomson, A., Thornton, P., van Vuuren, D. P., and Wang, Y. P.: Harmonization of land-use scenarios for the period 1500-2100: 600 years of global gridded annual land-use transitions, wood harvest, and resulting secondary lands, Climatic Change, 109, 117–161, doi:10.1007/s10584-011-0153-2, 2011.

IEA/OECD: CO_2 emissions from fuel combustion, International Energy Agency/Organisation for Economic Cooperation and Development, Paris, 152 pp., 2015.

IEW: International Energy Web, available at: http://gas.in-en.com/html/gas-2517194.shtml, last access: 11 October 2016 (in Chinese).

IMF: World Economic Outlook of the International Monetary Fund, available at: http://www.imf.org/external/ns/cs.aspx?id=29, last access: September 2016.

Inomata, S. and Owen, A.: COMPARATIVE EVALUATION OF MRIO DATABASES, Economic Systems Research, 26, 239–244, 2014.

Ito, A. and Inatomi, M.: Use of a process-based model for assessing the methane budgets of global terrestrial ecosystems and evaluation of uncertainty, Biogeosciences, 9, 759–773, doi:10.5194/bg-9-759-2012, 2012.

Jackson, R. B., Canadell, J. G., Le Quéré, C., Andrew, R. M., Korsbakken, J. I., Peters, G. P., and Nakicenovic, N.: Reaching peak emissions, Nature Climate Change, 6, 7–10, doi:10.1038/nclimate2892,, 2016.

Jacobson, A. R., Mikaloff Fletcher, S. E., Gruber, N., Sarmiento, J. L., and Gloor, M.: A joint atmosphere-ocean inversion for surface fluxes of carbon dioxide: 1. Methods and global-scale fluxes, Global Biogeochem. Cy., 21, GB1019, doi:10.1029/2005GB002556, 2007.

Jain, A. K., Meiyappan, P., Song, Y., and House, J. I.: CO_2 Emissions from Land-Use Change Affected More by Nitrogen Cycle, than by the Choice of Land Cover Data, Glob. Change Biol., 9, 2893–2906, 2013.

Joos, F. and Spahni, R.: Rates of change in natural and anthropogenic radiative forcing over the past 20,000 years, P. Natl. Acad. Sci. USA, 105, 1425–1430, 2008.

Karstensen, J., Peters, G. P., and Andrew, R. M.: Uncertainty in temperature response of current consumption-based emissions estimates, Earth Syst. Dynam., 6, 287–309, doi:10.5194/esd-6-287-2015, 2015.

Kato, E., Kinoshita, T., Ito, A., Kawamiya, M., and Yamagata, Y.: Evaluation of spatially explicit emission scenario of land-use change and biomass burning using a process-based biogeochemical model, Journal of Land Use Science, 8, 104–122, 2013.

Keeling, C. D., Bacastow, R. B., Bainbridge, A. E., Ekdhal, C. A., Guenther, P. R., and Waterman, L. S.: Atmospheric carbon dioxide variations at Mauna Loa Observatory, Hawaii, Tellus, 28, 538–551, 1976.

Keeling, R. F. and Manning, A. C.: 5.15 – Studies of Recent Changes in Atmospheric O_2 Content, in: Treatise on Geochemistry (Second Edition), edited by: Holland, H. D. and Turekian, K. K., Elsevier, Oxford, 385–404, doi:10.1016/B978-0-08-095975-7.00420-4, 2014.

Khatiwala, S., Primeau, F., and Hall, T.: Reconstruction of the history of anthropogenic CO_2 concentrations in the ocean, Nature, 462, 346–350, 2009.

Khatiwala, S., Tanhua, T., Mikaloff Fletcher, S., Gerber, M., Doney, S. C., Graven, H. D., Gruber, N., McKinley, G. A., Murata, A., Ríos, A. F., and Sabine, C. L.: Global ocean storage of anthropogenic carbon, Biogeosciences, 10, 2169–2191, doi:10.5194/bg-10-2169-2013, 2013.

Kirschke, S., Bousquet, P., Ciais, P., Saunois, M., Canadell, J. G., Dlugokencky, E. J., Bergamaschi, P., Bergmann, D., Blake, D. R., Bruhwiler, L., Cameron Smith, P., Castaldi, S., Chevallier, F., Feng, L., Fraser, A., Heimann, M., Hodson, E. L., Houweling, S., Josse, B., Fraser, P. J., Krummel, P. B., Lamarque, J., Langenfelds, R. L., Le Quéré, C., Naik, V., O'Doherty, S., Palmer, P. I., Pison, I., Plummer, D., Poulter, B., Prinn, R. G., Rigby, M., Ringeval, B., Santini, M., Schmidt, M., Shindell, D. T., Simpson, I. J., Spahni, R., Steele, L. P., Strode, S. A., Sudo, K., Szopa, S., van der Werf, G. R., Voulgarakis, A., van Weele, M., Weiss, R. F.,

Williams, J. E., and Zeng, G.: Three decades of global methane sources and sinks, Nat. Geosci., 6, 813–823, 2013.

Klein Goldewijk, K., Beusen, A., van Drecht, G., and de Vos, M.: The HYDE 3.1 spatially explicit database of human-induced global land-use change over the past 12,000 years, Glob. Ecol. Biogeogr., 20, 73–86, 2011.

Korsbakken, J. I., Peters, G. P., and Andrew, R. M.: Uncertainties around reductions in China's coal use and CO_2 emissions, Nature Climate Change, 6, 687–690, doi:10.1038/nclimate2963, 2016.

Krinner, G., Viovy, N., de Noblet, N., Ogée, J., Friedlingstein, P., Ciais, P., Sitch, S., Polcher, J., and Prentice, I. C.: A dynamic global vegetation model for studies of the coupled atmosphere-biosphere system, Global Biogeochem. Cy., 19, 1–33, 2005.

Landschützer, P., Gruber, N., Bakker, D. C. E., and Schuster, U.: Recent variability of the global ocean carbon sink, Global Biogeochem. Cy., 28, 927–949, doi:10.1002/2014GB004853, 2014.

Landschützer, P., Gruber, N., Haumann, F. A., Rödenbeck, C., Bakker, D. C. E., van Heuven, S., Hoppema, M., Metzl, N., Sweeney, C., Takahashi, T., Tilbrook, B., and Wanninkhof, R.: The reinvigoration of the Southern Ocean carbon sink, Science, 349, 1221–1224, 2015.

Landschützer, P., Gruber, N., and Bakker, D. C. E.: Decadal variations and trends of the global ocean carbon sink, Global Biogeochem. Cy., doi:10.1002/2015GB005359, online first, 2016.

Le Quéré, C.: Closing the global budget for CO_2, Global Change, 74, 28–31, 2009.

Le Quéré, C., Raupach, M. R., Canadell, J. G., Marland, G., Bopp, L., Ciais, P., Conway, T. J., Doney, S. C., Feely, R. A., Foster, P., Friedlingstein, P., Gurney, K., Houghton, R. A., House, J. I., Huntingford, C., Levy, P. E., Lomas, M. R., Majkut, J., Metzl, N., Ometto, J. P., Peters, G. P., Prentice, I. C., Randerson, J. T., Running, S. W., Sarmiento, J. L., Schuster, U., Sitch, S., Takahashi, T., Viovy, N., van der Werf, G. R., and Woodward, F. I.: Trends in the sources and sinks of carbon dioxide, Nat. Geosci., 2, 831–836, 2009.

Le Quéré, C., Andres, R. J., Boden, T., Conway, T., Houghton, R. A., House, J. I., Marland, G., Peters, G. P., van der Werf, G. R., Ahlström, A., Andrew, R. M., Bopp, L., Canadell, J. G., Ciais, P., Doney, S. C., Enright, C., Friedlingstein, P., Huntingford, C., Jain, A. K., Jourdain, C., Kato, E., Keeling, R. F., Klein Goldewijk, K., Levis, S., Levy, P., Lomas, M., Poulter, B., Raupach, M. R., Schwinger, J., Sitch, S., Stocker, B. D., Viovy, N., Zaehle, S., and Zeng, N.: The global carbon budget 1959–2011, Earth Syst. Sci. Data, 5, 165–185, doi:10.5194/essd-5-165-2013, 2013.

Le Quéré, C., Peters, G. P., Andres, R. J., Andrew, R. M., Boden, T. A., Ciais, P., Friedlingstein, P., Houghton, R. A., Marland, G., Moriarty, R., Sitch, S., Tans, P., Arneth, A., Arvanitis, A., Bakker, D. C. E., Bopp, L., Canadell, J. G., Chini, L. P., Doney, S. C., Harper, A., Harris, I., House, J. I., Jain, A. K., Jones, S. D., Kato, E., Keeling, R. F., Klein Goldewijk, K., Körtzinger, A., Koven, C., Lefèvre, N., Maignan, F., Omar, A., Ono, T., Park, G.-H., Pfeil, B., Poulter, B., Raupach, M. R., Regnier, P., Rödenbeck, C., Saito, S., Schwinger, J., Segschneider, J., Stocker, B. D., Takahashi, T., Tilbrook, B., van Heuven, S., Viovy, N., Wanninkhof, R., Wiltshire, A., and Zaehle, S.: Global carbon budget 2013, Earth Syst. Sci. Data, 6, 235–263, doi:10.5194/essd-6-235-2014, 2014.

Le Quéré, C., Moriarty, R., Andrew, R. M., Canadell, J. G., Sitch, S., Korsbakken, J. I., Friedlingstein, P., Peters, G. P., Andres, R. J.,

Boden, T. A., Houghton, R. A., House, J. I., Keeling, R. F., Tans, P., Arneth, A., Bakker, D. C. E., Barbero, L., Bopp, L., Chang, J., Chevallier, F., Chini, L. P., Ciais, P., Fader, M., Feely, R. A., Gkritzalis, T., Harris, I., Hauck, J., Ilyina, T., Jain, A. K., Kato, E., Kitidis, V., Klein Goldewijk, K., Koven, C., Landschützer, P., Lauvset, S. K., Lefèvre, N., Lenton, A., Lima, I. D., Metzl, N., Millero, F., Munro, D. R., Murata, A., Nabel, J. E. M. S., Nakaoka, S., Nojiri, Y., O'Brien, K., Olsen, A., Ono, T., Pérez, F. F., Pfeil, B., Pierrot, D., Poulter, B., Rehder, G., Rödenbeck, C., Saito, S., Schuster, U., Schwinger, J., Séférian, R., Steinhoff, T., Stocker, B. D., Sutton, A. J., Takahashi, T., Tilbrook, B., van der Laan-Luijkx, I. T., van der Werf, G. R., van Heuven, S., Vandemark, D., Viovy, N., Wiltshire, A., Zaehle, S., and Zeng, N.: Global Carbon Budget 2015, Earth Syst. Sci. Data, 7, 349–396, doi:10.5194/essd-7-349-2015, 2015a.

Le Quéré, C., Moriarty, R., Andrew, R. M., Peters, G. P., Ciais, P., Friedlingstein, P., Jones, S. D., Sitch, S., Tans, P., Arneth, A., Boden, T. A., Bopp, L., Bozec, Y., Canadell, J. G., Chini, L. P., Chevallier, F., Cosca, C. E., Harris, I., Hoppema, M., Houghton, R. A., House, J. I., Jain, A. K., Johannessen, T., Kato, E., Keeling, R. F., Kitidis, V., Klein Goldewijk, K., Koven, C., Landa, C. S., Landschützer, P., Lenton, A., Lima, I. D., Marland, G., Mathis, J. T., Metzl, N., Nojiri, Y., Olsen, A., Ono, T., Peng, S., Peters, W., Pfeil, B., Poulter, B., Raupach, M. R., Regnier, P., Rödenbeck, C., Saito, S., Salisbury, J. E., Schuster, U., Schwinger, J., Séférian, R., Segschneider, J., Steinhoff, T., Stocker, B. D., Sutton, A. J., Takahashi, T., Tilbrook, B., van der Werf, G. R., Viovy, N., Wang, Y.-P., Wanninkhof, R., Wiltshire, A., and Zeng, N.: Global carbon budget 2014, Earth Syst. Sci. Data, 7, 47–85, doi:10.5194/essd-7-47-2015, 2015b.

Li, W., Ciais, P., Wang, Y., Peng, S., Broquet, G., Ballantyne, A. P., Canadell, J. G., Cooper, L., Friedlingstein, P., Le Quéré, C., Myneni, R., Peters, G. P., Piao, S., and Pongratz, J.: Reducing uncertainties in decadal variability of the global carbon budget with multiple datasets, P. Natl. Acad. Sci. USA, doi:10.1073/pnas.1603956113, in press, 2016.

Liu, Z., Guan, D., Wei, W., Davis, S. J., Ciais, P., Bai, J., Peng, S., Zhang, Q., Hubacek, K., Marland, G., Andres, R. J., Crawford-Brown, D., Lin, J., Zhao, H., Hong, C., Boden, T. A., Feng, K., Peters, G. P., Xi, F., Liu, J., Li, Y., Zhao, Y., Zeng, N., and He, K.: Reduced carbon emission estimates from fossil fuel combustion and cement production in China, Nature, 524, 335–338, doi:10.1038/nature14677, 2015.

Manning, A. C. and Keeling, R. F.: Global oceanic and land biotic carbon sinks from the Scripps atmospheric oxygen flask sampling network, Tellus B, 58, 95–116, doi:10.1111/j.1600-0889.2006.00175.x, 2006.

Marland, G.: Uncertainties in accounting for CO_2 from fossil fuels, J. Ind. Ecol., 12, 136–139, 2008.

Marland, G., Andres, R. J., Blasing, T. J., Boden, T. A., Broniak, C. T., Gregg, J. S., Losey, L. M., and Treanton, K.: Energy, industry and waste management activities: An introduction to CO_2 emissions from fossil fuels, A report by the US Climate Change Science Program and the Subcommittee on Global Change Research, in: The First State of the Carbon Cycle Report (SOCCR): The North American Carbon Budget and Implications for the Global Carbon Cycle, edited by: King, A. W., Dilling, L., Zimmerman, G. P., Fairman, D. M., Houghton, R. A., Marland, G.,

Rose, A. Z., and Wilbanks, T. J., National Oceanic and Atmospheric Administration, Asheville, NC, 2007.

Marland, G., Hamal, K., and Jonas, M.: How Uncertain Are Estimates of CO_2 Emissions?, J. Ind. Ecol., 13, 4–7, 2009.

Masarie, K. A. and Tans, P. P.: Extension and integratino of atmospheric carbon dioxide data into a globally consistent measurement record, J. Geophys. Res.-Atmos., 100, 11593–11610, 1995.

McNeil, B. I., Matear, R. J., Key, R. M., Bullister, J. L., and Sarmiento, J. L.: Anthropogenic CO_2 uptake by the ocean based on the global chlorofluorocarbon data set, Science, 299, 235–239, 2003.

Melton, J. R. and Arora, V. K.: Competition between plant functional types in the Canadian Terrestrial Ecosystem Model (CTEM) v. 2.0, Geosci. Model Dev., 9, 323–361, doi:10.5194/gmd-9-323-2016, 2016.

Meyerholt, J., Zaehle, S., and Smith, M. J.: Variability of projected terrestrial biosphere responses to elevated levels of atmospheric CO_2 due to uncertainty in biological nitrogen fixation, Biogeosciences, 13, 1491–1518, doi:10.5194/bg-13-1491-2016, 2016.

Mikaloff Fletcher, S. E., Gruber, N., Jacobson, A. R., Doney, S. C., Dutkiewicz, S., Gerber, M., Follows, M., Joos, F., Lindsay, K., Menemenlis, D., Mouchet, A., Müller, S. A., and Sarmiento, J. L.: Inverse estimates of anthropogenic CO_2 uptake, transport, and storage by the oceans, Global Biogeochem. Cy., 20, GB2002, doi:10.1029/2005GB002530, 2006.

Moran, D. and Wood, R.: CONVERGENCE BETWEEN THE EORA, WIOD, EXIOBASE, AND OPENEU'S CONSUMPTION-BASED CARBON ACCOUNTS, Economic Systems Research, 26, 245–261, 2014.

Myhre, G., Alterskjær, K., and Lowe, D.: A fast method for updating global fossil fuel carbon dioxide emissions, Environ. Res. Lett., 4, 034012, doi:10.1088/1748-9326/4/3/034012, 2009.

Narayanan, B., Aguiar, A., and McDougall, R.: available at: https://www.gtap.agecon.purdue.edu/databases/v9/default.asp, last access: September 2015.

NBS: National Bureau of Statistic, Industrial Production Operation in September 2016, available at: http://www.stats.gov.cn/english/PressRelease/201610/t20161020_1411993.html, last access: October 2016.

NDRC: National Development and Reform Commission, Natural Gas, available at: http://www.sdpc.gov.cn/jjxsfx/201608/t20160826_816043.html, last access: 26 August 2016a.

NDRC: National Development and Reform Commission, Refined oil, available at: http://www.sdpc.gov.cn/jjxsfx/201608/t20160826_816042.html (last access: August 2016), 2016b.

NOAA/ESRL: available at: http://www.esrl.noaa.gov/gmd/ccgg/about/global_means.html, last access: 7 October 2015.

Oke, P. R., Griffin, D. A., Schiller, A., Matear, R. J., Fiedler, R., Mansbridge, J., Lenton, A., Cahill, M., Chamberlain, M. A., and Ridgway, K.: Evaluation of a near-global eddy-resolving ocean model, Geosci. Model Dev., 6, 591–615, doi:10.5194/gmd-6-591-2013, 2013.

Oleson, K. W., Lawrence, D. M., Bonan, G. B., Drewniak, B., Huang, M., Koven, C. D., Levis, S., Li, F., Riley, W. J., Subin, Z. M., Swenson, S. C., Thornton, P. E., Bozbiyik, A., Fisher, R., Heald, C. L., Kluzek, E., Lamarque, J., Lawrence, P. J., Leung, L. R., Lipscomb, W., Muszala, S., Ricciuto, D. M., Sacks, W., Tang, J., and Yang, Z.: Technical Description of version 4.5 of the Community Land Model (CLM),

National Center for Atmospheric Research, Boulder, CO, USA, available at: http://www.cesm.ucar.edu/models/cesm1.2/clm/CLM45_Tech_Note.pdf (last access: 8 November 2016), 2013.

Olin, S., Lindeskog, M., Pugh, T. A. M., Schurgers, G., Wårlind, D., Mishurov, M., Zaehle, S., Stocker, B. D., Smith, B., and Arneth, A.: Soil carbon management in large-scale Earth system modelling: implications for crop yields and nitrogen leaching, Earth Syst. Dynam., 6, 745–768, doi:10.5194/esd-6-745-2015, 2015.

Peters, G. P. and Hertwich, E. G.: Post-Kyoto Greenhouse Gas Inventories: Production versus Consumption, Climatic Change, 86, 51–66, doi:10.1007/s10584-007-9280-1, 2008.

Peters, G. P., Andrew, R., and Lennos, J.: Constructing a multi-regional input-output table using the GTAP database, Economic Systems Research, 23, 131–152, 2011a.

Peters, G. P., Minx, J. C., Weber, C. L., and Edenhofer, O.: Growth in emission transfers via international trade from 1990 to 2008, P. Natl. Acad. Sci. USA, 108, 8903–8908, 2011b.

Peters, G. P., Davis, S. J., and Andrew, R.: A synthesis of carbon in international trade, Biogeosciences, 9, 3247–3276, doi:10.5194/bg-9-3247-2012, 2012a.

Peters, G. P., Marland, G., Le Quéré, C., Boden, T. A., Canadell, J. G., and Raupach, M. R.: Correspondence: Rapid growth in CO_2 emissions after the 2008–2009 global financial crisis, Nature Climate Change, 2, 2–4, 2012b.

Peters, G. P., Andrew, R. M., Boden, T., Canadell, J. G., Ciais, P., Le Quéré, C., Marland, G., Raupach, M. R., and Wilson, C.: The challenge to keep global warming below 2 °C, Nature Climate Change, 3, 4–6, 2013.

Peters, G. P., Andrew, R. M., Canadell, J. G., Fuss, S., Jackson, R. B., Korsbakken, J. I., Le Quéré, C., and Nakicenovic, N.: Key indicators to track current progress and future ambition of the Paris Agreement, Nature Climate Change, in review, 2016.

Peters, W., Krol, M. C., van der Werf, G. R., Houweling, S., Jones, C. D., Hughes, J., Schaefer, K., Masarie, K. A., Jacobson, A. R., Miller, J. B., Cho, C. H., Ramonet, M., Schmidt, M., Ciattaglia, L., Apadula, F., Heltai, D., Meinhardt, F., Di Sarra, A. G., Piacentino, S., Sferlazzo, D., Aalto, T., Hatakka, J., Ström, J., Haszpra, L., Meijer, H. A. J., Van Der Laan, S., Neubert, R. E. M., Jordan, A., Rodó, X., Morguí, J.-A., Vermeulen, A. T., Popa, E., Rozanski, K., Zimnoch, M., Manning, A. C., Leuenberger, M., Uglietti, C., Dolman, A. J., Ciais, P., Heimann, M., and Tans, P. P.: Seven years of recent European net terrestrial carbon dioxide exchange constrained by atmospheric observations, Glob. Change Biol., 16, 1317–1337, 2010.

Pfeil, B., Olsen, A., Bakker, D. C. E., Hankin, S., Koyuk, H., Kozyr, A., Malczyk, J., Manke, A., Metzl, N., Sabine, C. L., Akl, J., Alin, S. R., Bates, N., Bellerby, R. G. J., Borges, A., Boutin, J., Brown, P. J., Cai, W.-J., Chavez, F. P., Chen, A., Cosca, C., Fassbender, A. J., Feely, R. A., González-Dávila, M., Goyet, C., Hales, B., Hardman-Mountford, N., Heinze, C., Hood, M., Hoppema, M., Hunt, C. W., Hydes, D., Ishii, M., Johannessen, T., Jones, S. D., Key, R. M., Körtzinger, A., Landschützer, P., Lauvset, S. K., Lefèvre, N., Lenton, A., Lourantou, A., Merlivat, L., Midorikawa, T., Mintrop, L., Miyazaki, C., Murata, A., Nakadate, A., Nakano, Y., Nakaoka, S., Nojiri, Y., Omar, A. M., Padin, X. A., Park, G.-H., Paterson, K., Perez, F. F., Pierrot, D., Poisson, A., Ríos, A. F., Santana-Casiano, J. M., Salisbury, J., Sarma, V. V. S. S., Schlitzer, R., Schneider, B., Schuster, U., Sieger, R., Skjel-

van, I., Steinhoff, T., Suzuki, T., Takahashi, T., Tedesco, K., Telszewski, M., Thomas, H., Tilbrook, B., Tjiputra, J., Vandemark, D., Veness, T., Wanninkhof, R., Watson, A. J., Weiss, R., Wong, C. S., and Yoshikawa-Inoue, H.: A uniform, quality controlled Surface Ocean CO_2 Atlas (SOCAT), Earth Syst. Sci. Data, 5, 125–143, doi:10.5194/essd-5-125-2013, 2013.

Pongratz, J., Reick, C. H., Raddatz, T., and Claussen, M.: Effects of anthropogenic land cover change on the carbon cycle of the last millennium, Global Biogeochem. Cy., 23, GB4001, doi:10.1029/2009GB003488, 2009.

Prather, M. J., Holmes, C. D., and Hsu, J.: Reactive greenhouse gas scenarios: Systematic exploration of uncertainties and the role of atmospheric chemistry, Geophys. Res. Lett., 39, L09803, doi:10.1029/2012GL051440, 2012.

Prentice, I. C., Farquhar, G. D., Fasham, M. J. R., Goulden, M. L., Heimann, M., Jaramillo, V. J., Kheshgi, H. S., Le Quéré, C., Scholes, R. J., and Wallace, D. W. R.: The Carbon Cycle and Atmospheric Carbon Dioxide. In: Climate Change 2001: The Scientific Basis. Contribution of Working Group I to the Third Assessment Report of the Intergovernmental Panel on Climate Change, edited by: Houghton, J. T., Ding, Y., Griggs, D. J., Noguer, M., van der Linden, P. J., Dai, X., Maskell, K., and Johnson, C. A., Cambridge University Press, Cambridge, United Kingdom and New York, NY, USA, 2001.

Randerson, J. T., Chen, Y., van der Werf, G. R., Rogers, B. M., and Morton, D. C.: Global burned area and biomass burning emissions from small fires, J. Geophys. Res.-Biogeo., 117, G04012, doi:10.1029/2012JG002128, 2012.

Raupach, M. R., Marland, G., Ciais, P., Le Quéré, C., Canadell, J. G., Klepper, G., and Field, C. B.: Global and regional drivers of accelerating CO_2 emissions, P. Natl. Acad. Sci. USA, 104, 10288–10293, 2007.

Regnier, P., Friedlingstein, P., Ciais, P., Mackenzie, F. T., Gruber, N., Janssens, I. A., Laruelle, G. G., Lauerwald, R., Luyssaert, S., Andersson, A. J., Arndt, S., Arnosti, C., Borges, A. V., Dale, A. W., Gallego-Sala, A., Goddéris, Y., Goossens, N., Hartmann, J., Heinze, C., Ilyina, T., Joos, F., La Rowe, D. E., Leifeld, J., Meysman, F. J. R., Munhoven, G., Raymond, P. A., Spahni, R., Suntharalingam, P., and Thullner M.: Anthropogenic perturbation of the carbon fluxes from land to ocean, Nat. Geosci., 6, 597–607, 2013.

Reick, C. H., T. Raddatz, V. Brovkin, and Gayler, V.: The representation of natural and anthropogenic land cover change in MPI-ESM, J. Adv. Model. Earth Syst., 5, 459–482, 2013.

Rhein, M., Rintoul, S. R., Aoki, S., Campos, E., Chambers, D., Feely, R. A., Gulev, S., Johnson, G. C., Josey, S. A., Kostianoy, A., Mauritzen, C., Roemmich, D., Talley, L. D., and Wang, F.: Chapter 3: Observations: Ocean. In: Climate Change 2013 The Physical Science Basis, Cambridge University Press, 2013.

Rödenbeck, C.: Estimating CO_2 sources and sinks from atmospheric mixing ratio measurements using a global inversion of atmospheric transport, Max Plank Institute, MPI-BGC, 2005.

Rödenbeck, C., Houweling, S., Gloor, M., and Heimann, M.: CO_2 flux history 1982–2001 inferred from atmospheric data using a global inversion of atmospheric transport, Atmos. Chem. Phys., 3, 1919–1964, doi:10.5194/acp-3-1919-2003, 2003.

Rödenbeck, C., Keeling, R. F., Bakker, D. C. E., Metzl, N., Olsen, A., Sabine, C., and Heimann, M.: Global surface-ocean $p$$CO_2$ and sea–air CO_2 flux variability from an observation-

www.earth-syst-sci-data.net/8/605/2016/

Earth Syst. Sci. Data, 8, 605–649, 2016

driven ocean mixed-layer scheme, Ocean Sci., 9, 193–216, doi:10.5194/os-9-193-2013, 2013.

Rödenbeck, C., Bakker, D. C. E., Metzl, N., Olsen, A., Sabine, C., Cassar, N., Reum, F., Keeling, R. F., and Heimann, M.: Interannual sea–air CO_2 flux variability from an observation-driven ocean mixed-layer scheme, Biogeosciences, 11, 4599–4613, doi:10.5194/bg-11-4599-2014, 2014.

Rödenbeck, C., Bakker, D. C. E., Gruber, N., Iida, Y., Jacobson, A. R., Jones, S., Landschützer, P., Metzl, N., Nakaoka, S., Olsen, A., Park, G.-H., Peylin, P., Rodgers, K. B., Sasse, T. P., Schuster, U., Shutler, J. D., Valsala, V., Wanninkhof, R., and Zeng, J.: Data-based estimates of the ocean carbon sink variability – first results of the Surface Ocean pCO_2 Mapping intercomparison (SOCOM), Biogeosciences, 12, 7251–7278, doi:10.5194/bg-12-7251-2015, 2015.

Rypdal, K., Paciornik, N., Eggleston, S., Goodwin, J., Irving, W., Penman, J., and Woodfield, M.: Chapter 1 Introduction to the 2006 Guidelines, in: 2006 IPCC Guidelines for National Greenhouse Gas Inventories, edited by: Eggleston, S., Buendia, L., Miwa, K., Ngara, T., and Tanabe, K., Institute for Global Environmental Strategies (IGES), Hayama, Kanagawa, Japan, 2006.

Schimel, D., Alves, D., Enting, I., Heimann, M., Joos, F., Raynaud, D., Wigley, T., Prater, M., Derwent, R., Ehhalt, D., Fraser, P., Sanhueza, E., Zhou, X., Jonas, P., Charlson, R., Rodhe, H., Sadasivan, S., Shine, K. P., Fouquart, Y., Ramaswamy, V., Solomon, S., Srinivasan, J., Albritton, D., Derwent, R., Isaksen, I., Lal, M., and Wuebbles, D.: Radiative Forcing of Climate Change, in: Climate Change 1995 The Science of Climate Change. Contribution of Working Group I to the Second Assessment Report of the Intergovernmental Panel on Climate Change, edited by: Houghton, J. T., Meira Rilho, L. G., Callander, B. A., Harris, N., Kattenberg, A., and Maskell, K., Cambridge University Press, Cambridge, United Kingdom and New York, NY, USA, 1995.

Schwietzke, S., Sherwood, O. A., Bruhwiler, L. M. P., Miller, J. B., Etiope, G., Dlugokencky, E. J., Michel, S. E., Arling, V. A., Vaughn, B. H., White, J. W. C., and Tans, P. P.: Upward revision of global fossil fuel methane emissions based on isotope database, Nature, 538, 88–91, 2016.

Schwinger, J., Goris, N., Tjiputra, J. F., Kriest, I., Bentsen, M., Bethke, I., Ilicak, M., Assmann, K. M., and Heinze, C.: Evaluation of NorESM-OC (versions 1 and 1.2), the ocean carbon-cycle stand-alone configuration of the Norwegian Earth System Model (NorESM1), Geosci. Model Dev., 9, 2589–2622, doi:10.5194/gmd-9-2589-2016, 2016.

Scripps: The Keeling Curve, available at: http://keelingcurve.ucsd.edu/, last access: 7 November 2013.

Séférian, R., Bopp, L., Gehlen, M., Orr, J., Ethé, C., Cadule, P., Aumont, O., Salas y Mélia, D., Voldoire, A., and Madec, G.: Skill assessment of three earth system models with common marine biogeochemistry, Clim. Dynam., 40, 2549–2573, 2013.

Shevliakova, E., Pacala, S. W., Malyshev, S., Hurtt, G. C., Milly, P. C. D., Caspersen, J. P., Sentman, L. T., Fisk, J. P., Wirth, C., and Crevoisier, C.: Carbon cycling under 300 years of land use change: Importance of the secondary vegetation sink, Global Biogeochem. Cy., 23, GB2022, doi:10.1029/2007GB003176, 2009.

Sitch, S., Smith, B., Prentice, I. C., Arneth, A., Bondeau, A., Cramer, W., Kaplan, J. O., Levis, S., Lucht, W., Sykes, M. T., Thonicke, K., and Venevsky, S.: Evaluation of ecosystem dynamics, plant geography and terrestrial carbon cycling in the LPJ dynamic global vegetation model, Glob. Change Biol., 9, 161–185, 2003.

Sitch, S., Friedlingstein, P., Gruber, N., Jones, S. D., Murray-Tortarolo, G., Ahlström, A., Doney, S. C., Graven, H., Heinze, C., Huntingford, C., Levis, S., Levy, P. E., Lomas, M., Poulter, B., Viovy, N., Zaehle, S., Zeng, N., Arneth, A., Bonan, G., Bopp, L., Canadell, J. G., Chevallier, F., Ciais, P., Ellis, R., Gloor, M., Peylin, P., Piao, S. L., Le Quéré, C., Smith, B., Zhu, Z., and Myneni, R.: Recent trends and drivers of regional sources and sinks of carbon dioxide, Biogeosciences, 12, 653–679, doi:10.5194/bg-12-653-2015, 2015.

Smith, B., Wårlind, D., Arneth, A., Hickler, T., Leadley, P., Siltberg, J., and Zaehle, S.: Implications of incorporating N cycling and N limitations on primary production in an individual-based dynamic vegetation model, Biogeosciences, 11, 2027–2054, doi:10.5194/bg-11-2027-2014, 2014.

Stephens, B. B., Gurney, K. R., Tans, P. P., Sweeney, C., Peters, W., Bruhwiler, L., Ciais, P., Ramonet, M., Bousquet, P., Nakazawa, T., Aoki, S., Machida, T., Inoue, G., Vinnichenko, N., Lloyd, J., Jordan, A., Heimann, M., Shibistova, O., Langenfelds, R. L., Steele, L. P., Francey, R. J., and Denning, A. S.: Weak Northern and Strong Tropical Land Carbon Uptake from Vertical Profiles of Atmospheric CO_2, Science, 316, 1732–1735, 2007.

Stocker, B. D. and Joos, F.: Quantifying differences in land use emission estimates implied by definition discrepancies, Earth Syst. Dynam., 6, 731–744, doi:10.5194/esd-6-731-2015, 2015.

Stocker, B. D., Feissli, F., Strassmann, K. M., Spahni, R., and Joos, F.: Past and future carbon fluxes from land use change, shifting cultivation and wood harvest, Tellus B, 66, 23188, doi:10.3402/tellusb.v66.23188, 2014.

Stocker, T., Qin, D., and Platner, G.-K.: Climate Change 2013 The Physical Science Basis, Cambridge University Press, 2013.

Sweeney, C., Gloor, E., Jacobson, A. R., Key, R. M., McKinley, G., Sarmiento, J. L., and Wanninkhof, R.: Constraining global air-sea gas exchange for CO_2 with recent bomb ^{14}C measurements, Global Biogeochem. Cy., 21, GB2015, doi:10.1029/2006GB002784, 2007.

Tans, P. and Keeling, R. F.: Trends in atmospheric carbon dioxide, National Oceanic & Atmospheric Administration, Earth System Research Laboratory (NOAA/ESRL) & Scripps Institution of Oceanography, available at: http://www.esrl.noaa.gov/gmd/ccgg/trends/ and http://scrippsco2.ucsd.edu/ (last access: 8 August 2014), NOAA/ESRL, 2014.

Tian, H., Liu, M., Z, h. C., Ren, W., Xu, X., Chen, G., Lu, C., and Tao, B.: The Dynamic Land Ecosystem Model (DLEM) for Simulating Terrestrial Processes and Interactions in the Context of Multifactor Global Change, Acta Geographica Sinica, 65, 1027–1047, 2010.

UN: United Nations Statistics Division: Energy Statistics, available at: http://unstats.un.org/unsd/energy/, last access: October 2015a.

UN: United Nations Statistics Division: Industry Statistics, available at: http://unstats.un.org/unsd/industry/default.asp, last access: October 2015b.

UN: United Nations Statistics Division: National Accounts Main Aggregates Database, available at: http://unstats.un.org/unsd/snaama/Introduction.asp (last access: December 2015), 2015c.

USGS: 2014 Minerals Yearbook – Cement, US Geological Survey, Reston, Virginia, 2016a.

USGS: Mineral Commodities Summaries: Cement, USGS, Reston, Virginia, 2016b.

van der Werf, G. R., Dempewolf, J., Trigg, S. N., Randerson, J. T., Kasibhatla, P., Giglio, L., Murdiyarso, D., Peters, W., Morton, D. C., Collatz, G. J., Dolman, A. J., and DeFries, R. S.: Climate regulation of fire emissions and deforestation in equatorial Asia, P. Natl. Acad. Sci. USA, 15, 20350–20355, 2008.

van der Werf, G. R., Randerson, J. T., Giglio, L., Collatz, G. J., Mu, M., Kasibhatla, P. S., Morton, D. C., DeFries, R. S., Jin, Y., and van Leeuwen, T. T.: Global fire emissions and the contribution of deforestation, savanna, forest, agricultural, and peat fires (1997–2009), Atmos. Chem. Phys., 10, 11707–11735, doi:10.5194/acp-10-11707-2010, 2010.

van Minnen, J. G., Goldewijk, K. K., Stehfest, E., Eickhout, B., van Drecht, G., and Leemans, R.: The importance of three centuries of land-use change for the global and regional terrestrial carbon cycle, Climatic Change, 97, 123–144, 2009.

Viovy, N.: CRUNCEP data set, available at: ftp://nacp.ornl.gov/synthesis/2009/frescati/temp/land_use_change/original/readme.htm (last access: June 2016), 2016.

Wanninkhof, R., Park, G.-H., Takahashi, T., Sweeney, C., Feely, R., Nojiri, Y., Gruber, N., Doney, S. C., McKinley, G. A., Lenton, A., Le Quéré, C., Heinze, C., Schwinger, J., Graven, H., and Khatiwala, S.: Global ocean carbon uptake: magnitude, variability and trends, Biogeosciences, 10, 1983–2000, doi:10.5194/bg-10-1983-2013, 2013.

Watson, R. T., Rodhe, H., Oeschger, H., and Siegenthaler, U.: Greenhouse Gases and Aerosols, in: Climate Change: The IPCC Scientific Assessment. Intergovernmental Panel on Climate Change (IPCC), edited by: Houghton, J. T., Jenkins, G. J., and Ephraums, J. J., Cambridge University Press, Cambridge, 1990.

Woodward, F. I. and Lomas, M. R.: Vegetation dynamics – simulating responses to climatic change, Biol. Rev., 79, 643–670, doi:10.1017/S1464793103006419, 2004.

Woodward, F. I., Smith, T. M., and Emanuel, W. R.: A global land primary productivity and phytogeography model, Global Biogeochem. Cy., 9, 471–490, 1995.

Yin, Y., Ciais, P., Chevallier, F., van der Werf, G. R., Fanin, T., Broquet, G., Boesch, H., Cozic, A., Hauglustaine, D., Szopa, S., and Wang, Y.: Variability of fire carbon emissions in Equatorial Asia and its non-linear sensitivity to El Niño, Geophys. Res. Lett., 43, 10472–10479, 2016.

Zaehle, S. and Friend, A. D.: Carbon and nitrogen cycle dynamics in the O-CN land surface model: 1. Model description, site-scale evaluation, and sensitivity to parameter estimates, Global Biogeochem. Cy., 24, GB1005, doi:10.1029/2009GB003521, 2010.

Zaehle, S., Ciais, P., Friend, A. D., and Prieur, V.: Carbon benefits of anthropogenic reactive nitrogen offset by nitrous oxide emissions, Nat. Geosci., 4, 601–605, 2011.

Zhang, H. Q., Pak, B., Wang, Y. P., Zhou, X. Y., Zhang, Y. Q., and Zhang, L.: Evaluating Surface Water Cycle Simulated by the Australian Community Land Surface Model (CABLE) across Different Spatial and Temporal Domains, J. of Hydrometeorol., 14, 1119–1138, 2013.